

8-1-2014

## Transport Properties of Nano-Silica Contained Self-Consolidating Concrete

Borhan Moradi

University of Nevada, Las Vegas, moradi.borhan@gmail.com

Follow this and additional works at: <https://digitalscholarship.unlv.edu/thesesdissertations>



Part of the [Civil Engineering Commons](#), [Environmental Engineering Commons](#), [Materials Science and Engineering Commons](#), and the [Nanoscience and Nanotechnology Commons](#)

---

### Repository Citation

Moradi, Borhan, "Transport Properties of Nano-Silica Contained Self-Consolidating Concrete" (2014). *UNLV Theses, Dissertations, Professional Papers, and Capstones*. 2198.  
<https://digitalscholarship.unlv.edu/thesesdissertations/2198>

This Thesis is protected by copyright and/or related rights. It has been brought to you by Digital Scholarship@UNLV with permission from the rights-holder(s). You are free to use this Thesis in any way that is permitted by the copyright and related rights legislation that applies to your use. For other uses you need to obtain permission from the rights-holder(s) directly, unless additional rights are indicated by a Creative Commons license in the record and/or on the work itself.

This Thesis has been accepted for inclusion in UNLV Theses, Dissertations, Professional Papers, and Capstones by an authorized administrator of Digital Scholarship@UNLV. For more information, please contact [digitalscholarship@unlv.edu](mailto:digitalscholarship@unlv.edu).

**TRANSPORT PROPERTIES OF NANO-SILICA CONTAINED  
SELF-CONSOLIDATING CONCRETE**

**By**

**Borhan Moradi**

**Bachelor of Science in Civil and Environmental Engineering**

**University of Nevada Las Vegas**

**2011**

**A Thesis Submitted in Partial Fulfillment**

**of the Requirements for the**

**Master of Science in Engineering – Civil and Environmental Engineering**

**Department of Civil and Environmental Engineering and Construction**

**Howard R. Hughes College of Engineering**

**The Graduate College**

**University of Nevada, Las Vegas**

**August 2014**

**Copyright by Borhan Moradi 2014**

**All rights reserved**



## THE GRADUATE COLLEGE

We recommend the thesis prepared under our supervision by

**Borhan Moradi**

entitled

**Transport Properties of Nano-Silica Contained Self-Consolidating Concrete**

is approved in partial fulfillment of the requirements for the degree of

**Master of Science in Engineering -- Civil and Environmental Engineering**

**Department of Civil and Environmental Engineering and Construction**

Nadar Ghafouri, Ph.D., Committee Chair

Mohamed Kaseko, Ph.D., Committee Member

Samaan Ladkany, Ph.D., Committee Member

Spencer Steinberg, Ph.D., Committee Member

Samir Moujaes, Ph.D., Graduate College Representative

Kathryn Hausbeck Korgan, Ph.D., Interim Dean of the Graduate College

**August 2014**

## **ABSTRACT**

### **Transport Properties of Nano-Silica Contained Self-Consolidating Concrete**

**By**

**Borhan Moradi**

**Dr. Nader Ghafoori, Examination Committee Chair**

**Professor of Civil Engineering**

**Department of Civil and Environmental Engineering and Construction**

**University of Nevada, Las Vegas**

In this research study, transport properties of various self-consolidating concretes (SCCs) containing nano-particles ( $\text{SiO}_2$ ) were investigated. Nano-silica replaced a portion of the cementitious materials at different replacement levels ranging from 1.5 to 7.5% by weight. For the purpose of this investigation, flow, bulk, and transport properties of SCCs were studied. The investigated transport properties were absorption, water penetration, rapid chloride permeability, capillary absorption, rapid migration, and chloride diffusion. Transport properties of nano-silica SCCs were also compared to those of equivalent silica fume (micro silica) contained concretes, as well as those of control mixture (concrete without nano or micro silica).

Test results showed that all transport properties of SCCs improved with inclusion of nano-silica. Improvement in transport properties increased with increases of nano-silica replacing a portion of cementitious materials, as well as extension of curing age. A comparison of transport properties between nano-silica contained SCCs and their equivalent silica fume (micro silica) contained SCCs revealed a slightly better

performance for concretes containing silica fume at both studied curing ages. This finding was primarily attributed to agglomeration of nano-silica particles during mixing process.

## **Acknowledgments**

I would like to express my profound gratitude to my academic advisor, Dr. Nader Ghafoori, for his scholastic advice and technical guidance throughout this investigation. His devotion, patience, and focus on excellence allowed me to reach this important milestone in my life. I also wish to extend my acknowledgment to my examination committee members, Dr. Samaan Ladkany, Dr. Mohamed S. Kaseko, Dr. Spencer M. Steinberg, and Dr. Samir Moujaes for their guidance and suggestions.

I wish to thank Mr. Peter Faught and Mr. Jon Becker, the research shop technicians, for providing unlimited assistance and technical supports during the experimental program. I thank extend special thanks to Ms. Rebecca Spitek and Mr. Meysam Najimi to offer countless assistance during this memorable journey.

Lastly, but not least, my sincere appreciation to my family for their love and patience throughout my education.

This study is dedicated to my parents, Mr. Bejatollah Moradi and Mrs. Tahereh Roohani.  
Without their continued and unconditional love and support, I would not be the person I  
am today.



## Table of Contents

Chapter 1 Introduction.....	1
1. Introduction .....	2
1.1 Self-Consolidating Concrete.....	3
1.2 History.....	4
1.3 Advantages and Disadvantages.....	5
1.4 Fresh Properties of SCC.....	7
1.4.1 Filling Ability/ Flowability .....	8
1.4.2 Passing Ability .....	9
1.4.3 Stability .....	9
1.5 Transport Properties of SCC.....	10
1.5.1 Water Permeability.....	10
1.5.2 Diffusion.....	11
1.5.3 Capillary Suction.....	11
1.5.4 Absorption.....	12
1.5.5 Migration.....	12
1.6 Mixture Proportioning Design of SCC .....	13
Chapter 2 Literature Review .....	15
2.1 Compressive Strength .....	15
2.2 Water Absorption (Permeability).....	21
2.3 Water Penetration.....	22
2.4 Rapid Chloride Permeability.....	23
2.5 Capillary Absorption.....	25
2.6 Chloride Diffusion.....	27
2.7 Rapid Migration .....	27
Chapter 3 Materials and Testing Programs .....	29
3.1 Materials.....	29
3.1.1 Aggregates.....	29
3.1.2 Portland Cement.....	31
3.1.3 Fly Ash.....	33
3.1.4 Water .....	34
3.1.5 Chemical Admixtures.....	34
3.1.6 Nano-Silica.....	35
3.1.7 Silica Fume.....	36

3.2	Particle Size Distribution .....	36
3.3	Mixture Proportioning.....	38
3.4	Particle Size Distributions of Cementitious Powder as Function of Nano-Silica Replacing a Portion of Cementitious Materials .....	45
3.5	Mixing Sequence.....	46
3.6	Experimental Program.....	48
3.6.1	Slump Flow, T <sub>50</sub> , and Dynamic Segregation (ASTM C1611).....	48
3.6.2	J-Ring Test (ASTM C1621).....	50
3.6.3	Compressive Strength (ASTM C39).....	52
3.6.4	Water Absorption (ASTM C642).....	53
3.6.5	Capillary Absorption (ASTM C1585) .....	55
3.6.6	Rapid Chloride Permeability Test (ASTM C1202) .....	59
3.6.7	Water Penetration (EN 12390).....	63
3.6.8	Chloride Diffusion (ASTM 1556).....	65
3.6.9	Rapid Migration Test (RMT- NT BUILD 492) .....	70
	Chapter 4 Results and Discussion .....	76
4.1	Nano-Silica Contained Concrete Test Results .....	76
4.1.1	Flow Properties .....	76
4.1.2	Compressive Strength .....	77
4.1.2.1	Compressive Strength of Studied Nano-Silica Contained SCCs at 28-, 90-, and 180-Day Curing Ages .....	78
4.1.3	Rapid Chloride Migration Test (RMT) .....	83
4.1.3.1	Rapid Migration of Studied SCCs at 28- and 90-Day Curing Ages.....	84
4.1.4	Water Penetration.....	88
4.1.4.1	Water Penetration of Studied Nano-Silica Contained SCCs at 28- and 90-Day Curing Ages.....	89
4.1.5	Capillary Absorption.....	93
4.1.5.1	Capillary Absorption of Studied Nano-Silica Contained SCCs at 28- and 90-Day Curing Ages .....	95
4.1.6	Water Absorption.....	100
4.1.6.1	Water Absorption after Immersion .....	101
4.1.6.2	Water Absorption after Immersion and Boiling of Studied Nano-Silica Contained SCCs at 28- and 90-day Curing Ages.....	103
4.1.6.3	Volume of Voids of Studied Nano-Silica Contained SCCs at 28- and 90-day Curing Ages .....	106
4.1.7	Rapid Chloride Permeability Test (RCPT) .....	108

4.1.7.1	Rapid Chloride Permeability of Studied Nano-Silica Contained SCCs at 28- and 90-Day Curing Ages .....	110
4.1.8	Chloride Diffusion Test.....	113
4.1.8.1	Chloride Diffusion of Studied SCCs at 28- and 90-Day Curing Ages .....	114
4.2	Comparison of Nano-Silica and Micro Silica Based Concretes .....	119
4.2.1	Flow Properties Comparison.....	119
4.2.2	Compressive Strengths Comparison .....	120
4.2.3	Rapid Migration Coefficients Comparison .....	122
4.2.4	Water Penetration Comparison .....	124
4.2.5	Chloride Diffusion Comparison.....	126
4.2.6	Differential Scanning Calorimetry and Thermogravimetric Analysis .....	129
4.3	Conclusions .....	134
Chapter 5 Correlations of Variables and Statistical Relationships.....		140
5.1	Linear Relationship between Compressive Strength and Transport Properties	140
5.2	Correlations between the Studied Tests .....	144
5.3	Classifications of Transport Properties of the Studied SCCs.....	154
5.4	Conclusions .....	158
Chapter 6 Conclusions and Recommendations .....		160
6.1	Conclusions .....	160
6.2	The Key Outcomes.....	165
6.3	Recommendations .....	167
Appendix A Conversion Factors .....		168
Appendix B Results of Individual Testing .....		169
Bibliography.....		177
Curriculum Vitae.....		189

## **List of Tables**

Table 2.1a: Summary of Past Studies on SCCs and Conventional Concretes Containing Nano and Micro Silica .....	15
Table 2.1b: Summary of Past Studies on SCCs and Conventional Concretes Containing Nano and Micro Silica .....	16
Table 2.1c: Summary of Past Studies on SCCs and Conventional Concretes Containing Nano and Micro Silica .....	17
Table 2.1d: Summary of Past Studies on SCCs and Conventional Concretes Containing Nano and Micro Silica .....	18
Table 2.1e: Summary of Past Studies on SCCs and Conventional Concretes Containing Nano and Micro Silica .....	19
Table 2.1f: Summary of Past Studies on SCCs and Conventional Concretes Containing Nano and Micro Silica .....	20
Table 3.1: Sieve Analysis and Material Finer than No.200 Sieve (ASTM Designation C117 and C136) .....	30
Table 3.2: Specific Gravity and Absorption of Fine Aggregate (ASTM C 128).....	30
Table 3.3: Deleterious Substances .....	31
Table 3.4: Alkali-Silica Reactions .....	31
Table 3.5: Physical Properties of Type V Cement (ASTM C150-09).....	32
Table 3.6: Chemical Properties of Type V Cement (ASTM C150-09) .....	32
Table 3.7: Optimum Requirements (ASTM C150-09) .....	33
Table 3.8: Fly Ash Properties (ASTM C 618/AASHTO M 295 Testing of Fly Ash) .....	34
Table 3.9: Chemical Admixture Specifications .....	35

Table 3.10: Properties of Porous Silicon Oxide Nano Particles .....	35
Table 3.11: Chemical and Physical Properties of Undensified Silica Fume .....	36
Table 3.12: Coarse Aggregate Gradation.....	41
Table 3.13: Selected Coarse Aggregate Gradation by Weight .....	41
Table 3.14: Example Calculation of Workability and Coarseness Factors for 9:1 Coarse to Fine Ratio.....	42
Table 3.15: Workability and Coarseness Factors for Various Coarse to Fine Ratios.....	42
Table 3.16: Mixture Proportions and Constituents of Nano-Silica Contained SCCs .....	44
Table 3.17: Mixture Proportions and Constituents of Silica Fume Contained SCCs.....	44
Table 3.18: Visual Stability Index (VSI) of SCC Rating Criteria. ....	50
Table 3.19: Passing ability Rating .....	52
Table 3.20: Apparatus and Materials Needed for ASTM C642 .....	54
Table 3.21: Apparatus and Materials Required for Capillary Absorption Test.....	56
Table 3.22: RCPT Ratings (Per ASTM C1202) .....	61
Table 3.23: Apparatus and Materials Required for RCPT Test.....	61
Table 3.24: Apparatus and Materials Required for Water Penetration Test.....	64
Table 3.25: Apparatus and Materials Required for Chloride Diffusion Test .....	66
Table 3.26: Apparatus and Materials Required for Rapid Migration Test .....	71
Table 3.27: Test Voltage and Duration for Concrete Specimens (NT BUILD 492) .....	74
Table 4.1: Flow Properties of Self-Consolidating Concretes .....	76
Table 4.2: Average Compressive Strength Comparison of SCCs (MPa) .....	79
Table 4.3: Percent Increase in Compressive Strength between Nano-Silica and Control SCCs.. .....	80

Table 4.4: Rapid Migration Coefficients ( $m^2/s \times 10^{-12}$ ).....	85
Table 4.5: 28- and 90-Day Average Water Penetration Depths (mm) of Studied SCCs..	90
Table 4.6: Primary Capillary Absorption of Studied SCCs ( $\times 10^{-5} mm/s^{0.5}$ ) .....	95
Table 4.7: Secondary Capillary Absorption of Studied SCCs ( $\times 10^{-5} mm/s^{0.5}$ ) .....	96
Table 4.8: Average Percentage Absorption after Immersion of Studied SCCs.....	101
Table 4.9 Average Percentage Absorption after Immersion and Boiling of Studied SCCs.....	104
Table 4.10: Percentage Volume of Permeable Pore Space, Voids .....	106
Table 4.11: Total Charge Passed through Studied SCC Specimens (Coulombs).....	110
Table 4.12: Average Chloride Content Measured at Selected Depths of Studied SCCs (gram).....	115
Table 4.13: Percent Reduction from Curing Ages and Control SCC .....	116
Table 4.14: Flow Properties Comparison of Nano-Silica and Silica Fume Contained SCCs.....	119
Table 4.15: Compressive Strength Comparison of Nano and Micro Silica Contained SCCs (MPa).....	120
Table 4.16: Rapid Migration Coefficient Comparison of Nano and Micro Silica Contained SCCs ( $m^2/s \times 10^{-12}$ ) .....	122
Table 4.17: Water Penetration Depth Comparison of Nano and Micro Silica Contained SCCs (mm) .....	124
Table 4.18: 28-Day Chloride Content (%) Comparison of Nano and Micro Silica Contained SCCs at Selected Depths .....	126
Table 4.19: 180-Day Nano-Silica and 90-Day Silica Fume	

Chloride Content (%) Comparison at Selected Depths.....	127
4.20: Percent Difference in Chloride Content at Selected Depths from Micro to Nano-Silica Contained SCCs .....	127
Table 4.21: Constituents of Nano and Micro Silica Contained Samples Used for TGA Test.....	130
Table 5.1: Correlation for Explanatory Variables.....	142
Table 5.2: Derived Equations from Multiple Regression Analysis of Nano-Silica Contained SCCs.....	142
Table 5.3: Summary of Regression Analyses of Selected Tests.....	143
Table 5.4: Correlation between the Studied Tests for 28-Day Cured Nano-Silica Contained SCCs .....	145
Table 5.5: Correlation between the Studied Tests for 90-Day Cured Nano-Silica Contained SCCs. ....	145
Table 5.6: Properties of Concrete Matrix, Transport Properties, and Deterioration Processes Caused by the Transport Processes .....	155
Table 5.7: Rapid Chloride Permeability Range of Chloride Ion Penetrability Based on Charge Passed.....	156
Table 5.8: Chloride Ingress Resistance Criteria Based on Rapid Migration Coefficients .....	156
Table 5.9: Durability Classification Based on Apparent Volume of Permeable Voids..	156
Table 5.10: Nano-Silica Contained SCC Classification .....	157

## List of Figures

Figure 1.1: Excess Paste Theory (Douglas, 2004).....	8
Figure 3.1: Particle Size Distribution Comparison of SCCs Constituents.....	37
Figure 3.2: Coarseness and Workability Factors versus Coarse to Fine Ratios .....	43
Figure 3.3: HRWRA Dosage Comparison of Nano and Micro Silica Contained SCCs ..	45
Figure 3.4: Particle Size Distributions of Cementitious Powder as Function of Nano-Silica Replacing a Portion of Cementitious Materials .....	46
Figure 3.5: Arrangement of Slump Flow Test .....	48
Figure 3.6: Schematic of J-ring Test for Concrete (Boukendakdji et al., 2009).....	51
Figure 3.7: Concrete Cylinder Experiencing Axial Load .....	53
Figure 3.8: Schematic of the Capillary Absorption Test Setup .....	57
Figure 3.9: Schematic of RCPT Test Setup (ACI) .....	60
Figure 3.10: Actual Setup of RCPT Test.....	60
Figure 3.11: Concrete Water Penetration Testing Apparatus .....	64
Figure 3.12: Profile of Penetrated Water through Concrete Cubes .....	65
Figure 3.13: Test Arrangement of Rapid Migration Test .....	72
Figure 3.14: Rapid Migration Test Setup .....	72
Figure 3.15: Chloride Penetration Depth after Applying Silver Nitrate to the Freshly Split Sections .....	74
Figure 4.1: Average Compressive Strength Comparison of Studied SCCs.....	79
Figure 4.2: Rapid Migration Coefficients of Studied SCCs .....	85
Figure 4.3: Water Penetration Depth of All Concretes.....	90
Figure 4.4: Primary Capillary Absorption of Studied SCCs (28-Day Curing Age) .....	97



Figure 4.5: Primary Capillary Absorption of Studied SCCs (90-Day Curing Age) .....	97
Figure 4.6: Secondary Capillary Absorption of Studied SCCs (28-Day Curing Age) .....	98
Figure 4.7: Secondary Capillary Absorption of Studied SCCs (90-Day Curing Age) .....	98
Figure 4.8: Percentage Absorption after Immersion in Water of Studied SCCs. ....	102
Figure 4.9: Percentage Absorption after Immersion and Boiling in Water of Studied SCCs.....	104
Figure 4.10: Percentage of Voids in Studied SCCs .....	107
Figure 4.11: Charges Passed through Studied SCCs .....	111
Figure 4.12: Chloride Content of 28-Day Studied SCCs after 35 Days in Salt bath.....	117
Figure 4.13: Chloride Content of 180-Day Studied SCCs after 60 Days in Salt bath....	117
Figure 4.14: Compressive Strength Comparison of NS and SF Contained SCCs.....	121
Figure 4.15: Rapid Migration Coefficient Comparison of NS and SF Contained Concretes .....	123
Figure 4.16: Water Penetration Depth Comparison of NS and SF Studied SCCs.....	125
Figure 4.17: Chloride Content of 28-Day Studied Nano and Micro Silica Contained SCCs.....	128
Figure 4.18: Chloride Content of 180-Day Studied Nano-Silica and 90-Day Micro Silica Contained SCCs .....	128
Figure 4.19: Nano-Silica TGA/DSC Test Result (TG Scale in %). ....	131
Figure 4.20: Nano-Silica TGA/DSC Test Result (TG Scale in mg) .....	131
Figure 4.21: Silica Fume TGA/DSC Test Result (TG Scale in %) .....	132
Figure 4.22: Silica Fume TGA/DSC Test Result (TG Scale in mg).....	132

Figure 5.1: Correlation between Secondary Capillary Absorption and Rapid Chloride Coefficients of 28- and 90-Day Cured Nano-Silica Contained SCCs .....	146
Figure 5.2: Correlation between Secondary Capillary Absorption and Percent Volume of Voids of 28- and 90-Day Cured Nano-Silica Contained SCCs .....	147
Figure 5.3: Correlation between Secondary Capillary Absorption and Water Penetration Depths of 28- and 90-Day Cured Nano-Silica Contained SCCs .....	148
Figure 5.4: Correlation between Water Penetration Depths and Rapid Migration Coefficients of 28- and 90-Day Cured Nano-Silica Contained SCCs .....	149
Figure 5.5: Correlation between Compressive Strength and Rapid Chloride Permeability of 28- and 90-Day Cured Nano-Silica Contained SCCs.....	150
Figure 5.6: Correlation between Compressive Strength and Rapid Migration of 28- and 90-Day Cured Nano-Silica Contained SCCs .....	151
Figure 5.7: Correlation between Compressive Strength and Water Penetration Depth of 28- and 90-Day Cured Nano-Silica Contained SCCs.....	152
Figure 5.8: Correlation between Compressive Strength and Percent Volume of Voids of 28- and 90-Day Cured Nano-Silica Contained SCCs.....	153
Figure 5.9: Correlation between Compressive Strength and Secondary Capillary Absorption of 28- and 90-Day Cured Nano-Silica Contained SCCs.....	154

## **Chapter 1**

### **Introduction**

#### *Research Significance and Objectives*

The increase in convolution of construction and complex reinforcement design of modern age concrete structure, have increased the demanded of self-consolidating concrete (SCC). In recent years, the concrete mixture design has emphasized on not only compressive strength, but also flow-ability where access is hindered in narrow gaps of formworks. For this reason, self-consolidating concrete has captured significant attention. Use of nano-silica in concrete matrix, particularly in self-consolidating concrete, is among the most advanced technologies to break into concrete design field. Nano-sized particles improve the strength bearing crystals of cement pastes. Nano-level materials have diverted researcher's directions in the building materials. Nano-level has been claimed to be a need and have strong potential for the future.

Awareness of self-consolidating concrete has spread across the world; however, concerns with poor consolidation and transport properties of SCC remain unanswered. It is believed that addition of nano-particle materials such as nano-silica can enhance the mechanical, transport, and rheological properties of SCC.

The main objectives of this research were the following:

- Investigate the state of the art regarding the influence of addition of nano-silica and silica fume on the mechanical and transport performances of fresh and hardened self-consolidating concrete.
- Investigate the state of the art regarding methods of measuring transport properties of self-consolidating concrete.

- Investigate the distinctions in transport properties of self-consolidating concrete containing nano-silica and silica fume particles.

## **1. Introduction**

Self-consolidating concrete (SCC) in fresh state is well recognized for its ability to be placed without vibration or compaction. High deformability and resistance to segregation are among the most known characteristics of this type of concrete. This type of concrete is often used in congested reinforced structures where casting is difficult. In general, the materials used in production of SCC are the same as those used for conventional concrete except for the additives. High content of powders combined with incorporation of superplasticizer make this type of concrete distinctive from conventional concrete. Moreover, Filling ability, passing ability, and resistance to segregation are the key fresh properties of any SCC.

Properties of concrete that have a direct relation to transportation of ions into concrete are called transport properties. In all concrete deteriorative processes, external ions are transported through concrete pores by means of migration, diffusion, permeation, or penetration; these ions modify concrete's chemical and physical characteristics. Instances of these deteriorative processes are sulfate attack and corrosion of reinforcements in concrete. Hence, it is essential to understand these ions, their movements, and mechanisms of their attacks.

This study examines the transport properties of SCCs containing nano-silica particles as a partial replacement of ordinary Portland cement (OPC). It is believed that incorporation of fine additives, such as nano-silica, enhances the transport properties of SCC. For this reason, transport properties of SCCs containing nano-silica are compared

to the control SCCs, which are SCCs without additives, and to SCCs that contain micro silica.

### **1.1 Self-Consolidating Concrete**

The increase in convolution of construction and complex reinforcement design of modern age concrete structures have increased the demand for SCC. In recent years, concrete mixture design has emphasized not only on strength but also on flowability where access is hindered in narrow gaps of formworks. For this reason, SCC has captured significant attention. Self-consolidating concrete is known as a high performance concrete, which is very deformable in fresh states and very resistance to segregation. It is well-known that SCC does not require vibration in order to be placed. In reality, SCC can be compacted and placed under its own weight.

Self-consolidating concrete is distinguished from conventional concrete by three characteristics namely; appropriate flowability, non-segregation, and no blocking tendency. In general, the materials used for SCC are the same as those used for conventional concrete such as cement, aggregates, and water, yet the additives are different. The most common difference between SCC and conventional concrete is higher superplasticizer dosage combined with a relatively high powder content (powder being materials with particles less than 0.125 mm) such as Portland cement, mineral additives, ground filler or very fine sands, and lower coarse aggregate content (Domone, 2006). Desirable powder content for initial testing is 385.45 to 474.4 kg/m<sup>3</sup> (650 to 800 lb/ft<sup>3</sup>).

Self-consolidating concrete is mostly well-known for its flowability and stability. The high flowability of SCC is achieved by incorporating high-range-water-reducing admixtures (HRWRA) instead of using excess water. Stability of SCC refers to its

resistance to bleeding and segregation. Stability of SCC is achieved by increasing fine component of matrix or by using admixtures. One way to increase the fine content is to increase cementitious material content. In general, SCC mixtures have a higher paste volume. The ratio of fine aggregate to coarse aggregate in these mixtures is higher than that of conventional concrete (National Ready Mix Concrete Association, 2004).

Mixture proportioning plays a crucial role in achieving desired fluidity and cohesiveness of SCC. To ensure fluidity, coarse aggregate content needs to be low enough in order to be lubricated by layer of mortar paste (Domone, 2006). Limiting the fine aggregate and water/powder ratio, adding superplasticizer and viscosity modifying agent (VMA) all assist the mortar to obtain adequate fluidity and viscosity (Domone, 2006).

## **1.2 History**

During 1960s to 1970s, Professor Hajime Okamura at Kochi University of Technology proposed the concept of SCC in Japan. He predicted the need for workable concrete, which did not require any compaction as a solution to the growing concrete durability concerns of the Japanese government. The demand for this type of concrete began when many defects in concrete were found due to quick construction, which resulted in high water to cement ratio and poor compaction. To make durable concrete structures, sufficient compaction by skilled workers was required. However, reduction in numbers of skilled workers and human error in compaction of concrete resulted in reduction in quality of construction work. Okamura realized that the main reason for the poor durability performance of concrete in structures was the insufficient consolidation of the concrete in casting stage (Goodier, 2003).

The first SCC prototype was used in 1988 in Japan. Following the Japanese prototype, European researches and development into SCC first began in the middle of 1990's where it was used for civil works in transportation projects in Sweden. European countries, however, focused on addition of inert materials such as limestone to increase plastic viscosity of SCC to eliminate the use of VMA. Development of SCC spread quickly from Sweden to other Scandinavian countries. North Americans expanded the use of inert material and designed SCC with large silica fume composite in several projects in the late 1989's (Goodier, 2003). Presently, the use of SCC in both concrete field and institutional research projects is well-spread in Japan and European countries more than any other places in the world due to their advances in concrete technology. Nowadays, East Asia and Pacific Conference on Structural Engineering and Construction (EASEC-2), American Concrete Institute (ACI), and many other institutions and organizations report on ongoing researches and investigations to make SCC a standard type of concrete.

### **1.3 Advantages and Disadvantages**

There are many advantages to use SCC, such as faster rate of placement, improved pumpability, improved surface finish, and shorter construction period, all of which lead to saving in labor and cost. Self-consolidating concrete also offers benefits for fabricators, ready-mix producers, and contractors. Some of these benefits are (Yang, 2004):

- “Reduction in vibration effort and noise generated during placement,
- Filling complex forms with limited accessibility,
- Uniformity in distribution in areas of closely grouped rebars,

- Rapid pumping,
- Uniform and compact surface,
- Aesthetics of flatwork,
- Faster placing with no mechanical vibration resulting in saving in overall placement cost,
- Shorter construction period, and
- Increase field safety by eliminating the need for consolidation.”

Even though SCC is accepted as a premium concrete for its special characteristics and suitability for complex designs, there are still obstacles in the way of its ever-increasing development and applications. Shortcomings of SCC are seen more in the field of construction, where it is used outside of workshops and research institutes. Segregation is one of the essential concerns associated with SCC. Detrimental effects of SCC to structures due to segregation are more of concern than conventional concrete. Some of the shortcomings of SCCs are:

- Segregation: Segregation of SCC is directly related to the coarse aggregate used in its production. For instance, frequency of aggregate contacts while SCC is being transported can increase the internal stress of SCC, which decreases fluidity especially in the case of large coarse aggregates. Sensitivity of SCC to water content, temperature, and moisture content are other disadvantages of SCC in industrial production (Azamirad and Beheshti zadeh, 2005).
- Self-compatibility test is very difficult to be performed for entire volume of ready-mixed SCC. In addition, it is very difficult to use SCC for economic



reasons due to incorporation of high cementitious materials, different superplasticizers, fillers, and some new and rare materials such as nano-silica.

- Careless protection and curing of SCC after placement can cause bleeding and plastic shrinkage cracking. Special attention must be given to coarse aggregate content, paste fraction, powder content, fine aggregate, water content, water to cement ratio, and air content while designing SCC to prevent possible segregation, and excessive creep and shrinkage.
- Higher drying shrinkage is another potential shortcoming of SCCs. Due to high cement fineness and content, higher drying shrinkage is expected for SCCs. The aggregates used in SCCs act to restrain the shrinkage of cement paste. Hence, SCCs with lower aggregate content have higher shrinkage than those with higher aggregate content. In addition, higher water/cement ratio produced greater drying shrinkage.
- Autogeneous shrinkage is another potential disadvantage of SCCs due to high cement content, which is greatly affected by water/cement ratio and incorporation of mineral fillers. The higher the water/cement ratio, the lower the autogeneous shrinkage would be.
- More strict requirements in selection, measuring, and monitoring of materials used for SCCs is another disadvantage of SCCs.

#### **1.4 Fresh Properties of SCC**

All of the aforementioned advantages of SCC are directly related to its fresh and hardened properties. Fresh state properties can be categorized in three groups: 1) filling ability, 2) passing ability, and 3) stability

### **1.4.1 Filling Ability/ Flowability**

Filling ability is the ability of concrete to flow smoothly and fill all spaces in formwork without any external compaction or vibration. Flowability is best described by concretes' fluidity and cohesion and can be evaluated by the slump flow test. According to a theory by C.T. Kennedy called 'Excess Paste Theory,' workability of concrete is achieved if and only if there is enough paste to cover the surface area of aggregates (Figure. 1). The excess paste serves to minimize the friction among the aggregates to offer better flowability (Douglas, 2004). Flowability cannot be achieved if there is no paste layer. Without paste layer, excessive friction between aggregates could diminish flowability.

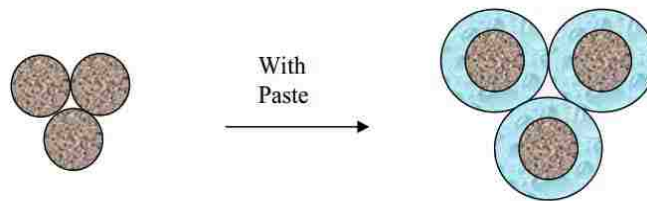


Figure 1.1 Excess Paste Theory (Douglas, 2004)

The V-funnel and slump tests are the most common tests to examine this property of concrete. The V-funnel determines the filling ability of concrete under confined flow, whereas slump test is used to determine flowability of concrete under unconfined flow.

#### ***1.4.2 Passing Ability***

This is the ability of concrete mix to flow through limited spaces without blocking. Aggregate size and volume play a significant role in passing ability of SCCs. The L-Box test is the most common test to examine this property (Douglas, 2004). The blockage occurs as the distance between coarse aggregates decreases. Therefore, it is recommended that the aggregate content be decreased to avoid blockage. Shear stress is another phenomenon that occurs due to relative displacement from the change in aggregate location. Hence, shear stress must be minimized for concrete to flow smoother (Douglas, 2004). Lastly, segregation should be prevented by increasing high paste viscosity to prevent blockage.

#### ***1.4.3 Stability***

This unique property assures that there is sufficient uniformity and cohesion in concrete mix throughout the entire construction process. To assure the stability of concrete mix, there should be minimum, if possible no segregation and bleeding. Some bleeding is normal for SCC, but excessive bleeding can cause reduction in strength (Douglas, 2004). Stability is directly related to viscosity and cohesiveness of concrete. Viscosity can be increased by reduction in free water content and increase in fine aggregate content. There are two mixture proportioning methods to ensure adequate stability: 1) low water-to-cement ratio (w/c) and high content of fines, and 2) incorporating viscosity modifying admixture (VMA). The suggested tests to evaluate segregation resistance are column segregation test, electrical conductivity test, penetration tests, flow test, and sieve stability test.

## **1.5 Transport Properties of SCC**

In addition to fresh and hardened properties of SCC, transport property is among the most decisive properties when studying SCC. Deterioration of concrete structural members is a result of many different processes such as transport of ions to concrete. In all of the deteriorative processes, harmful ions are transported through concrete. Thus, transport properties of concrete are essential to better understand and improve the durability of concrete structures. Transport properties of SCC are mostly affected by pore structures of the paste and the paste volume. Low water/cementitious (w/cm) ratio and water content can assist in optimum pore formation. Supplementary cementitious materials can also improve the pore structure of concrete. Additionally, increase in hydration of cementitious materials can decrease the permeability and diffusivity. Damages to SCCs may also be caused by water or chemical dissolved in water. An example of these chemicals is sodium chloride (NaCl) which dissociates into  $\text{Na}^+$  and  $\text{Cl}^-$  (Claisse, 2005).

Some of the important transport properties of concrete are diffusion, electro-migration, thermal migration, pressure driven flow, and absorption. The transport properties studied in this research are introduced below.

### ***1.5.1 Water Permeability***

This property of concrete measures how fast a fluid (in this case water) can flow through concrete under air pressure. An application of this property can be found in dams where there is an external water pressure. This mode of transport is feasible for concrete members in contact with liquid under a pressure head. It is proven that permeability of concrete can vary from  $10^{-16}$  to  $10^{-10}$  m/s (Claisse, 2005). The permeability of concrete

depends on the pore structure and the viscosity of the liquids or gases (Claisse, 2005). The water permeability is used to examine the pore structure and continuity of pores in concretes.

### **1.5.2 Diffusion**

In this process, ions can penetrate into saturated concrete without help of water. When a strong solution becomes in contact with a weak solution, they will both tend to reach towards the same concentration. The chloride ion transport studied for this research refers to movement of chloride ions under a concentration gradient in two cells separated by a concrete specimen. This mode of transport takes place only in fully saturated media. Ultimately, diffusion coefficient is determined from the difference in concentration of chloride ions. Pore structure and chloride binding capacity of concretes are the two main findings of this test method.

### **1.5.3 Capillary Suction**

This phenomenon occurs in fine voids of concrete with wetting surfaces and is caused by surface tension. In general, concrete with finer pore structures encounters greater capillary suction pressures. On the other hand, concretes with fewer pores experience lower capillary suction. This property of concrete is greatly influenced by the viscosity, density, and surface tension of the liquid and the pore structure and surface energy of the concrete (Cement and Aggregate Concrete Australia, 2009). In this important mechanism, water can be taken up by capillary forces in non-saturated concrete. A non-steady state of transport occurs when concrete is not in permanent contact with a liquid such as in the tidal zone. In this state, the absorbed liquid at the surface and transported liquid at any distance from the surface is a function of time.

However, a steady state occurs when all suitable boundary conditions are kept constant over time, such as when a concrete member is in contact with water at all the time (Cement and Aggregate Concrete Australia, 2009).

#### **1.5.4 Absorption**

An exposed concrete undergoes wetting and drying cycles. Concrete has a tendency of absorbing water while in wetting process. Absorption is generally used to determine the amount of water absorbed under specified conditions. It must be noted that water absorption mechanism is different from water capillary absorption of concrete. Water absorption indicates the degree of porosity of material (Siddique, 2013). In majority of concrete researches, dried specimens are completely immersed in water at room temperature for 3 days and the amount of water absorbed per unit initial mass in percentage is noted. Other parameters can be determined through absorption characteristic of concrete such as percent volume of voids, absorption percentage after immersion, absorption percentage after boiling, and absorption percentage after suspension in water.

#### **1.5.5 Migration**

Migration refers to transport of ions in electrolytes under electrical force. In an electrical field, positive ions tend to migrate toward negative ions and vice versa. This mechanism may generate a difference in concentration in a homogeneous solution or may provoke a species flux in the direction of concentration gradients (Cement and Aggregate Concrete Australia, 2009). Rapid chloride permeability and rapid migration are the two well-known test methods utilized to measure and monitor migration of ions through SCC specimens. Rapid migration test indicates the quality of pore structure and pores

connectivity, whereas rapid chloride permeability test deals with the quality of pore solution.

### **1.6 Mixture Proportioning Design of SCC**

Mixture design is the process of determining required characteristics of concrete. Desirable workability, durability, and strength are among the decisive factors when designing a concrete mixture. Economy is another factor that needs to be considered in mixture proportioning of concrete. The selected materials should be available locally. The first step in designing a concrete mixture is to determine the water-to-cement ratio (w/c) ratio. Among concrete properties, compressive strength and durability are most related to water/cement ratio. Afterward, the quantities of air, water, cement, coarse and fine aggregates, and admixtures can be determined. However, when designing for SCCs' water/cementitious ratio, aggregates with higher passingability and mortar/paste ratio should be considered. A mixture design method by Okamura and Ouchi; that concentrates on fixed coarse and fine aggregates percentage as a function of total aggregate volume, as well as adjusting the water/powder ratio and superplasticizer dosage; is listed below (Okamura and Ouchi, 2003):

- Coarse aggregate content is fixed at 50% of the solid volume,
- The fine aggregate content is fixed at 40% of the mortar volume,
- The water-to-powder ratio is assumed 0.9 to 1.0 by volume, and
- The superplasticizer dosage and the final water/powder ratio need to be determined by keeping other aforementioned factors constant.

American Concrete Institute (ACI) has also provided a series of procedures for SCC mixture design that is listed below:

- The slump flow performance is determined. The slump flow must range from 18 to 30 in., depending on the application of SCCs (ACI 237, 2007).
- Coarse aggregates are selected and quantified (coarse aggregate content must be remained at 28% to 32% range). Additionally, for 1/2 in. and larger nominal maximum size of coarse aggregates, the bulk density of the coarse aggregate is first determined and 50% of the total concrete volume is filled with that bulk volume of coarse aggregate. On the other hand, for coarse aggregates smaller than 1/2 in., an initial proportion of 50% fine aggregate and 50% coarse aggregate by volume is the starting point for the first trial batch.
- Required water content and cementitious materials are determined,
- Paste and mortar volume are calculated (paste volume needs to be between 34% to 40%, whereas mortar volume is kept at 68% to 72% range),
- Proper type of admixture is selected,
- A trial mixture is batched,
- Workability, filling ability, passing ability, segregation, and bleeding of the mixture (J-ring, L-box, and column segregation test) are tested, and
- Mixture proportions are adjusted based on the first results and further testing is performed until the required fresh properties are achieved.



## Chapter 2

### Literature Review

The main objective of this chapter is to provide an overview of past studies related to transport properties and resulting durability of SCCs containing nano-silica or silica fume. Some of the major results, discussions, and conclusions of these studies are summarized in this chapter to better understand the nature of transport properties and characteristics of nano-silica or silica fume contained SCCs.

#### 2.1 Compressive Strength

Compressive strength is one of the major factors in determining durability of concretes. This hardened property of concrete is a well-known indication of internal pore structure of concretes. Several studies on strength properties of SCCs and conventional concretes containing nano materials and silica fume are presented in Tables 2.1a through 2.1f.

Table 2.1a: Summary of Past Studies on SCCs and Conventional Concretes Containing Nano and Micro Silica

Author(s), Year	Subject of the Study	Summary of Findings/Outcomes of the Study
Zhang and Li, 2004	Effect of nano-SiO <sub>2</sub> and nano-TiO <sub>2</sub> on strength properties of SCCs	Increase in nano-material content resulted in increase in strength. In addition, nano-TiO <sub>2</sub> contained concretes showed higher strengths than concretes containing nano-SiO <sub>2</sub> . Strength improvement was due to reduction in total specific pore volume and most probable pore diameter decrease, which resulted in a denser pore structure.
Li et al, 2004	Effects of nano-SiO <sub>2</sub> and nano-Fe <sub>2</sub> O <sub>3</sub> on microstructural properties of cement mortars	Nano-silica particles provided more profound effects in strength than micro silica particles. While increasing nano-silica content increased compressive strength of mortars, increasing nano-Fe <sub>2</sub> O <sub>3</sub> content did the contrary.

Table 2.1b: Summary of Past Studies on SCCs and Conventional Concretes Containing Nano and Micro Silica

Author(s), Year	Subject of the Study	Summary of Findings/Outcomes of the Study
Li, 2004	Comparison of hardened properties of high performance concretes containing nano-silica and high volume fly ash with concretes containing Portland cement and fly ash only	High-volume fly ash concrete containing nano-silica showed 81% higher compressive strength than high-volume fly ash concrete without nano-silica after 3 days of curing. After 2 years, the compressive strengths were 115.9 MPa and 108 MPa for high-volume fly ash concretes with and without nano-silica, respectively. The pozzolanic activity of the fly ash was greatly improved in the presence of nano-silica particles.
Li et al., 2006	Effect of nano-alumina on the mechanical properties of mortars	While there was not obvious improvement in compressive strength of mortars containing nano-alumina, elastic modulus of mortars considerably increased. This improvement was correlated to the filling ability of nano-alumina. Nano-alumina increased the density of ITZ, which effectively improved the modulus of elasticity.
Qing et al., 2007	Comparison of effects of nano-SiO <sub>2</sub> and silica fume on properties of hardened cement pastes	Addition of nano-SiO <sub>2</sub> produced a thicker cement paste. It also accelerated the cement hydration process. Additionally, compressive strengths of hardened cement paste increased with increasing nano-SiO <sub>2</sub> content, especially at early ages. By increasing the silica fume content, the strengths of hardened cement paste decreased slightly at early ages, but increased at later ages. In comparison with silica fume, nano-SiO <sub>2</sub> showed more effectiveness in consuming calcium hydroxide (CH) crystals, decreasing the orientation of CH crystals, reducing the size of CH crystals at interface, and improving interface structure.

Table 2.1c: Summary of Past Studies on SCCs and Conventional Concretes Containing Nano and Micro Silica

Author(s), Year	Subject of the Study	Summary of Findings/Outcomes of the Study
Jo et al., 2007	Comparison of nano-silica and silica fume effects on compressive strength and microstructure of cement mortars	Better performance in mortars containing nano-silica in comparison with control mortars containing silica fume was observed. Nano-SiO <sub>2</sub> behaved not only as a filler to improve mortar cement microstructure, but also as a promoter of pozzolanic reaction. A scanning electron microscopy (SEM) investigation showed that microstructure of the mixture containing nano-SiO <sub>2</sub> revealed a compact formation of hydration products and reduction in number of Ca(OH) <sub>2</sub> crystals.
Dolado et al., 2007	Effect of addition nano-silica to fly ash Belite cement pastes held in sulfate solution	Nano-silica addition resulted in a lower strength at the ages of 28 and 90 days and higher strength at the age of 180 days when compared to the pastes without nano-silica. The results were in contrary with the results obtained for ordinary Portland cement pastes.
Wang et al., 2007	Effect of nano-silica and on strength properties of SCCs	Compressive strengths of mortars with nano-silica were all higher than those mortars containing silica fume at 7 and 28 days. The strength of the mortars increased as the nano-silica content increased from 3% to 12%. The optimum nano-silica content for maximizing strength was 6% at the w/c ratio of 0.23.
Maghsoudi and Dahooei, 2007	Effect of nano-silica and silica fume on fresh and hardened properties of SCCs	Engineering properties of SCCs were not improved by adding nano-silica solely. However, micro silica showed promising improvement in engineering properties of SCC when added solely. Additionally, incorporation of both nano-silica and micro silica to the SCCs resulted in the best effects on the engineering properties of SCC. The binary SCCs showed improvement in compressive strength by 7% and 1% at 28 days and 7% and 4% at the 90 days.

Table 2.1d: Summary of Past Studies on SCCs and Conventional Concretes Containing Nano and Micro Silica

Author(s), Year	Subject of the Study	Summary of Findings/Outcomes of the Study
Naji Givi et al., 2012	Influence of two different sizes of nano-silica (15 nm and 80 nm) on the mechanical properties of concrete	All of the concretes containing nano-silica gained higher compressive and flexural strengths than control concretes. It was found that concretes containing 15 nm nano-silica powders showed higher early age strengths (7 days) than the concretes containing 80 nm nano-silica powders. However, final strengths (90 days) showed an opposite behavior.
Sneff et al., 2010	Effect of nano-silica and silica fume on rheological properties and compressive strength of mortars	The results revealed that 3.5% nano-silica replacement improved compressive strength, water absorption, and apparent porosity of mortars. Although using nano-silica increased the compressive strength, high level replacement (i.e. 7% nano-silica) decreased performance of mortars due to difficulty of molding. Similar negative trend was observed for mortars containing 20% silica fume.
Nazari and Riahi, 2010	Effects of nano-silica on the physical and mechanical properties of high strength compacting concrete	Four percent replacement was found to be the optimum level of replacement.
Oltulu and Sahin, 2011	Effect of various nano-particles (nano-SiO <sub>2</sub> , nano-Al <sub>2</sub> O <sub>3</sub> and nano-Fe <sub>2</sub> O <sub>3</sub> ) in single, binary and ternary combinations on the strength properties of cement mortars containing 5% silica fume	The best results for compressive strength were obtained for 1.25% nano-Al <sub>2</sub> O <sub>3</sub> in alone use, 0.5% in binary combination of nano-SiO <sub>2</sub> and nano-Al <sub>2</sub> O <sub>3</sub> , and 0.5% in ternary combination. Nano-silica contained mortars showed 58-66% increase for 180-day strength, while nano-Al <sub>2</sub> O <sub>3</sub> and nano-Fe <sub>2</sub> O <sub>3</sub> contained samples displayed 64-71% and 93-96% increase, respectively. The authors concluded that most of the improvements in the mechanical and physical properties of mortars were due to pozzolanic activity rather than the filler effect.

Table 2.1e: Summary of Past Studies on SCCs and Conventional Concretes Containing Nano and Micro Silica

Author(s), Year	Subject of the Study	Summary of Findings/Outcomes of the Study
Querica et al., 2012	Influence of two kinds of amorphous nano-silica (fumed powder silica and precipitated silica in colloidal suspension) on mechanical properties of SCCs	Colloidal nano-silica was more reactive at early age that improved all mechanical properties of SCCs. The 28 and 90-day compressive strengths of SCCs containing colloidal nano-silica were nearly identical.
Uysal et al., 2012	Effect of Limestone powder, fly ash, granulated blast furnace slag, basalt powder, and marble powder on engineering properties of SCC	The highest compressive strength obtained by addition of marble powders. The 7-day compressive strengths of control SCCs were higher than the rest of SCCs containing mineral admixtures. This indicated that there was not sufficient pozzolanic reactivity by none of the mineral admixtures. On the other hand, the 28-day compressive strength of all SCCs were higher than of the control SCCs and among all mineral admixtures granulated blast furnace slag achieved the highest strength. The improvement in strength of SCCs was due to filling ability of mineral admixtures and well-dispersed cement grains.
Said et al., 2012	Effects of colloidal nano-SiO <sub>2</sub> on concretes containing ordinary cement and concretes containing ordinary cement in addition to Class F fly ash	The mixtures containing nano-silica showed higher strengths at 28 days and continued to gain strength with a higher rate after 28 days. The compressive strength increased regardless of addition of fly ash. The authors concluded that the low rate of strength development of fly ash contained concretes could be controlled by addition of nano-silica. Enhancements were due to filling ability and pozzolanic effects of nano-silica, which improved the pore structure advantageously.

Table 2.1f: Summary of Past Studies on SCCs and Conventional Concretes Containing Nano and Micro Silica

Author(s), Year	Subject of the Study	Summary of Findings/Outcomes of the Study
Jalal et al., 2012	Study of mechanical, rheological, durability and microstructural properties of high performance SCC incorporating nano and micro silica	Two percent replacement of Portland cement by nano-silica in binary mixtures increased compressive strength of SCCs. On the other hand, micro silica contained concretes showed strength increase at older ages. Compressive strength increased by increases in binder content at all ages. The authors concluded that the increase in compressive and splitting tensile strengths was due to accelerated C-S-H gel formation as a result of increased crystalline Ca(OH) <sub>2</sub> at the early ages.
Zhang and Islam, 2012	Comparison of the effects of nano-silica and silica fume on strength development of pastes, mortars and concretes containing 50% fly ash or slag	Nano-silica showed more profound effect on the strength enhancement than the silica fume, especially at early ages. The results showed that 1% addition of nano-silica to fly ash mortars increased the strength by 61% and 25% for 1 and 3 days, respectively. On the other hand, 1% silica fume addition to fly ash mortars increased the strength by only 13% and 15% for 1 and 3 days.
Sabet et al., 2013	Study on mechanical and durability properties of high performance SSCs containing natural zeolite, silica fume and fly ash	28-day compressive strengths of all SCCs ranged from 57-80.5 MPa while the 180-day compressive strength varied from 61 to 87 MPa. The highest 28-day compressive strength was obtained for the mix containing 20% fly ash and lowest compressive strength was achieved for the mix containing 20% natural zeolite.
Siddique, 2013	Influence of water/powder ratio on strength properties of SCCs containing coal fly ash and bottom ash	Compressive strength decreased with the increases of coal bottom fly ash content at all ages. The optimum fly ash percentage replacement to obtain the maximum strength was 25 to 35% and bottom ash optimal replacement percentage was up to 20%.

## 2.2 Water Absorption (Permeability)

Sneff et al. (Sneff et al., 2010) studied water absorption and apparent porosity of mortars previously described in section 2.1. Mortars containing 7% nano-silica showed less water absorption and porosity than mortars without nano-silica. Mortars containing nano-silica had smaller densities due to high surface area of nano-SiO<sub>2</sub>.

Querica et al. (Querica et al., 2012) have also studied the permeable porosity of nano-silica contained SCCs. Detailed description of this investigation is given in section 2.1. The authors concluded that the water permeability of nano-silica contained SCCs did not improve significantly. The pore volume was not changed, but larger pores were subdivided into smaller ones for mixtures containing nano-SiO<sub>2</sub>. The microstructural analysis revealed that nano-silica addition produced a denser Interfacial Transition Zone (ITZ) and refined the microstructure. The enhancement of microstructure also improved mechanical properties.

Jalal et al. (Jalal et al., 2012) investigated the water absorption of concretes containing both nano and micro silica. Details related to this study are described in section 2.1. In this study, water absorption decreased in the samples containing 2% nano-silica, especially for binder content of 500 kg/m<sup>3</sup>. Combination of micro and nano-silica enhanced water impermeability of concrete specimens significantly.

Siddique (Siddique, 2013) studied water absorption and sorptivity of SCCs containing bottom ash. The author concluded that all SCC samples had low absorption (less than 10%). The water absorption of SCC samples varied from 5.8% to 7.1%. The results also showed that sorptivity increased with an increase in bottom ash content.

Sabet et al. (Sabet et al., 2013) in a study of high performance SCCs containing natural zeolite, silica fume and fly ash investigated water absorption of SCCs after 30 minutes and 72 hours, respectively. The results revealed that all SCCs had absorption of less than 5% and among all mineral admixtures, silica fume showed to be the most effective in reduction of final absorption. Replacement of 10 to 20% of Portland cement content with silica fume resulted in the highest reduction in water absorption of all studied SCCs.

### **2.3 Water Penetration**

Ji (Ji, 2005) studied the water permeability and microstructure of concretes containing fly ash and 3% nano-SiO<sub>2</sub>. Water permeability test showed lower water permeability and denser microstructure for concrete containing nano-silica when compared to the control concretes (concretes containing fly ash without nano-silica). The SEM images of fly ash contained concretes with and without nano-silica showed that fly ash particles were available in the binding paste matrix of control concretes at 28 days. In addition, great deal of hydration products (C–S–H) was available in concrete containing nano-SiO<sub>2</sub> only at 28 days. This observation revealed that the pozzolanic reactivity of fly ash was accelerated due to presence of nano-silica. Calcium hydroxide crystals existed in control concrete in the form of clusters, lapped and jointed together after 180 days, whereas the texture of hydrate products of nano-SiO<sub>2</sub> contained concretes was very dense and compact, and big crystals such as Ca(OH)<sub>2</sub> and ettringite disappeared.

The results of the water penetration test showed that the average penetration depth was 14.6 cm. The author correlated the improvements in properties of concretes containing nano-silica to the following mechanisms:



- A great deal of  $\text{Ca}(\text{OH})_2$  crystals was produced due to the hydration reaction between cement and water. Nano- $\text{SiO}_2$  had very high activity due to its very high specific surface area, so it reacted with  $\text{Ca}(\text{OH})_2$  crystals quickly and produced C–S–H gel which resulted in reduction of size and amount of the calcium hydroxide crystals. The C–S–H gel filled the voids to improve the density of the interfacial transition zone (ITZ) (Ji, 2005).
- The nano- $\text{SiO}_2$  particles filled the voids of C–S–H gel structure and made the binding paste matrix denser. In the C–S–H gel structure, nano- $\text{SiO}_2$  particles acted as a nucleus to tightly bond with C–S–H gel particles. Thus, the integration and stability of hydration product structure were improved and long-term mechanical properties and durability of concrete were enhanced (Ji, 2005).

Querica et al. (Querica et al., 2012) have also studied the water resistivity of nano-silica contained SCCs under water pressure. Detailed description of this investigation is given in section 2.1. The results of this study showed that all samples showed less than 30 mm of penetration depth, which is considered low permeability. The authors concluded that nano-silica contained SCCs have low effective water permeability due to less interconnected pores regardless of similar permeable porosity obtained from permeable porosity test. The same phenomenon was observed by Yogendran and Lengan in their investigation on high performance concrete containing silica fume.

#### **2.4 Rapid Chloride Permeability**

Zhang and Li (Zhang and Li, 2011) have studied the chloride permeability of concrete pavements containing nano-materials (nano- $\text{TiO}_2$  and nano- $\text{SiO}_2$ ). The addition of nano-particles improved the resistance to chloride penetration of concretes. The

authors concluded that the pore structure and resistance to chloride penetration of nano-TiO<sub>2</sub> contained concretes were higher than those containing nano-SiO<sub>2</sub>. The authors also believed that nano-particles in cement paste acted as kernel to further promote cement hydration due to their high pozzolanic activity. A comparison of pore structure of nano-SiO<sub>2</sub> with nano-TiO<sub>2</sub> showed that the pore structure of concrete containing nano-SiO<sub>2</sub> was coarser than that of concretes containing nano-TiO<sub>2</sub>. The authors believed that this was due to larger specific surface area of nano-SiO<sub>2</sub> particles. As a result, uniform dispersion of nano-SiO<sub>2</sub> particles was more difficult than that of nano-TiO<sub>2</sub> particles. In summary, nano-particles refined pore structure of concretes and acted as fillers to further enhance density and reduce porosity of concrete.

Querica et al. (Querica et al., 2012) studied the resistivity of two types of nano-silica contained SCCs (fumed powder silica and precipitated silica in colloidal suspension) to chloride migration. The SCCs with colloidal nano-silica showed the best performance due to their finer porosity and more precipitated C-S-H gel, which were able to decrease the movement of chloride ions into the SCC pore solution.

Uysal et al. (Uysal et al, 2012) investigated the chloride resistivity of SCCs mentioned in section 2.1 to chloride ingress. Among all SCCs, the mixtures that had pozzolanic admixtures such as fly ash and granulated blast furnace slag showed lower chloride ion permeability. This was due to development of discontinuous pore system resulted from pozzolanic reactivity. The authors believed that the chloride ion penetration also depended on the chloride binding capacity of constituent materials. Some of the penetrated chlorides may reacted with the cement compounds, mainly tricalciumaluminates (C<sub>3</sub>A), forming stable chlorocomplexes.

Said et al. (Said et al., 2012) investigated the resistivity of concretes containing nano and micro silica. A detailed description of this investigation is stated in section 2.1. Results obtained from rapid chloride permeability revealed that in most cases, the charges passing through concrete specimens decreased as dosage of nano-silica increased. The authors believed that the pore structure was refined by addition of nano-silica, which resulted in less conductivity of concretes. The charged passed through concretes containing nano-silica, silica fume did not differ significantly, and they both showed less than 1000 coulombs passing through.

Siddique (Siddique, 2013) examined the chloride resistivity of SCCs containing fly ash and bottom ash. Detailed description of this study is given in section 2.1. The author reported that fly ash decreased rapid chloride penetration due to its ability of transforming large pores to small pores. However, SCCs containing bottom ash showed higher coulomb charge with an increase in bottom ash content.

## **2.5 Capillary Absorption**

Capillary water absorption of concretes containing wollastonite and micro silica were investigated by Kumar and Kumar (Ransinchung et al., 2009). The replacement levels of cement by wollastonite were at a regular interval of 2.5% up to 30% and by micro silica at an interval of 2.5% up to 12.5%. This study showed that mixtures with 15% of wollastonite and 7.5% of micro silica admixed with cement reduced the pore spaces and refined the microstructure advantageously. It was concluded that the mineral admixtures affected the physical arrangement of aggregate surface system by acting as fillers. In addition, pozzolanic activities reduced the size of C-S-H crystals, which resulted in stronger interfacial zone. Lastly, the author concluded that concretes

containing pozzolans decreased pores size and their connectivity/continuity over a longer time period than concretes containing Portland cement.

The results of capillary water absorption test showed that water absorption percentage decreased as moist curing time increased from 3 to 365 days for all mixtures, which proved the fact that the permeable voids reduced with prolonged curing. Authors also concluded that secondary rate of absorption became closer to the initial rate of absorption with an increase in curing time.

Sonebi and Nanukuttan (Sonebi and Nanukuttan, 2009) studied the effect of various mineral and chemical admixtures on transport properties of SCCs. Limestone powder, pulverized fuel ash and VMA were used in SCCs. The results of this study showed that both mineral admixtures had great effect on reducing permeability of SCCs. However, SCCs made with VMA had a higher sorptivity, air and water permeability due to the higher water-to-cement ratio (w/c). In addition, SCCs containing limestone powder had a lower capillary absorption than the SCCs containing VMA due to the improvement of packing density of concrete. The authors concluded that water permeability and sorptivity of SCCs were greatly influenced by the size and type of pores. In the VMA contained SCCs, high water-to-binder ratio and low binder-to-coarse aggregates resulted in a higher porosity and poor ITZ area.

Capillary absorption of samples containing nano-SiO<sub>2</sub>, nano-Al<sub>2</sub>O<sub>3</sub> and nano-Fe<sub>2</sub>O<sub>3</sub> were examined by Oltulu and Sahin (Oltulu and Sahin, 2011). Different effects on capillary absorption were observed for different type of mineral additive. This study showed that addition of 0.5% and 1.25% nano-silica into fly ash contained mixtures decreased capillary absorption by 2% and 9%, respectively. In contrary, 2.5% addition of

nano-silica showed 20% increase in capillary absorption. Nano- $\text{Al}_2\text{O}_3$  contained mortars showed increased capillary absorption despite their improvement in compressive strength. Capillary absorption of 0.5% and 1.25% nano- $\text{Fe}_2\text{O}_3$  contained mortars decreased by 5% and 1%, respectively. However, an increase of 3% in capillary absorption was observed for 2.5% nano- $\text{Fe}_2\text{O}_3$  contained mortars.

Jalal et al. (Jalal et al., 2012) studied capillary absorption of concrete samples containing nano and micro silica. A description of this study is given in section 2.1. The authors found that the height of absorbed water decreased by an increase in the binder content from 400 to 500  $\text{kg/m}^3$ , and addition of micro and nano-silica admixtures. It was believed that this behavior was due to more packed and refined microstructure of concretes containing nano and micro silica.

## **2.6 Chloride Diffusion**

Sonebi and Nanukuttan (Sonebi and Nanukuttan, 2009) in a study examined the chloride diffusivity of SCCs containing limestone powder, pulverized fuel ash (PFA), and VMA. The results showed that chloride diffusivity was lower for mixtures with pulverized fuel ash (PFA) than other SCCs. The particle density in the matrix and the interfacial transition zone between aggregates and paste was enhanced in SCCs containing PFA. In addition, presence of aluminate phases and C-S-H formation filled pore spaces, resulting in reduction in chloride diffusivity.

## **2.7 Rapid Migration**

Edvardsen (Edvardsen, 1998) studied chloride migration on green concretes containing silica fume and fly ash. Concrete samples with fly ash replacement levels of 18% and 40% by cement weight were prepared. Additionally, one series of samples

containing ash originated from the combustion of sludge from a sewage plant replaced by ordinary fly ash were examined. The author concluded that the pore-blocking effect due to the pozzolanic reaction of fly ash was able to improve microstructure of concretes, which, in turn, reduced rapid migration of chloride ions through concrete specimens. It is believed that an increase in chloride binding capacity of concretes containing fly ash was another reason for high resistance of studied concrete specimens to chloride ingress.

## Chapter 3

### Materials and Testing Programs

#### 3.1 Materials

Special attention and care is required to achieve the unique properties of SCC. Material selection and preparation are among the special cares to prevent variation in material properties. Moisture content, gradation, and fines content of the aggregates are significant factors causing complexity during production of SCC and must be addressed to ensure consistent results. The raw materials used in SCC production and their physical and chemical characteristics are mentioned in the next sections.

##### 3.1.1 Aggregates

The selection of aggregates is important in order to meet certain specifications and standards proposed for SCC. Coarse aggregate size, shape and volume play a crucial role in performance of SCC. Generally, rounded coarse aggregates have a better filling ability as compared to crushed stones of a similar size. Fine aggregate and its gradation are also very important to have a homogenous concrete mixture. Both coarse and fine aggregates for this study were provided by a Southern Nevada quarry. The coarse aggregate conformed to the ASTM C33 size designation 7 and the fine aggregates were in accordance with ASTM C33.

Both fine and coarse aggregates were delivered in 55-gallon metallic drums. Liners were used to prevent moisture contact. Sample gradation was performed and the results showed that fine aggregate's gradation was consistent for all of the drums. On the other hand, gradation of coarse aggregates varied for different drums. Hence, to minimize influencing factors in mixing, such as variations in moisture content and gradation, coarse

aggregates were placed in horse troughs and air-dried and sieved into four different size categories: (1) aggregates greater than ½-in., (2) aggregates from 3/8 to ½-in., (3) aggregates from No. 4 sieve to 3/8-in., (4) and aggregates finer than No. 4 sieve. The moisture content of aggregates was monitored periodically and kept at 0.1% at all the times. The fine aggregates were also air-dried in horse troughs to achieve moisture content of 0.1% and then stored in 5-gallon containers inside the laboratory room at the temperature of  $21 \pm 2$  °C ( $70 \pm 3$  °F). Particle size distribution, physical and chemical properties of fine aggregates are presented in Tables 3.1 through 3.4.

Table 3.1: Sieve Analysis and Material Finer than No.200 Sieve (ASTM Designation C117 and C136)

Sieve Size	Mass Percent Passing	Range
3/8 in	100	100
#4	100	95 to 100
#8	95	80 to 100
#16	65	50 to 85
#30	43	25 to 60
#50	24	5 to 30
#100	9	0 to 10
#200	2.7	0 to 3

Table 3.2: Specific Gravity and Absorption of Fine Aggregate (ASTM C 128)

Relative Density (Specific Gravity) Oven-Dry	2.755
Relative Density (Specific Gravity) Saturated-Surface Dry	2.777
Apparent Relative Density (Apparent Specific Gravity)	2.818
Absorption (%)	0.81
Damp Loose Unit Weight ASTM C 29	85 pcf@1.5% moisture



Table 3.3: Deleterious Substances

	Results	Maximum Allowable
Organic Impurities (ASTM C40)	Less than Color Plate	Not Detrimental
Clay Lumps and Friable Particles (ASTM C142)	No.1	
Lightweight Particles (ASTM C123)	0%	3.00%
Soundness of Aggregates (ASTM C88)	0 Specific Gravity 2.0	0.30%
Sand Equivalent Value (ASTM D2419)	Sodium Sulfate 1.7%	
	Loss	10.00%
	93	NA

Table 3.4: Alkali-Silica Reactions

	Results	Maximum Allowable
Potential Alkali-Reactivity of Aggregate (Mortar Bar Method) ASTM C1260	0.06%	0.10%
Accelerated Detection of Potentially Deleterious Expansion of Mortar Bars Due to Alkali-Silica Reaction AASHTO T303	0.03%	0.10%

### 3.1.2 Portland Cement

Portland cement, as a key ingredient of SCC, should meet one of the following ASTM standards: ASTM C150, ASTM C595, or ASTM C1157. Type V Portland cement, which complied with ASTM C150, was used for this study. Type V Portland cement is well-known for its resistance to sulfate attack. Special care was taken to deliver the cement. It was placed in plastic bags and stored in sealed barrels. Twenty-four hours prior to use, it was transferred into 5-gallon sealed containers and placed in the laboratory room at temperature of  $21 \pm 2$  °C ( $70 \pm 3$  °F) for use. The chemical and physical properties and characteristics of the cement used for this study are presented in Tables 3.5 through 3.7

Table 3.5: Physical Properties of Type V Cement (ASTM C150-09)

Item	ASTM Test Method	Spec. Limit	Test Result
Air Content of Mortar (volume %)	C185	12 max	8
Fineness (cm <sup>2</sup> /g)			
Air Permeability	C204	2600 min	4160
Autoclave Expansion (%)	C151	0.80 max	0.02
Compressive Strength (psi)			
1 Day	C109	NA	2165
3 Day	C109	1160 min	3630
7 Day	C109	2180 min	4611
28 Day	C109	3050 min	None
Time of Setting (minutes) (Vicat)			
Initial: Not less than	C109	45	112
Initial: Not more than		375	

Table 3.6: Chemical Properties of Type V Cement (ASTM C150-09)

Compounds	ASTM Test Method	Spec. Limit	Test Results
SiO <sub>2</sub> (%)	C114	NA	20.33
Al <sub>2</sub> O <sub>3</sub> (%)	C114	6.0 max	4.1
Fe <sub>2</sub> O <sub>3</sub> (%)	C114	6.0 max	3.98
CaO (%)	C114	NA	63.34
MgO (%)	C114	6.0 max	2.25
SO <sub>3</sub> (%)	C114	A*	2.85
Loss on Ignition (%)	C114	3.0 max	2.33
Na <sub>2</sub> O (%)	C114	NA	0.05
K <sub>2</sub> O (%)	C114	NA	0.74
Insoluble Residue (%)	C114	0.75 max	0.3
CO <sub>2</sub> (%)	C114	NA	1.34
Limestone (%)	C114	5.0 max	3.2
CaCO <sub>3</sub> (%)		70 min	95
Potential Compounds (%)			
C <sub>3</sub> S	C114	NA	57
C <sub>2</sub> S	C114	NA	15
C <sub>3</sub> A	C114	5 max	4
C <sub>4</sub> AF	C114	NA	12
C <sub>4</sub> AF+2(C <sub>3</sub> A)	C114	25.0 max	20

A\*: C1038 expansion in water does not exceed 0.02% at 14 days

Table 3.7: Optimum Requirements (ASTM C150-09)

Chemical			
Item	ASTM Test Method	Spec. Limit	Test Result
C <sub>3</sub> S+C <sub>3</sub> A (%)	C114	None	61
Equivalent Alkalies (%)	C114	0.6	0.53
Physical			
False Set (%)			
Heat of Hydration (KJ/Kg)			
7 Days	C186	NA	None
Compressive Strength (psi)			
28 Days	C109	NA	None

### 3.1.3 Fly Ash

Class F fly ash used for this study conformed to the ASTM C618/AASHTO M295. It was provided by the same supplier of the cement. Liners were also used to seal the drums of fly ash for prevention of moisture entry and contamination. Twenty-four hours prior to use, fly ash was transferred into 5-gallon containers and stored in the laboratory room at temperature of  $21 \pm 2$  °C ( $70 \pm 3$  °F). The physical and chemical properties of the fly ash are presented in Table 3.8.

Table 3.8: Fly Ash Properties (ASTM C 618/AASHTO M 295 Testing of Fly Ash)

Chemical Compositions		ASTM/AASHTO Limits		ASTM Test Method
		Class F	Class C	
Silicon Dioxide (SiO <sub>2</sub> )	59.93			
Aluminum Oxide (Al <sub>2</sub> O <sub>3</sub> )	22.22			
Iron Oxide (Fe <sub>2</sub> O <sub>3</sub> )	5.16			
Total Constituents	87.31	70% min	50% min	D4326
Sulfur Trioxide (SO <sub>3</sub> )	0.38	5% max	5% max	D4326
Calcium Oxide (CaO)	4.67			D4326
Moisture	0.04	3% max	3% max	C311
Loss of Ignition	0.32	6% max	6% max	C311
		5% max	5% max	AASHTO M295
Total Alkalies, as Na <sub>2</sub> O	1.29	Not Required		C311
When required by purchaser		1.5% max	1.5% max	AASHTO M295
Physical Properties				
Fineness, % Retained on # 325	18.08	34% max	34% max	C311, C430
Strength Activity Index-7 or 28 Day Requirement				C311, C109
7day, % of Control	83	75% min	75% min	
28day, % of Control	79	75% min	75% min	
Water Requirement, % Control	97	105% max	105% max	
Autoclave Soundness	-0.02	0.8% max	0.8% max	C311, C151
Density	2.31			C604

### 3.1.4 Water

Tap water complying with the requirements of ACI 310 Specifications for Structural Concrete for Buildings was used throughout the entire experimental program.

### 3.1.5 Chemical Admixtures

A polycarboxylate-based high-range water-reducing admixture (HRWRA) was used to achieve the required flow properties for the studied SCCs. Its specifications satisfied the requirements of AASHTO M194 (Types A and F), ASTM C 494 (Types A

and F), and ASTM C1017. The admixture was stored in 5-gallon containers in the laboratory at room temperature of  $21 \pm 2$  °C ( $70 \pm 3$  °F) prior to use. The chemical properties of the HRWRA are presented in Table 3.9.

Table 3.9: Chemical Admixture Specifications

Designation	HRWRA
Chemical Type	Polycarboxylate Acid
Volatiles (%)	59.70%
Specific Gravity	1.09
pH	3 to 8
Water Reduction Range	up to 40%

### 3.1.6 Nano-Silica

It is believed that cement paste is composed of very small grains of hydrated calcium silicate gel, capillary pores, nano-sized pores, and large crystals of hydrated products. As a result, there is sufficient room for nano-silica particles to fill the pores in the cement paste (Jo et al., 2007). Amorphous type of nano-silica was used in this investigation. The chemical and physical properties of the nano-silica powder used in this investigation are presented in Table 3.10.

Table 3.10: Properties of Porous Silicon Oxide Nano Particles

Color	White
APS (nm)	15-20
Specific Surface Area (m <sup>2</sup> /g)	640
Porosity (mL/g)	0.6
Morphology	Porous and Nearly Spherical
Bulk Density (g/cm <sup>3</sup> )	0.08-0.10

### 3.1.7 Silica Fume

Silica fume, a very fine pozzolanic material, composed of amorphous silica produced by electric arc furnaces as a byproduct of the production of elemental silicon or ferrosilicon alloys, has been used in concrete since 1970. Silica fume is produced in accordance with the ASTM C 1240 specification and can be used in a variety of cementitious products such as concrete, grouts, mortars, and fiber cement products. An undensified type of silica fume was used in this study. The chemical and physical properties of the silica fume used in this investigation are summarized in Table 3.11.

Table 3.11: Chemical and Physical Properties of Undensified Silica Fume

Chemical Characteristics	
SiO <sub>2</sub> (%)	94.72
SO <sub>3</sub> (%)	0.23
CL (%)	0.11
Total Alkali (%)	0.49
Moisture Content (%)	0.27
Loss of Ignition (%)	2.82
pH	8.47
Physical Characteristics	
Color	Gray
% Retained on 45 um (%)	2.88
Density (specific gravity)	2.23
Bulk Density (kg/m <sup>3</sup> )	322.96
Specific Surface Area (m <sup>2</sup> /g)	22.65
Accelerated Pozzolanic Activity Index-with Portland Cement (%)	133.04

### 3.2 Particle Size Distribution

Particle size analysis of all SCCs constituent such as silica fume, nano-silica, Portland cement, and Class F fly ash was performed using Laser Diffraction Particle Size Analyzer. The results of this analysis are shown in Figure 3.1, which is focused on particle size less than 100 micrometers.

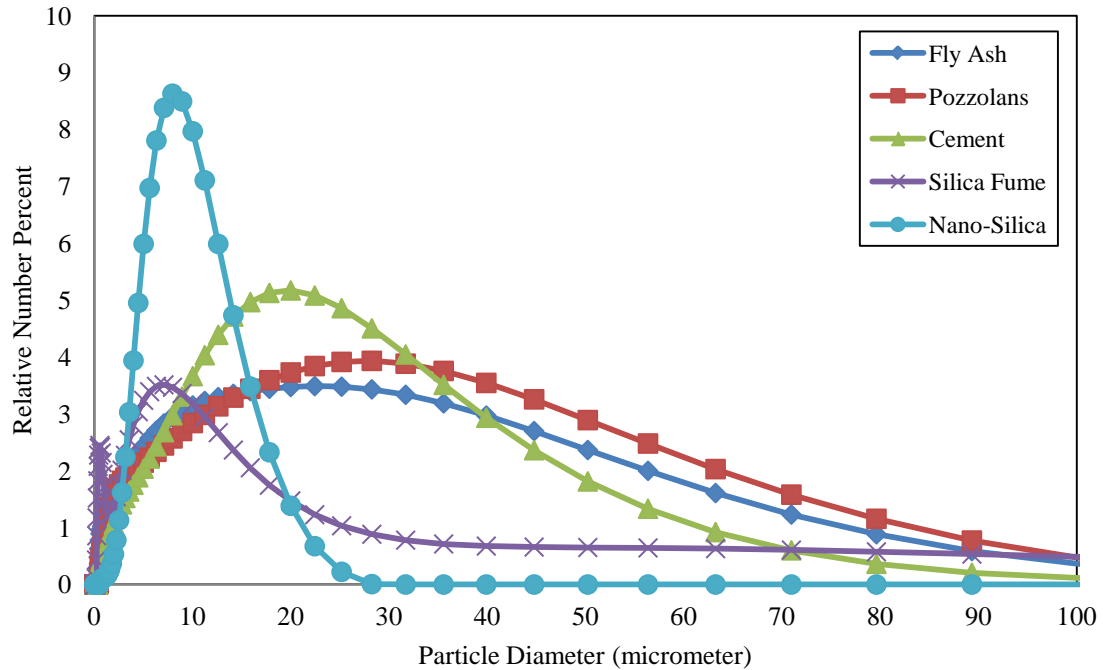


Figure 3.1: Particle Size Distribution Comparison of SCCs Constituents

Particle sizes of dry nano-silica varied from 15 to 20 nanometers, whereas only 2.88% of silica fume particle particles retained on 45-micrometer sieve. Although nano-silica particles were finer in the dry state, their surface area changed once they were blended with water for particle size distribution analysis. Particle size analysis showed that silica fume particles sizes were ranged from 0.2 to 502 micrometers, and amongst all of the constituents, higher size concentration was observed for nano-silica particle, which was within 3.17 to 20 micrometers interval. From particle size distribution analysis it can be concluded that although nano-silica particle sizes were the finest prior to blending for particle size distribution analysis purposes, silica fume covered a wider particle sizes range once blended. Blending of nano-silica particles with water prior to particle size

distribution analysis caused nano-silica particles lose their high surface area due to grain growth and agglomeration and concentrate within size interval of 17 to 20 micrometers.

### **3.3 Mixture Proportioning**

The mixture proportions used in this investigation were developed based on the required engineering properties and mixture economy of various SCCs using the raw materials described in the previous sections.

General considerations were taken to achieve the desired flow properties of the SCCs such as:

- Optimum coarse-to-fine aggregate ratio,
- Appropriate water-to-cementitious materials ratio ( $w/cm = 0.45$ ) to subside potential formation of autogeneous shrinkage. In general, autogenous shrinkage dominates when the  $w/cm$  ratio is below 0.40. The shrinkage becomes less dependent on cement content when a  $w/cm$  ratio higher than 0.4 is used,
- Minimum cementitious materials content,
- And optimum dosage of the HRWRA and VMA (if needed).

American Concrete Institute (ACI) has also provided a series of procedures for SCC mixture design, which is listed below:

- The slump flow performance is determined: the slump flow must range from 18 to 30 in. depending on the application of SCCs (ACI 237, 2007).
- Coarse aggregates are selected and quantified (coarse aggregate content must be remained at 28% to 32% of the volume of concrete). Additionally, for 1/2 in. and larger nominal maximum size of aggregates, the bulk density of the coarse aggregate is first determined and 50% of the total concrete volume is filled with



that bulk volume of coarse aggregate. On the other hand, for coarse aggregates smaller than 1/2 in., an initial proportion of 50% sand and 50% coarse aggregate by volume is a starting point for the first trial batch.

- Required water content and cementitious materials are determined,
- Paste and mortar volume are calculated (paste volume needs to be between 34% to 40%, whereas mortar volume is kept at 68% to 72% of total concrete volume),
- Proper types of admixtures are selected,
- A trial mixture is batched,
- Workability, filling ability, passing ability, segregation, and bleeding of the mixture (J-ring, L-box, and column segregation test) are tested, and
- Mixture proportions are adjusted based on the first results and further testing is performed until the desired/required fresh properties are achieved.

In accordance with the testing standards related to the target flow properties, the following target limits were utilized:

- Lower and upper limits slump flow: : 635 to 711 ± 25 mm (25 to 28 ± 1 inch)
- Visual Stability Index (VSI) : 0 to 1 (Highly stable to Stable)
- T<sub>50</sub> Time : 2 to 5 seconds
- J-ring value : SF – J-ring ≤ 50 mm (2.0 inches).

SCC is typically proportioned with relatively high cementitious materials content and chemical admixtures, leading to a relatively high material cost. To achieve the most economical matrices, the following items were considered:

- Use of minimum possible cement content without sacrificing the desired rheological properties,

- Use of secondary cementitious material to improve fresh properties and mixture economy,
- Use of minimum dosage of the combined admixtures to produce the intended flow properties.

A total number of 10 SCCs were designed with a constant water/cementitious materials ratio and coarse and fine aggregate contents. The total cementitious materials content, which is the combination of nano-silica or silica fume, fly ash and Portland cement, was varied to achieve different replacement rates of Portland cement with nano-silica or silica fume.

The minimum coarse to fine ratio was another important factor to achieve desired workability of SCCs. Self-consolidating concrete should have an optimum coarseness factor below 40 and its workability factor to remain above 40. The coarseness factor is obtained from  $\frac{Q}{Q+I} \times 100$ , or as the percent retained above the 9.5 mm sieve divided by the percent retained above the 2.36 mm sieve multiplied by 100. In this equation Q (Quality) is the percent of combined aggregate, which is all materials including sand, retained on the 9.5 mm sieve and I (Intermediate) is the percent of combined aggregate passing the 9.5 mm sieve and retained on the No.8 sieve. The workability factor is calculated based on the percent passing 2.36 mm sieve. The combined gradation of both coarse and fine aggregates was required to calculate the workability and coarseness factors. Therefore, sieve analysis was performed on both coarse and fine aggregates. The coarse aggregate gradation was determined by averaging the standard specifications for ASTM 7 for percent passing 12.7 mm sieve and percent passing the 9.51 mm sieve. From test results, the percent passing the 4.76 mm sieve averaged around 0.22 percent and was considered

unnecessary in the coarse aggregate gradation as ASTM No. 7 allowed for 0-15% passing. The ASTM 7 coarse aggregate specifications and coarse aggregate gradation are summarized in Tables 3.12 and 3.13.

Table 3.12: Coarse Aggregate Gradation

Sieve Size		Percent Passing					
Sieve No.	Opening (mm)	Sample 1	Sample 2	Sample 3	Sample 4	ASTM 7	Selected Gradation
1/2	12.5	94	92	99.1	97.7	90-100%	95%
3/8	9.5	55	40.6	64.1	48	40-70%	55%
No. 4	4.75	0.5	0.28	2.6	0.22	0-15%	0%
Pan		0	0	0	0		

Table 3.13: Selected Coarse Aggregate Gradation by Weight

Sieve No.	Percent Passing	Percent Retained	Percent Utilized
3/4 sieve	100	0	0
1/2 sieve	95	5	5
3/8 sieve	55	45	40
No.4	0	100	55

To determine the ratio of coarse aggregate to fine aggregate, various ratios of coarse to fine were examined. The ratios were 9:1 coarse to fine, 8:2, 7:3 and so on until 1:9 coarse to fine ratio. From these ratios, the combined percent passing and percent retained, the coarseness factor (CF) and workability factor (WF) were calculated. A sample calculation for the 9:1 ratio is provided in Table 3.14. From these calculations, Table 3.15 was derived to present the coarse to fine ratio, coarseness factor, and workability factor. Figure 3.2 displays the two factors plotted against the coarseness to fine ratio.

From Figure 3.2, the ratio that held the coarseness factor below 40 and the workability factor above 40 was determined to be 0.426. For simplicity, this value was rounded off to 0.43. The aggregate volume is then finalized as 43% coarse aggregate and 57% fine aggregate. This aggregate proportion was kept constant for all studied SCCs.

Table 3.14: Example Calculation of Workability and Coarseness Factors for 9:1 Coarse to Fine Ratio

Sieve Size	Coarse	Fine	Total Coarse	Total Fine	Cumulative Retained	Percent Retained	Percent Passing
	5 lb.	5 lb.	9:1	9:1			
1/2 Sieve	0.25		0.45		0.450	4.500	95.500
3/8 Sieve	2		3.6		4.050	40.500	59.500
No. 4	2.75	0.002	4.95	0.0004	9.100	91.005	8.995
No. 8		0.5		0.10008	9.100	91.005	8.995
No. 16		1.6		0.320256	9.421	94.207	5.793
No. 30		1.074		0.214972	9.636	96.357	3.643
No. 50		0.9		0.180144	9.816	98.159	1.841
No. 100		0.542		0.108487	9.924	99.243	0.757
Pan		0.378		0.075661	10	100	0
Workability factor equals percent passing No. 8							
8.995							
Coarseness factor equals percent retained of 3/8 in sieve divided by percent retained above No.8							
44.503							

Table 3.15: Workability and Coarseness Factors for Various Coarse to Fine Ratios

Coarse to fine ratio	WF	CF
0.9	8.995196	44.503145
0.8	17.99039	43.897296
0.7	26.98559	43.142168
0.6	35.98078	42.174837
0.5	44.97598	40.891233
0.4	53.97118	39.105931
0.3	62.96637	36.453356
0.2	71.96157	32.098801
0.1	80.95677	23.630439

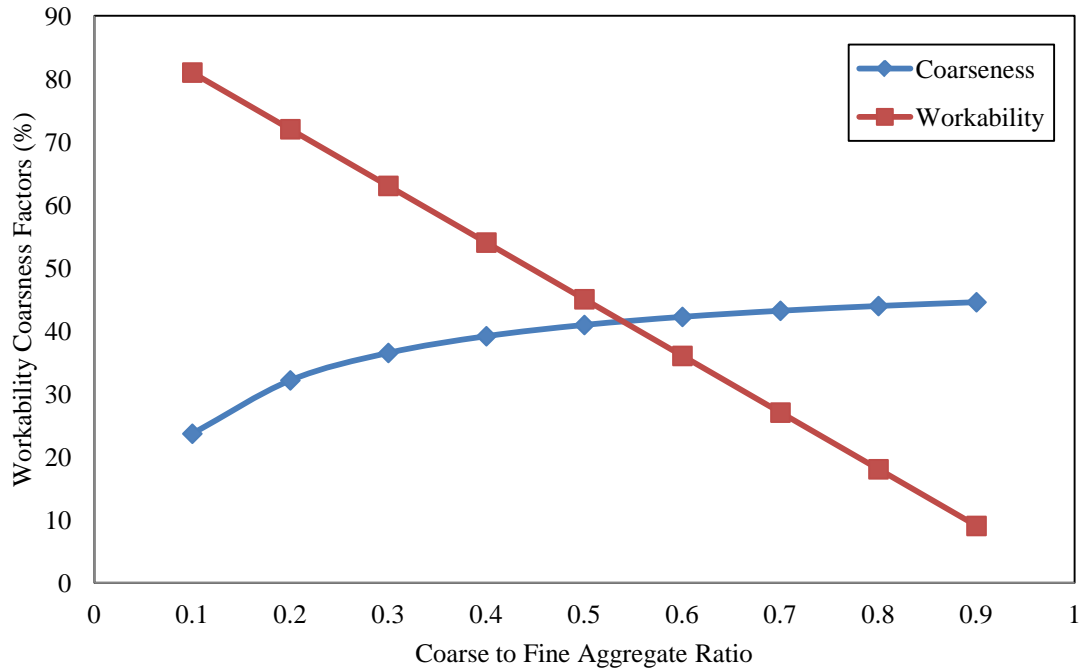


Figure 3.2: Coarseness and Workability Factors versus Coarse to Fine Ratios

The mixture proportions of the studied SCCs are given in Tables 3.16 and 3.17. The abbreviations used in the study for referring to the mixtures were adopted in a manner that they clearly show the main constituents and their content percentages. Mixtures are designated by their percentages by weight replacing a portion of cementitious materials in SCCs, followed by nano-silica and silica fume denoted as NS and SF, respectively.

Table 3.16: Mixture Proportions and Constituents of Nano-Silica Contained SCCs

Mixture	Portland Cement (kg/m <sup>3</sup> )	Fly ash (kg/m <sup>3</sup> )	Nano-Silica (kg/m <sup>3</sup> )	W/CM	Water (kg/m <sup>3</sup> )	Coarse Agg. (kg/m <sup>3</sup> )	Fine Agg. (kg/m <sup>3</sup> )	HRWR Admix. Dosage (kg/m <sup>3</sup> )
0-NS	396.9	79.4	0	0.45	214.335	725.2	962	1.02
1.5-NS	390.9	78.2	7.1	0.45	214.29	725.2	962	2.05
3-NS	385	77	14.3	0.45	214.335	725.2	962	3.24
4.5-NS	379	75.8	21.4	0.45	214.29	725.2	962	4.33
6-NS	373.1	74.6	28.6	0.45	214.335	725.2	962	5.75
7.5-NS	367.1	73.4	35.7	0.45	214.29	725.2	962	7.37

\*Total cementitious materials = Portland cement, fly ash, and nano-silica

Table 3.17: Mixture Proportions and Constituents of Silica Fume Contained SCCs

Mixture	Portland Cement (kg/m <sup>3</sup> )	Fly ash (kg/m <sup>3</sup> )	Silica Fume (kg/m <sup>3</sup> )	W/CM	Water (kg/m <sup>3</sup> )	Coarse Agg. (kg/m <sup>3</sup> )	Fine Agg. (kg/m <sup>3</sup> )	HRWR Admix. Dosage (kg/m <sup>3</sup> )
3-SF	385.0	77.0	14.3	0.45	214.335	725.2	962	1.54
4.5-SF	379.0	75.8	21.4	0.45	214.29	725.2	962	1.75
6-SF	373.1	74.6	28.6	0.45	214.335	725.2	962	1.97
7.5-SF	367.1	73.4	35.7	0.45	214.29	725.2	962	2.26

\*Total cementitious materials = Portland cement, fly ash, and silica fume

Figure 3.3 presents a comparison in dosages of HRWRA used for both nano-silica and silica fume contained SCCs. As it can be seen, all silica fume contained SCCs required less amount of admixture to achieve the target flow properties. This figure also shows that as the content of nano-silica and silica fume were increased, the need for additional amount of HRWRA to meet the required flow properties also increased. This finding can be attributed to the larger surface area of nano-silica or silica fume replacing a portion of cementitious materials, necessitating the use of a higher amount of HRWRA to meet the target flow properties.

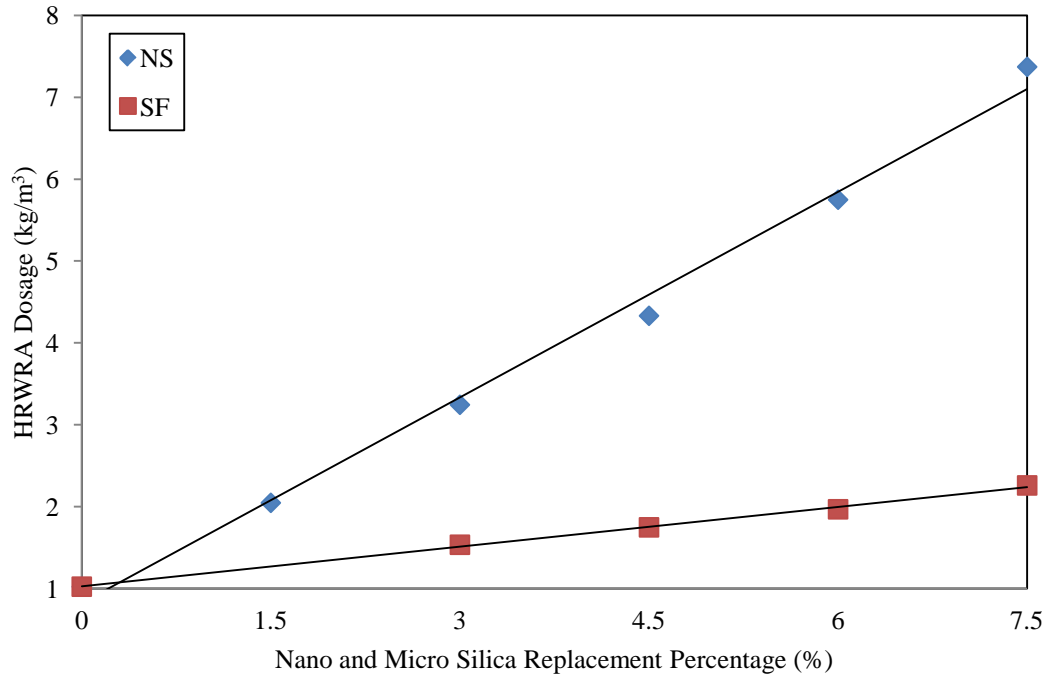


Figure 3.3: HRWRA Dosage Comparison of Nano and Micro Silica Contained SCCs

### 3.4 Particle Size Distributions of Cementitious Powder as Function of Nano-Silica Replacing a Portion of Cementitious Materials

The particle size distribution of studied SCCs was determined to analyze nano-silica particle size effect on studied SCC's physical characteristics. Figure 3.4 displays the particle size distribution of the powder (cement, fly ash, and nano-silica) and is focused on particle size less than 2 micrometers to examine nano-silica effect on finer size distribution.

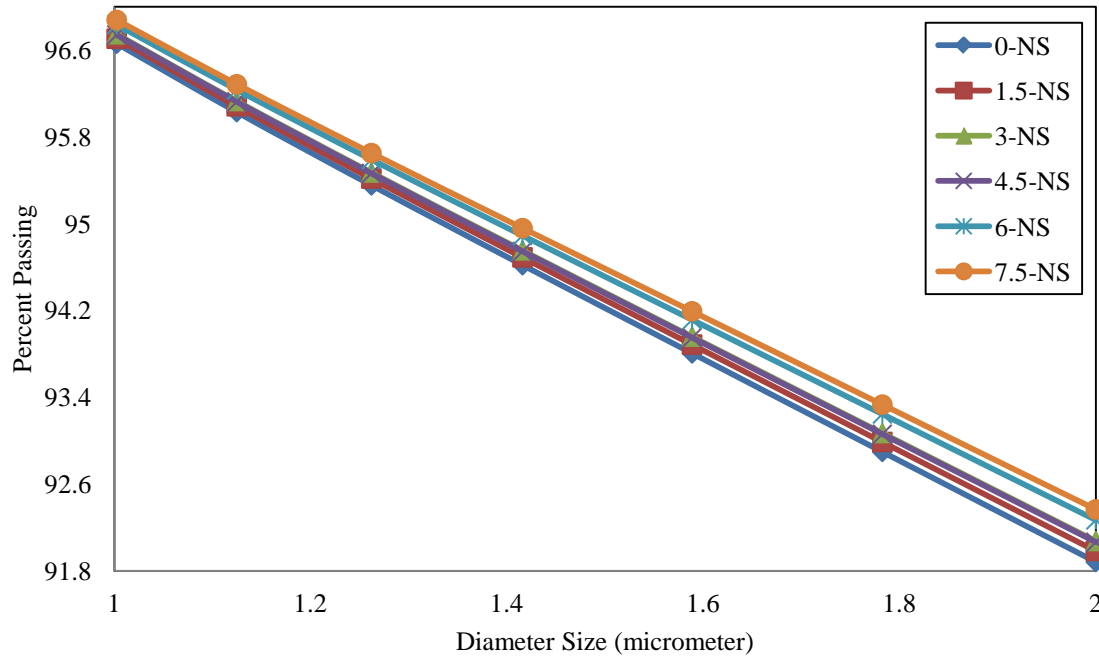


Figure 3.4: Particle Size Distributions of Cementitious Powder as Function of Nano-Silica Replacing a Portion of Cementitious Materials

From Figure 3.4, it was apparent that increasing nano-silica partial replacement created a finer particle size distribution especially for distribution of particles in diameter of 2 micrometers or less. It is also evident that nano-silica contained SCCs had more finer gradation than that of the control SCC.

### 3.5 Mixing Sequence

The adopted mixing sequence was primarily in accordance with ASTM C 192, “Standard Practice for Making and Curing Concrete Test Specimens in the Laboratory” with some modifications to meet challenges associated with the use of micro and nano particles. The following steps were taken in mixing all concrete mixtures presented in this study:



- (1) Nano-silica or silica fume, water, and a portion of the needed HRWRA were mixed in a blender to assure that fine particles of nano-silica and silica fume are mixed thoroughly with water.
- (2) The mixing drum was moistened to prevent loss of moisture once SCC's dry solid constituents were added.
- (3) Coarse aggregates were added and mixed for 2 minutes.
- (4) Fine aggregates were added and mixed for 2 minutes.
- (5) Nano-silica or silica fume powders were mixed with water and portion of admixture in a blender at high speed for 3 minutes to produce slurry.
- (6) Portland cement, fly ash, and slurry of nano-silica or silica fume were added to the coarse and fine aggregates and mixed for 3 minutes.
- (7) High-range water-reducing admixture was added within 3 minutes of mixing. The mix was monitored constantly to assure there was no bleeding or coning while the admixtures were being added into the mixing drum.
- (8) A 3-minute rest was allowed, once the entire amount of HRWRA was added to the mix, this followed by 3 minutes of additional mixing.
- (9) Finally, freshly-mixed SCC was used to perform slump test, J-ring test, and casting molds for all other transport properties tests.

### 3.6 Experimental Program

This section summarizes the tests performed to evaluate flow, mechanical, and transport properties of the studied SCCs.

#### 3.6.1 Slump Flow, $T_{50}$ , and Dynamic Segregation (ASTM C1611)

This test is designed to indicate the degree of flowability of SCCs. For this test, Abram's cone and slump flow board made of rigid metal plate were used. The Abram's cone was placed in the center point of the plate and was filled with SCC. Then, the cone was raised in nearly 3 seconds to the height of  $9 \pm 3$  inches allowing the mix to flow on a leveled steel plate. At last, the average diameter of the resulting concrete was measured. In addition to the slump flow,  $T_{50}$  was obtained from this test method.  $T_{50}$  is the time that it takes the concrete to reach a diameter of 50 cm (20 inches) and is an indirect indicator of concrete's viscosity. Segregation tendency is another way of evaluation SCC that was observed visually. The visual stability index (VSI) was used to examine the dynamic segregation resistance of fresh SCC by measuring the thickness of cement paste extended beyond the coarse aggregate. The accepted VSI ranges from 0 to 1. Zero being a highly stable matrix corresponding to no evidence of segregation or bleeding, and 1 being a stable matrix corresponded to no evidence of segregation and slight bleeding. Equipment used for this test are shown in Figure 3.5.

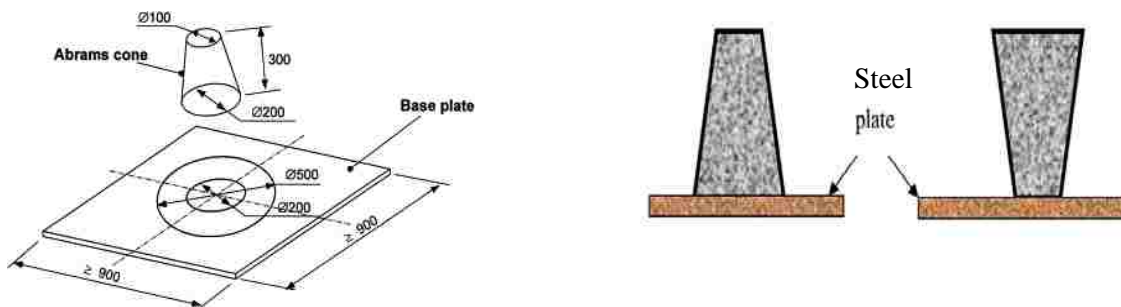


Figure 3.5: Arrangement of Slump Flow Test

The apparatus used for this test were:

- A flat steel plate with dimensions of at least  $900 \times 900$  mm ( $35 \times 35$  inches) with two centroidal circular marks of 200 and 508 mm (8 and 20 inches).
- A tape measure to measure the diameter of spread mix.
- A stopwatch to time concrete to reach diameter of 50 cm.
- A mold with a height of 300 mm (11.8 inches), upper diameter of 100 mm (3.9 inches) and lower diameter of 200 mm (7.8 inches).
- A tamping rod.
- A scoop to fill the cone.

The procedures followed to perform this test were as follows:

- After making a desired concrete mix, the slump cone and base plate were cleaned and dampened.
- The base plate was leveled and the cone was centered on the base plate with the bigger diameter on the plate.
- The cone was filled without any vibration, rodding, or tapping.
- Excess concrete was removed from the top surface of the cone as well as the base plate.
- The cone was then raised vertically for a distance of  $225 \pm 75$  mm ( $9 \pm 3$  inches) within 3 seconds.
- $T_{50}$  was measured immediately after the cone was lifted and recorded when the concrete reached the 508 mm (20 inches) circular mark.

- When concrete settled, the maximum diameter of the slump flow was measured in two perpendicular directions to the nearest 12.5 mm (0.5 inches) and the average of the two measurements was recorded.
- Visual examination was used to check segregation and Table 3.18 was used to evaluate the dynamic segregation (VSI).

Table 3.18: Visual Stability Index (VSI) of SCC Rating Criteria

Rating	Criteria
0 Highly stable	No evidence of segregation or bleeding in slump flow, mixer drum/pan, or sampling receptacle (e.g. wheelbarrow).
1 Stable	No mortar halo or coarse aggregate heaping in the slump flow, but some slight bleeding and/or air popping is evident on the surface of the slump flow, or concrete in the mixer drum/pan or sampling receptacle (e.g. wheelbarrow).
2 Unstable	Slight mortar halo, 10 mm $\leq$ 0.5 inch mm) wide, and/or coarse aggregate heaping in the slump flow, and highly noticeable bleeding in the mixer drum/pan or sampling receptacle (e.g. wheelbarrow).
3 Unstable	Clearly segregated by evidence of a large mortar halo, > 10 mm (0.5 inch), and/or large coarse aggregate pile in the slump flow, and a thick layer of paste on the surface of the concrete sample in the mixer drum or sampling receptacle (e.g. wheelbarrow).

### 3.6.2 J-Ring Test (ASTM C1621)

J-ring test is used to determine the passing ability of SCC. A difference less than 25 mm (1 inch) indicates good passing ability and a difference greater than 50 mm (2 inches) indicates poor passing ability. Figure 3.6 shows the apparatus used to evaluate passing ability of the studied SCCs.

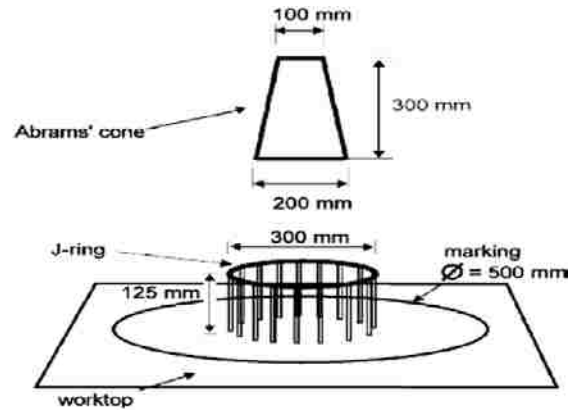


Figure 3.6: Schematic of J-ring Test for Concrete (Boukendakdji et al., 2009)

The apparatus used for this test are as follows:

- The J-ring used for this study held a diameter of 305 mm (12 inches) with a height of 100 mm (4 inches). J-ring is an open steel ring, drilled vertically and threaded sections of reinforcing bars.
- A flat plate with dimensions of at least 900 × 900 mm (35 × 35 inches) with two centroidal circular marks of 200 and 508 mm (8 and 20 inches).
- A tape measure to measure the diameter of spread mix.
- A mold with a height of 300 mm (11.8 inches), upper diameter of 100 mm (3.9 inches) and lower diameter of 200 mm (7.8 inches).
- A tamping rod.
- A scoop to fill the cone.

The adopted procedure to perform this test is as follows:

- The slump cone, J-ring, and base plate were cleaned and dampened.
- The plate was leveled and J-ring was placed on the plate. Then, the cone was centered within the J-ring with the smaller diameter on the plate.

- The cone was filled with fresh concrete with no help of vibration, rodding, or tapping.
- Excess concrete on the base plate and on the top of the cone were removed.
- The cone was then raised vertically for a distance of  $225 \pm 75$  mm ( $9 \pm 3$  inches) within 3 seconds.
- When concrete settled, the maximum diameter of the slump flow was measured in two perpendicular directions to the nearest 12.5 mm (0.5 inches) and the average of the two measurements was recorded. The J-ring value was calculated as the difference between the J-ring flow and the unobstructed slump flow as tested according to slump flow test of the same representative sample.

The passing ability of the mix was rated according to Table 3.19:

Table 3.19: Passing Ability Rating

J-ring Value mm (in)	Passing ability Rate	Remarks
0-25 (0-1)	0	High Passing ability
>25-50 (>1-2)	1	Moderate Passing ability
>50(>2)	2	Low Passing ability

### 3.6.3 **Compressive Strength (ASTM C39)**

Compressive strength test established by American Society of Testing Materials (ASTM C39) is used to determine compressive strength of cylindrical specimens. The results of this test are used characterizing the strengths of the studied SCCs. Ultimate compressive strength of concrete is defined as its maximum resistance to axial loading. Compressive strength is dependent on quality of concrete constituents and proportions,

water-to-cement ratio, the extent to which hydration has progressed, curing and environmental conditions, and age of concrete. In this test method, compressive axial load is applied to concrete cylinders at the rate of 20 to 50 psi/sec until specimen fails. It is calculated from the failure load divided by the cross sectional area resisting the load. After completion of desired curing ages (28, 90, and 180 days), the test specimens were placed on spherical bearing blocks and positioned with the centroid of upper platen of a static testing compression machine (see Figure 3.7). Afterward, compressive force was applied until concrete specimen failed.



Figure 3.7: Concrete Cylinder Experiencing Axial Load

#### **3.6.4 Water Absorption (ASTM C642)**

This standard test method is designed to measure density, absorption, and volume of voids in hardened concrete. This test method is useful for conversion between mass and volume for concrete. Water permeability and sorptivity are both affected by size and continuity of pores available in concrete (Soneby and Nanukhuttan, 2009). The apparatus

and materials required for this test are listed in Table 3.20. Oven-dried mass, saturated mass after immersion in water, saturated mass after boiling in water, and immersed apparent mass in water are the different properties obtained from this test. Volume of permeable voids and bulk densities are also calculated from these properties.

Table 3.20: Apparatus and Materials Needed for ASTM C642

Balance	Sensitive to 0.025% of the mass of the specimen
Container	To immerse specimens in
Concrete discs	4"×2" (volume greater than 350 cm <sup>3</sup> ) free of shattered edges

The systematic procedure, in sequence, used to perform this test is listed below.

- Test specimen was placed in a dry oven at a temperature of 100 to 110°C for at least 24 hours. After 24 hours of drying, they were air-dried at a room temperature of 20 to 25°C and mass of test specimen was recorded (to make certain that the specimens were completely dry, specimens were re-dried in an oven until the difference between concrete mass did not exceed 0.5%).
- Test specimen was placed in water at temperature of 21°C for 48 hours. Excess water was removed from surface of test specimen and its mass was measured.
- Test specimen was placed in a covered container filled with tap water and boiled for 5 hours. It was allowed to cool for 14 hours at room temperature of 20 to 25°C. Excess moisture was removed from surface of test specimen and mass was measured.
- Test specimen was suspended by wire in water and its mass was measured.

The following calculations were performed to determine absorption, bulk and apparent densities, and volume of permeable pore space.



$$\text{Absorption after immersion, \%} = [(B - A)/A] \times 100$$

$$\text{Absorption after immersion and boiling, \%} = [(C - A)/A] \times 100$$

$$\text{Bulk density, dry} = [(A/(C - D)]\rho = g_1$$

$$\text{Bulk density after immersion} = [B/(C - D)]\rho$$

$$\text{Bulk density after immersion and boiling} = [C/(C - D)]\rho$$

$$\text{Apparent density} = [A/(A - D)]\rho = g_2$$

$$\text{Volume of permeable pore space (voids), \%} = (g_2 - g_1)/g_2 \times 100$$

Where:

A = mass of oven-dried sample in air (g)	D = apparent mass of sample in water after immersion and boiling (g)
B = mass of surface-dry sample in air after immersion (g)	$g_1$ = bulk density, dry, Mg/m <sup>3</sup>
C = mass of surface-dry sample in air after immersion and boiling (g)	$g_2$ = apparent density, Mg/m <sup>3</sup>
	$\rho$ = density of water = 1 Mg/m <sup>3</sup> = 1 g/cm <sup>3</sup>

### **3.6.5 Capillary Absorption (ASTM C1585)**

This standard test method measures the rate of absorption (sorptivity) of water by hydraulic cement concrete by measuring the increase in the mass of a specimen resulting from absorption of water as a function of time. In this method, only one surface of a specimen is exposed to water. The water absorption of a concrete surface depends on several factors such as mixture proportions, presence of microcracks, and the degree of hydration. The main difference between this test method and ASTM C642 is that ASTM C642 is used to estimate the maximum amount of water that can be absorbed by a dry

specimen and, therefore, provides a measure of the total water permeable pore space. Capillary is the transport of liquids due to surface tension acting in capillaries. This phenomenon is influenced by viscosity, density and surface tension of the liquid and pores structure (radius, tortuosity and continuity of capillaries) and surface energy of the concrete (Yang et al., 2006). Generally, concretes with finer pores structures will experience greater capillary suction pressures. Capillary pores are those voids remaining that were originally filled with mixing water (Yang et al., 2006). These pores are known to be larger than the CSH gel pores and so dominate transport processes. The apparatus and materials required for this test are documented in Table 3.21 and the test setup is shown in Figure 3.8.

Table 3.21: Apparatus and Materials Required for Capillary Absorption Test

Pan	Corrosion resistant pan
Support device	Rods, pins, or other devices resistant to corrosion
Top-pan balance	Accuracy of $\pm 0.01$ g and capacity of test specimens (not less than 3 kg)
Timing device	Stop watch with accuracy of $\pm 1$ second
Paper towel	To wipe excess water from surface of specimen
Dry oven	To maintain temperature of $50 \pm 2^\circ\text{C}$
Desiccator	To contain specimens in
Saturated solution of potassium bromide (solubility of 80.2g/100 g of water at $50^\circ\text{C}$ )	To control the relative humidity of $80 \pm 5\%$ in the desiccator
Polyethylene storage containers	With sealable lid to store specimens in
Caliper	To measure specimen dimensions to the nearest 0.1 mm
Concrete discs	4"×2"
Sealing material (Waterproof Plasti Dip)	To seal sides of specimen
Plastic sheeting	To control evaporation from the top surface of specimen

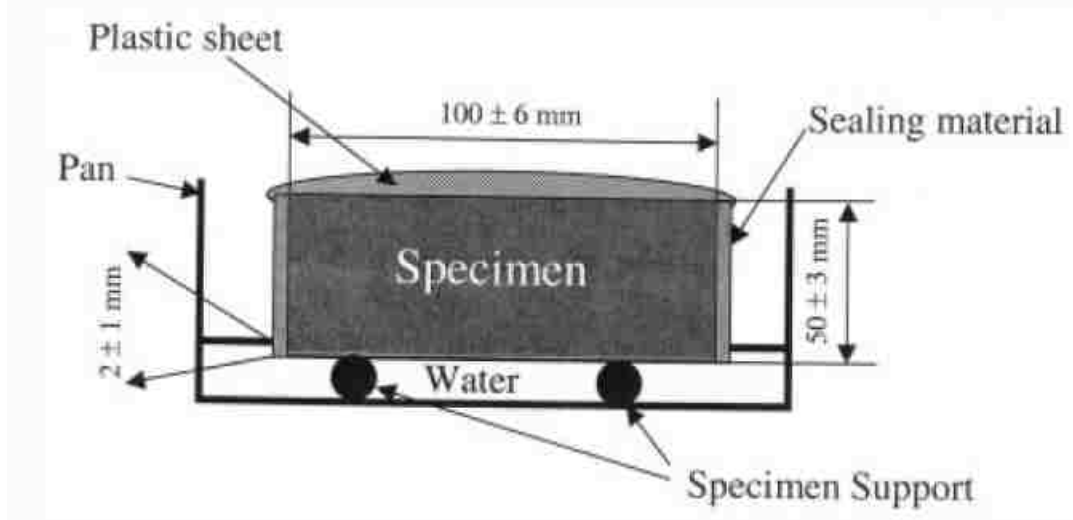


Figure 3.8: Schematic of the Capillary Absorption Test Setup

The orderly preconditioning steps for this test method are listed below.

- Specimens were placed in a desiccator for 3 days. The desiccator contained solution of potassium bromide to control the relative humidity. The test specimens did not have contact with the solution.
- Each specimen was then placed inside a sealable container at a room temperature of  $23 \pm 2^\circ\text{C}$  for 15 days.
- Test specimen was removed from the container and its mass was recorded to the nearest 0.01 gram.
- Four diameters of test specimen at the surface exposed to water were measured to the nearest 0.1 mm and the average was taken.
- The sides of test specimen were sealed with a sealing material (Waterproof Plasti Dip) and the top surfaces were covered with plastic sheet.
- The mass of the sealed test specimen was measured to the nearest 0.01 gram.

- The container was filled with tap water and the specimens were placed on the support device so that the water level was 2 mm above the top of the support device.
- The timing device was started and the test surface of the test specimens was placed on the support device.
- The mass of the test sample was recorded after 60 seconds, 5 minutes, 10 minutes, 20 minutes, 30 minutes, 1 hour, 2 hours, 3 hours, 4 hours, 5 hours, 6 hours, 1 day, 2 days, 3 days, 5 days, 6 days, 7 days, and 8 days. The actual time was recorded within  $\pm 10$  seconds. For each mass determination, test specimen was removed from the pan, time was stopped, and excess water was wiped off the surface. The dry side of the specimen was placed on the balance and within 15 seconds of removal from the pan the mass was measured.

The following calculations were performed to determine absorption of the test samples. The change in mass divided by the product of the cross sectional area of the specimen and the density of water yielded in absorption.

$$I = m_t/a/d \quad (1)$$

Where:

I = absorption	a = the exposed area of the specimen
$m_t$ = the change in specimen mass(g), at	( $\text{mm}^2$ )
the time t	d = density of the water in $\text{g}/\text{mm}^3$

The initial rate of absorption was obtained from the slope of the line for the graph plotting absorption versus square root of time using all collected data from 1 minute to 6

hours. The secondary rate of water absorption was obtained from the slope of the line for the graph of absorption versus square root of time using all collected data from 1 to 7 days.

### **3.6.6 Rapid Chloride Permeability Test (ASTM C1202)**

This standard test method evaluate electrical conductance of concrete in order to provide a rapid indication of its resistance to penetration of chloride ions. In this test, the total charges passed through hardened cement matrix over a known time interval is measured. These charges are then correlated to the amount of chloride permeability through established relationships between chloride permeability and total charges (Wee et al., 1999). Chloride ions migrate inside concrete by means of liquid present in the pores. The pore liquid is a solution containing the dissolved components of hydrated cement (Zofia and Adam 2013). It is believed that the pore liquid has an electrolyte nature due to presence of several ions such as sodium, potassium, calcium, and hydroxide ions. In this test, the ionic movement is measured (Zofia and Adam 2013).

Concrete electroconductivity is affected by both concrete pore structure (to lesser extent) and the chemistry of the pore solution (to larger extent). Pore structure is a function of pore size, distribution, and connectivity of pores, which are all affected by hydration of cement, freeze and thaw, and deterioration processes. On the other hand, pore solution is greatly affected by cement composition, supplementary cementitious materials, and inclusion of aggregates (Shi, 2006).

In this test method, electrical current passes through a 2-in. thick concrete disk (4"×2") during a 6 hours period of time. One end of the specimen is immersed in a 3% sodium chloride solution and the other end is immersed in a 0.3M sodium hydroxide

solution. The potential difference of 60 volts is maintained across these two ends for 6 hours. The total charges passed, in coulombs, determines the resistance of the test specimen to chloride ion penetration. A schematic setup including test apparatus are shown in Figures 3.9 and 3.10.

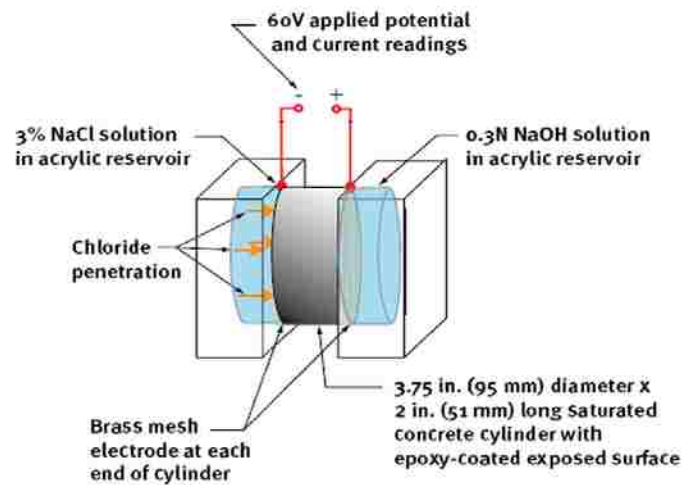


Figure 3.9: Schematic of RCPT Test Setup (ACI)

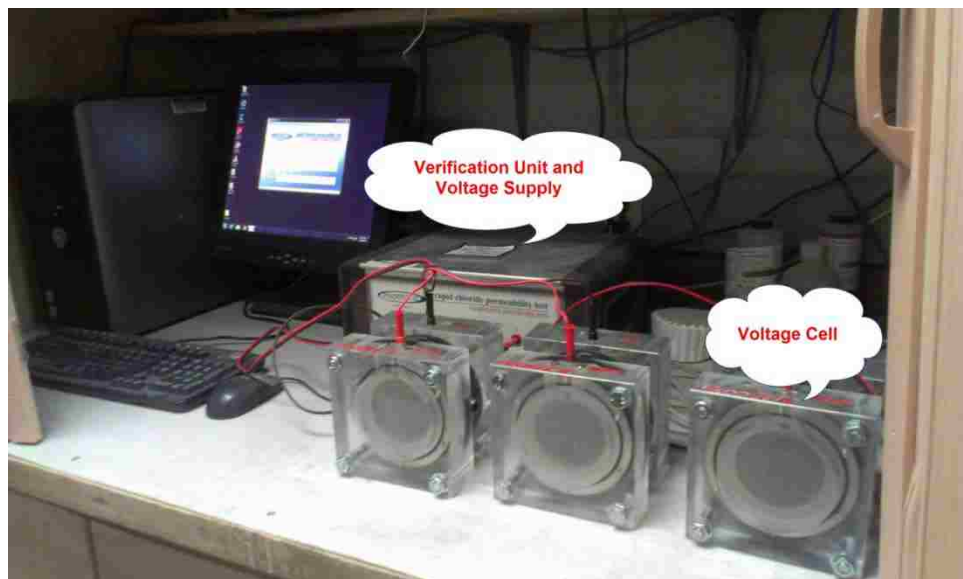


Figure 3.10: Actual Setup of RCPT Test

Chloride ion penetration is rated according to Table 3.22.

Table 3.22: RCPT Ratings (Per ASTM C1202)

Charge passed (Coulombs)	Chloride Ion Penetrability
> 4000	High
2000 - 4000	Moderate
1000 - 2000	Low
100 - 1000	Very low
< 100	Negligible

There have been numbers of criticisms about this test method. One of the criticisms is that the current passed through the specimen is related to all ions in the pore solution and not just chloride ions. In addition, the measurements are made before steady state migration is achieved, and the high voltage applied leads to an increase in temperature (Stanish et al., 2000).

The apparatus and materials used for this test are documented in Table 3.23.

Table 3.23: Apparatus and Materials Required for RCPT Test

Vacuum desiccator	10 inches or more in diameter with two hose connections
Vacuum pump	To maintain pressure of less than 1 mm Hg (133 Pa) in desiccator
Manometer	With $\pm 0.5$ mm Hg ( $\pm 66$ Pa)
Applied voltage cells (Proove'it cells)	To place specimens in as well as containing sodium chloride and sodium hydroxide solutions
Voltage application and date readout apparatus	To hold $60 \pm 0.1$ V dc across the cell
Verification unit	To control the microprocessor controlled power supply
Windows based software	For testing and report preparation
Sodium chloride solution	3.0% by mass
Sodium hydroxide solution	0.3 N in distilled water
Filter paper	No.2
Concrete discs	4"×2"

The preconditioning procedures used to prepare the samples are listed below.

- The side surfaces of specimen were coated. All apparent holes in the coating were filled.
- Test specimen was placed in desiccator and both end faces of the specimen were exposed.
- Vacuum was maintained for 3 hours in the desiccator.
- With vacuum pump running, the stopcock connected to the container filled with tap water was opened and sufficient water was drained into the desiccator to cover specimen (precautions were taken to make sure air was not entered to the desiccator).
- The water stopcock was closed and vacuum pump ran for an additional hour.
- Vacuum stopcock was closed and the pump was turned off. Then, vacuum line stopcock was opened to allow air to re-enter the desiccator.
- Test sample was soaked under water in the desiccator for another 18 hours.

After preconditioning of test specimen, the following test procedures were followed.

- Test specimen was removed from water and placed in RCPT cells in addition to the filter paper.
- Rubber rings were placed on faces of test specimen as well as the side to restrict moisture movement. The two halves of the test cell then were clamped together to seal the sample.
- One side of the cell was filled with 3.0% NaCl solution and the other side was filled with 0.3 N NaOH solution.



- Wires were attached to cell banana posts. Power supply was turned on and set to 60 volts. Temperature of the test sample, cells, and solutions were measured to be 22 to 25°C (68 to 77°F).
- Computer software was used to record current at every 30 minutes. The software converted voltage readings to amperes for 6 hours. A plot of current versus time was drawn by the software and the area underneath the curve was obtained to determine the ampere-seconds, or coulombs of charge passed during the 6 hours test period.

### **3.6.7 Water Penetration (EN 12390)**

This test determines the depth of penetration of water under pressure in hardened concrete. In this method, water is applied under pressure to bottom surface of hardened concrete. Then, test specimen is split into half and the depth of penetration of the water front is measured. The permeability of concrete is strongly affected by pore structure of concrete and is mainly a function of pore size distribution (Zhang and Li 2011). The permeability of concrete is related to the pore connectivity and pore size distribution. There are mainly three types of factors affecting the permeability of concrete: 1) factors affecting the original pore structure of concrete such as water-to-binder ratio, mineral admixtures and additive agents, 2) factors affecting the development of pore structure of concrete such as curing condition, age and activity of binders, and 3) penetration condition such as hydraulic gradient and penetration time (Zhang and Li 2011). The apparatus and materials required for this testing method are documented in Table 3.24.

Concrete impermeability apparatus (EL34-4620)	With 3 measuring locations and central spindle
Air compressor	To apply pressure
Concrete cubes	6"×6"×6"
Pressure regulator and gage	To control air pressure

The actual testing apparatus and setup are shown in Figures 3.11.



Figure 3.11: Concrete Water Penetration Testing Apparatus

The following test procedure was conducted to perform water penetration tests of the studied SCCs.

- After removing test sample from the curing room, the sample's surface intended to be exposed to water pressure was roughen with a wire brush.
- Test specimen was placed in the test apparatus under water pressure of  $500 \pm 30$  kPa for 72 hours. The dry surface of the specimens was observed periodically to make sure there was no leakage (leakage makes the test results invalid).

- Test specimen was then removed from the test apparatus and split in two halves perpendicularly to the face on which water pressure was applied.
- Water penetration into the test specimen was marked. The maximum depth of penetration under the test area was then recorded to the nearest millimeter. In addition to the maximum penetrated depth, a profile of water penetration was drawn by measuring the depth of penetrated water every 5.08 mm across the width of specimen as shown in Figure 3.12.

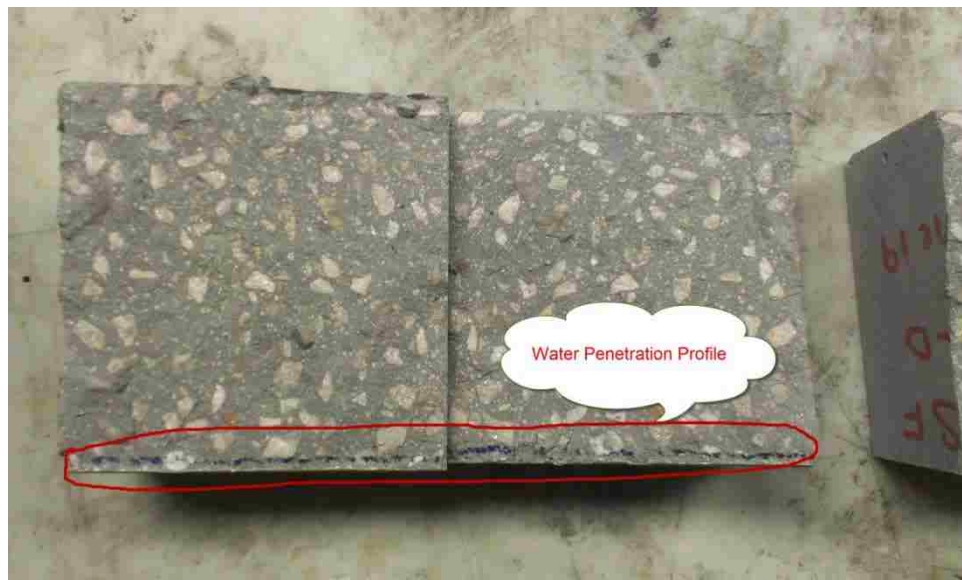


Figure 3.12: Profile of Penetrated Water through Concrete Cubes

### 3.6.8 Chloride Diffusion (ASTM 1556)

This standard test method is used to determine the apparent chloride diffusion coefficient of hardened concrete by bulk diffusion. Apparent chloride diffusion coefficient is a chloride transport parameters calculated from acid soluble chloride profile data obtained from saturated specimens exposed to chloride solutions (without correction

for chloride binding). In this method, initial chloride ion content is measured by crushing the specimen prior in contact with calcium hydroxide and sodium chloride solutions. Then, the chloride ion content is measured at different depths after an exposure of a concrete specimen to calcium hydroxide and sodium chloride. Diffusion is a process by which ions can pass through a saturated concrete without the flow of water. The driving factor in diffusion is the concentration gradient. Diffusion is observed in cases where a strong solution is in contact with a weak solution; in these cases, ions will migrate between the solutions until they both reach an equal concentration.

The apparatus and materials required for the adopted chloride diffusion test are documented in Table 3-21.

Table 3.25: Apparatus and Materials Required for Chloride Diffusion Test

Balance	With accuracy of $\pm 0.01$ g
Thermometer	With accuracy of $\pm 1.0^\circ\text{C}$
Plastic container with lid	To store specimens in
Drill and drill bit	To grind off and collect powder from specimens as well as coring
Automated Titrator	To perform chloride analysis
Distilled water	For titration
Calcium hydroxide	Technical grade
Sodium chloride	Technical grade
Calcium hydroxide solution	3 g/L
Sodium chloride solution (exposure liquid)	165 g of NaCl per liter of solution
Epoxy-resin based paint	To form a barrier resistant to chloride ion diffusion
Concrete discs	4"×2" with minimum depth of 75 mm
Burette, class A	With 10 mL capacity and 0.05 mL divisions
Sodium chloride	Primary standard grade
Silver nitrate	Reagent grade
Potassium chloride	Reagent grade

The preconditioning procedure associated with this test method is given below.

- All sides of test sample were sealed except for the finished surface.
- Test specimen was then immersed in a saturated calcium hydroxide water bath at  $23 \pm 2^\circ\text{C}$  in a closed plastic container for 24 hours.
- Test specimen was removed from the test container and their surface dry mass was measured (specimen was kept in a saturated calcium hydroxide water bath until its mass did not change by more than 0.1 % in 24 hours).
- Test sample was removed from the calcium hydroxide water bath and rinsed with tap water. Next, it was placed in a sealed container filled with exposure liquid (sodium chloride) for 35 days. Precaution was taken to make sure that water did not evaporate from the exposure liquid or there was no leakage from the container.
- After 35 days, specimen was removed from the exposure liquid and rinsed with tap water and dried for 24 hours at temperature of  $23 \pm 2^\circ\text{C}$  and  $50 \pm 3\%$  relative humidity.
- Powdered samples were obtained by grinding off materials in 7 layers parallel to the exposed surface (depth 1: 0-2 mm; depth 2: 2-4 mm; depth 3: 4-6 mm; depth 4: 6-8 mm; depth 5: 8-11 mm; depth 6: 11-14. mm; and depth 7: 14.-17 mm).
- Three gram of powder was obtained from each layer and from the depth below the exposed surface.
- The powdered sample was then transferred to a container and pulverized so that all the material passed  $850 \mu\text{m}$  (No. 20) sieve.
- The 3 grams powdered sample was then introduced into a 250 mL beaker.

- The collected powder from test sample was dispersed with 75 mL of water and with no delay 25 mL of nitric acid (1+1) was added slowly. In a case of strong hydrogen sulfide smell, 3 mL of hydrogen peroxide (30% solution) was added. Afterward, 3 drops of methyl orange indicator was added and stirred.
- The solution was heated rapidly to boiling.
- The beaker was then covered with watch glasses and allowed to rest for 1 to 2 minutes.
- Next, filter papers were soaked to filter the heated solutions. Sample solution was filtered and beaker was rinsed with additional 50 mL of water. The filtrate was transferred to a 250 mL beaker and cooled to room temperature. Volume of filtrate was kept below 175 mL.
- Two mL of standard 0.05 N NaCl solution was added to the cooled sample beakers by pipet.
- The beaker was then placed on a magnetic stirrer and a TFE-fluorocarbon-coated magnetic stirring bar was added into the beaker. The electrodes were then immersed into the solution. The delivery tip of the 10 mL burette, filled to the mark with a standard 0.05 N silver nitrate solution placed above the solution.
- While titrating, the amount of standard 0.05 N silver nitrate solution required to bring the millivoltmeter reading to 60.0 mV of the equivalence point was recorded.
- Titration continued with 0.20 mL increments and burette reading and corresponding millivolt was recorded accordingly.

- Titration was carried out by the titration machine until three readings exceeded the approximate equivalence point.
- A blank determination using 75 mL of water in place of the test sample was prepared. The results obtained were then corrected by subtracting the measured chloride content of test sample from the blank's chloride content.

The following calculations were performed to determine the percent chloride to the nearest 0.001%.

$$CI, \% = \frac{3.545 [(V_1 - V_2)N]}{W} \quad (2)$$

Where:

$V_1$  = milliliters of 0.05 N  $AgNO_3$   
solution used for sample titration  
(equivalence point)

$N$  = exact normality of 0.05 N  $AgNO_3$   
solution

$W$  = weigh of sample (g)

$V_2$  = milliliters of 0.05 N  $AgNO_3$   
solution used for blank titration  
(equivalence point)

$$C(x,t) = C_s - (C_s - C_i) \operatorname{erf} \left( \frac{x}{\sqrt{4 D_a t}} \right) \quad (3)$$

Where:

$C(x,t)$  = chloride concentration  
measured at depth  $x$  and exposure time  $t$ ,  
mass %

$C_s$  = projected chloride concentration at  
the interface between the exposure liquid  
and test specimen that is determined by  
the regression analysis

$C_i$  = initial chloride ion concentration of the mixture prior to submersion in the exposure liquid

$x$  = depth below the exposed surface, to the middle of a layer (m)

$D_a$  = apparent chloride diffusion coefficient ( $m^2/s$ )

$t$  = exposure time (s)

erf = error function

$$S = \sum_{n=2}^N \Delta C^2(n) = \sum_{n=2}^N (C_m(n) - C_c(n))^2 \quad (4)$$

Where:

$S$  = sum of squares to be minimized, (mass %)<sup>2</sup>

$N$  = number of layers ground off

$\Delta C(n)$  = difference between the measured and calculated chloride concentration of the  $n$ th layer, mass %

$C_m(n)$  = measured chloride concentration of the  $n$ th layer, mass %

$C_c(n)$  = calculated chloride concentration in the middle of the  $n$ th layer, mass %  
The plots of measured chloride contents at all points versus the depth below the surface, as well as the best fit curve of the same graph, were also drawn.

### **3.6.9 Rapid Migration Test (RMT- NT BUILD 492)**

Rapid Migration Test (RMT) resembles the Rapid Chloride Permeability Test (RCPT) in some respects. In both tests 50 mm × 100 mm concrete disks that are exposed to NaCl solution on one side and NaOH solution on the other side are used. The concentration of NaOH solution is 0.3N for both tests, yet the NaCl solution concentration in the RMT is 10% by mass compared with 3% in the RCPT. In the RMT,



chloride ions migrate into the specimen by an external potential applied force across the specimens. The applied voltage in RMT varies depending on the initial current measured at 30V and the various test duration. This test resembles a non-steady migration experiment. In the electrical field, positive ions move toward negative electrode and negative ions to the positive one. The chloride resistance of concrete is highly dependent on the porosity of concrete in terms of pore size, pore distribution and interconnectivity of the pore system (Cement and Aggregate Concrete Australia, 2009).

The apparatus and materials required for this test are documented in Table 3.26 and the test setup and apparatus are shown in Figures 3.13 and 3.14.

Table 3.26: Apparatus and Materials Required for Rapid Migration Test

Balance	With accuracy of $\pm 0.01$ g
Thermometer	With accuracy of $\pm 1.0^{\circ}\text{C}$
Rubber sleeve	For migration setup arrangement
Anode	For migration setup arrangement
Cathode	For migration setup arrangement
Plastic support	For migration setup arrangement
Plastic container (reservoir)	For migration setup arrangement
Spray bottle	To spray silver nitrate
Power supply	To apply voltage to the tank
Sodium chloride solution	3.0% by mass
Sodium hydroxide solution	0.3 N in distilled water
Vacuum desiccator	10 inches and more in diameter with two hose connections
Vacuum pump	To maintain pressure of less than 1 mm Hg (133 Pa) in desiccator
Silver nitrate	Reagent grade
Distilled water	

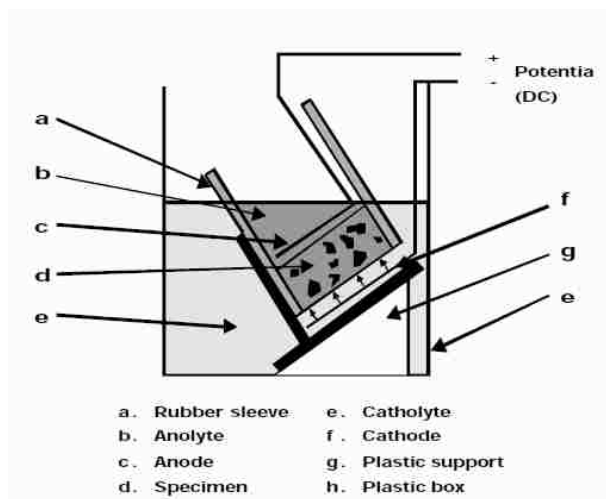


Figure 3.13: Test Arrangement of Rapid Migration Test



Figure 3.14: Rapid Migration Test Setup

The preconditioning procedure required for this method is described below.

- One liter of tap water was boiled and allowed to cool to ambient temperature while capped tightly.

- The side surface of test specimen was coated with a waterproof agent and cured. All apparent holes in the coating were filled.
- Test sample was placed in a desiccator and both end faces of test specimen were exposed.
- Vacuum was maintained for 3 hours in the desiccator.
- With vacuum pump running, the stopcock connected to the container filled with tap water was opened and sufficient water was drained into the desiccator to cover test specimen (precautions were taken to make sure air was not entered to the desiccator).
- The water stopcock was closed and vacuum pump ran for one more hour.
- Vacuum stopcock was closed and the pump was turned off. Afterward, vacuum line stopcock was opened to allow air to re-enter the desiccator.
- Test specimen was soaked under water in the desiccator for another 18 hours.
- The initial currents of test specimen were measured with the voltage preset at 30 V.
- The voltage was adjusted based on the values presented in Table 3-23 and the new currents were measured.
- Initial temperature was recorded and the appropriate test duration was chosen based on the initial current.
- After the specified duration was over, test specimen was removed from the NaCl tank and rinsed with tap water.
- Test specimen was split axially into two halves and 0.1M silver nitrate was sprayed on the freshly split sections.

- Penetration depth was measured to both edges at internal of 10 mm to an accuracy of 0.1 mm (see Figure 3.15).

Table 3.27: Test Voltage and Duration for Concrete Specimens (NT BUILD 492)

Initial Current $I_{30V}$ (with 30 V) (mA)	Applied Voltage U (After Adjustment) (V)	Possible New Initial Current $I_0$ (mA)	Test Duration t (hour)
$I_0 < 5$	60	$I_0 < 10$	96
$5 \leq I_0 < 10$	60	$10 \leq I_0 < 20$	48
$10 \leq I_0 < 15$	60	$20 \leq I_0 < 30$	24
$15 \leq I_0 < 20$	50	$25 \leq I_0 < 35$	24
$20 \leq I_0 < 30$	40	$25 \leq I_0 < 40$	24
$30 \leq I_0 < 40$	35	$35 \leq I_0 < 50$	24
$40 \leq I_0 < 60$	30	$40 \leq I_0 < 60$	24
$60 \leq I_0 < 90$	25	$50 \leq I_0 < 75$	24
$90 \leq I_0 < 120$	20	$60 \leq I_0 < 80$	24
$120 \leq I_0 < 180$	15	$60 \leq I_0 < 90$	24
$180 \leq I_0 < 360$	10	$60 \leq I_0 < 120$	24
$I_0 \geq 360$	10	$I_0 \geq 120$	6



Figure 3.15: Chloride Penetration Depth after Applying Silver Nitrate to the Freshly Split Sections

The following relationship was used to determine coefficient of migration.

$$D_{nssm} = \frac{0.0239(273+T)L}{(U-2)t} (x_d - 0.0238) \sqrt{\frac{(273+T)Lx_d}{U-2}} \quad (5)$$

Where:

$D_{nssm}$ : non-steady migration coefficient

( $\times 10^{-12} \text{ m}^2/\text{s}$ )

U: absolute value of the applied voltage,

V

T: average value of the initial and final

temperatures in the analyte solution, °C

L: thickness of the specimen, mm

$X_d$ : average value of the penetration

depths, mm

t: test duration, hours

## Chapter 4

### Results and Discussion

In the first part of this chapter, all test results for the studied nano-silica contained self-consolidating concretes are presented and discussed. The second part of this chapter deals with the comparison of the test results obtained for silica fume contained SCCs and those of the equivalent concretes containing nano-silica.

#### 4.1 Nano-Silica Contained Concrete Test Results

Flow properties, compressive strength, rapid migration, water penetration, capillary absorption, water absorption, rapid chloride penetration, and chloride diffusion tests results of nano-silica contained concretes are presented and discussed below.

##### 4.1.1 Flow Properties

The optimum dosages of polycarboxylate-based High-Range-Water-Reducing Admixture (HRWRA) required in attaining the target slump flows of  $635 \pm 25$  mm, J-ring of 50 mm, and visual stability of stable (1) to highly stable (0) indexes are summarized in Tables 4.1. In addition, workability of concrete mixtures was evaluated by measuring slump flow,  $T_{50}$ , J-ring, and VSI, which are also presented in Table 4.1.

Table 4.1: Flow Properties of Self-Consolidating Concretes

Mixture Designation	Slump Flow Diameter (mm)	VSI	$T_{50}$ (sec)	J-Ring Diameter (mm)	HRWR Admixture Dosage ( $\text{kg/m}^3$ )
0-NS	635	1	1.04	25	1.02
1.5-NS	660	1	1.00	19	2.05
3-NS	635	1	0.79	25	3.24
4.5-NS	635	1	1.00	25	4.33
6-NS	648	1	1.80	38	5.75
7.5-NS	635	1	2.70	38	7.37

As it is shown in Table 4.1, admixture dosage increased with increases in nano-silica content. The slump flow diameters of the studied mixtures varied in the range of 635 to 660 mm, well within the target slump flow of  $635 \pm 25$  mm. It took less than 2.66 seconds for all concretes to reach 50 centimeter diameter. J-ring results ranged from 19 mm to 38 mm, well within the limit of 51 mm. The observed visual stability indices were 1, indicating stable. No segregation, bleeding, or coning was observed in any of the studied SCCs.

#### ***4.1.2 Compressive Strength***

Compressive strength test established by American Society of Testing Materials (ASTM C39) is used to determine the compressive strength of moist-cured cylindrical specimens. The results of this test are used as a basis to characterize maximum resistance of concrete specimen to a uniaxial loading. Compressive strength is mainly affected by concrete ingredients and proportions, degree of hydration reactivity, densification (void content), water-cement-ratio, curing and environmental conditions, age of concrete, and interfacial zone between aggregate and paste.

There are a number of studies on compressive strength of nano-silica contained pastes, mortars, and concretes. Zhang and Islam showed that early-age (1 through 28 days) strengths of cement pastes, mortars, and concretes were increased by using a small amount of nano-silica (Zhang and Islam, 2012). Higher strength at early ages, through addition of nano-silica, were attributed to accelerated cement hydration and pozzolanic reaction, reduced pores, and improved interface bonding between hardened cement paste and aggregates (Zhang and Islam, 2012). Qing et al. (Qing et al., 2007) studied the properties of hardened cement paste containing nano-silica. In this study, the authors

concluded that nano-silica made cement paste thicker and accelerated the cement hydration process. Aggregate-paste interface, which is regarded as one of the critical area within the structure of concrete, was significantly improved by addition of nano-silica due to its reactions with free calcium hydroxides (CH), which decreased the orientation of CH crystals and reduced the crystal size of CH gathered at the interface (Qing et al., 2007). Li has also evaluated the influence of incorporating nano-silica on properties of high volume fly ash concrete. He concluded that addition of nano-silica increased the low initial pozzolanic activity of fly ash (Li, 2004). Nazari and Riahi also showed that compressive strength of mixtures containing nano-silica increased due to additional formation of hydrated products in presence of nano-silica particles (Nazari and Riahi, 2011).

Early age strength gain was observed by Usyal et al. when the authors used a combination of fly ash and nano-silica as a partial replacement of Portland cement. The surface of the mixtures containing nano-silica and fly ash acted as nucleation sites for the early reaction products of calcium hydroxide and calcium silicate hydrates, which accelerated hydration of cement clinkers (especially  $C_3S$ ) and consequently increased the early age strength (Usyal et al., 2012).

#### **4.1.2.1 Compressive Strength of Studied Nano-Silica Contained SCCs at 28-, 90-, and 180-Day Curing Ages**

For the purpose of this study, a total of forty-eight 28-, 90-, and 180-days moist-cured cylindrical samples containing different dosages of nano-silica were tested in compression. The average compressive strength test results and the percent difference between 28- to 90- and 90- to 180-day curing ages are presented in Table 4.2, while the



average strengths as a function of nano-silica content are shown in Figure 4.1. Individual sample's compressive strengths are presented in Appendix B.

Table 4.2: Average Compressive Strength Comparison of SCCs (MPa)

Mixture Designation	28-Day	90-Day	180-Day	% Gained from 28 to 90	% Gained from 90 to 180
0-NS	55.5	70.9	81.6	28	15
1.5-NS	57.6	72.4	80.3	26	11
3-NS	59.5	72.5	82.5	23	12
4.5-NS	64.3	74.9	84.3	17	12
6-NS	66.6	76.5	85.8	15	12
7.5-NS	72.5	83.9	90.2	16	7

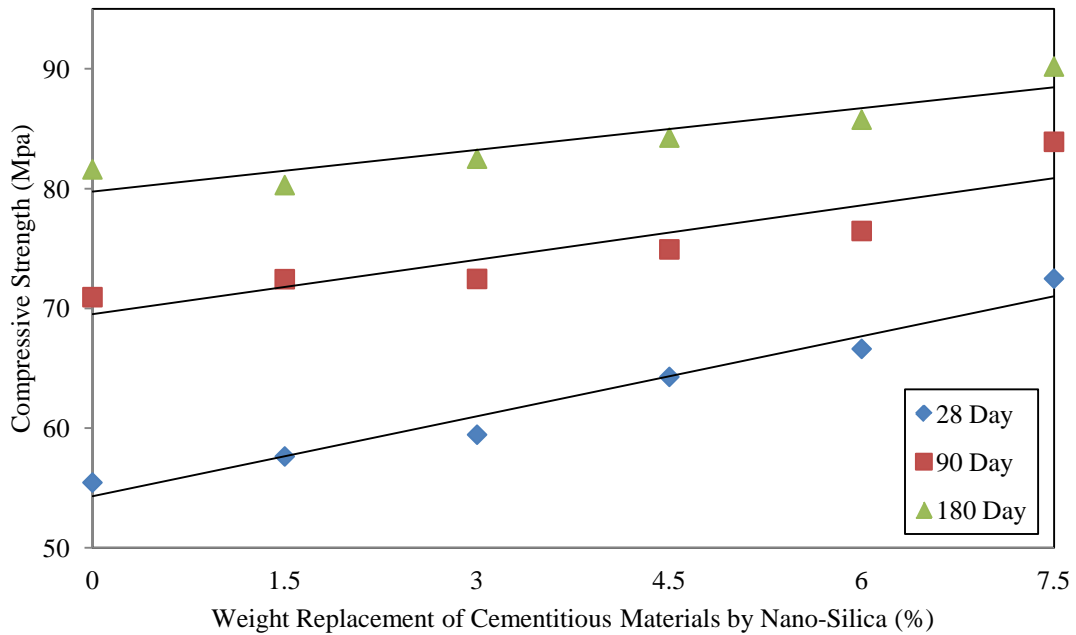


Figure 4.1: Average Compressive Strength Comparison of Studied SCCs

Table 4.3 presents the percent difference in compressive strength between nano-silica contained SCCs and control SCC at curing ages of 28 through 180 days.

Table 4.3: Percent Increase in Compressive Strength between Nano-Silica and Control SCCs

Mixture Designation	% Gained from Control at 28 Day	% Gained from Control at 90 Day	% Gained from Control at 180 Day
1.5-NS	3.9	2.1	-1.6
3-NS	7.2	3.4	1.1
4.5-NS	15.9	5.6	3.3
6-NS	20.1	7.8	5.1
7.5-NS	30.7	18.3	10.5

The results show that the overall increase in compressive strength with each 1.5% by weight replacement of cementitious materials with nano-silica was moderate at 28-day curing age. The 28-day compressive strength increases ranged from 4 to 31% when nano-silica contained SCCs compared to that of control SCC. Mixture 1.5-NS had only 4% increase in compressive strength from that of the control SCC. From this point on, for every 1.5% replacement level of cementitious materials by nano-silica up to 6%, an average of 5% increase in compressive strength was observed when compared to that of control SCC up to mixture 6-NS. Nearly a 10% increase in compressive strength was observed once nano-silica content increased from 6 to 7.5% as a percentage of cementitious materials.

The improvement in the 28-day strength of the SCCs can be attributed to the rapid consumption of free calcium hydroxide ( $\text{Ca}(\text{OH})_2$ ) by reactive nano-silica particles and formation of larger calcium silicate hydrate crystals, which ultimately improved the pore structure by filling up the capillary pores and by thickening of paste. Moreover, incorporation of nano-silica in all concretes containing fly ash resulted in an accelerated

pozzolanic activity of fly ash earlier than anticipated; resulting in production of additional C-S-H compounds to increase compressive strength.

Another reason for 28-day compressive strength improvement of nano-silica contained SCCs is the fact that nano-silica particles are smaller in size than cement and fly ash and are capable of reducing volume of larger pores in the cement paste. As mentioned in Chapter 3 of this study (section 3.4), increasing a portion of cementitious materials by nano-silica has created finer particle size distribution of studied concrete (see Figure 3.4 in Chapter 3). The finer particle size distribution of nano-silica enhanced the pore structure of concrete and filled various size voids. Pore structure refinement by nano-silica not only was achieved by transformation of calcium hydroxide into smaller calcium silicate hydrates (chemical effect), but it was also attained by filler effects of nano-silica (physical effect).

The compressive strength test results of the studied SCCs at 90-day curing age demonstrated marginal improvements when compared to those of 28-day results. The 90-day compressive strength increase ranged from 2 to 18% when nano-silica contained SCCs compared to that of control SCC. On average, for every 1.5% replacement of cementitious materials, an increase of 2% in compressive strength was observed up to Mixture 6-NS as compared to that of control SCC. Mixture 7.5-NS showed a nearly 10% increase in compressive strength when compared to that of Mixture 6-NS. This improvement was nearly a half of that was observed for the 28-day cured nano-silica contained SCCs. The compressive strength of control SCC gained higher improvement in compressive strength when compared to nano-silica SCCs. The gain in 90-day compressive strength gradually reduced with increase in nano-silica content. The

reduction in 90-day compressive strengths of nano-silica SCCS, as compared to that of the control concrete, can be attributed to the reduced reactivity of nano-silica and increased reactivity of fly ash. This attribute is also responsible for the difference between 90-day and 28-day nano-silica contained concretes.

The 90-day compressive strength increase ranged from 1 to 10% when nano-silica contained SCCs compared to that of control SCC. On average, for every 1.5% replacement of cementitious materials, an increase of 2% in compressive strength was observed up to Mixture 6-NS as compared to that of control SCC. Mixture 7.5-NS showed a nearly 5% increase in compressive strength when compared to that of Mixture 6-NS. For every 1.5% replacement of cementitious materials, 180-day cured nano-silica concrete produced compressive strength that was higher by an average of 11% than 90-day cured specimens. This improvement was nearly a half of that from 28- to 90-day curing age.

The gap between compressive strength of SCCs containing nano-silica and control concretes decreased with increases in curing age. According to Wild et al. (Wild et al., 1995), the difference in strength development in control concrete and concrete containing silica over time can be attributed to the rapid formation of an inhibiting layer of reaction product preventing further reaction of silica with calcium hydroxide beyond 90 days. As a result, it is reasonable to say that compressive strength of SCCs did not improve significantly over time due to reduction in reactivity of silica with free calcium hydroxides. The control concrete had the highest improvement in compressive strength over 180 days of curing; however, the control concrete still produced compressive strength lower than nano-silica contained concretes. The highest strength gain over time

for the control SCC can be attributed to higher content of reactive fly ash in control SCCs than of all other nano-silica contained SCCs. The higher strength gain from 28- to 90-day curing age compared to that of 90- to 180-day curing age indicated that fly ash was mainly reactive between 28 and 90 days of continuous curing. After 90 days of curing, it was apparent that some pozzolanic reaction was still present, yet not as significant as prior to 90 days.

#### **4.1.3 Rapid Chloride Migration Test (RMT)**

Among all rapid test methods to determine chloride ingress in concrete, Rapid Migration Test, which has been elaborated by Tang, proved to be the most precise, simplest, and theoretically clearest test. Migration refers to transport of ions in electrolytes due to the action of an electrical fields as the driving force. In an electrical field, positive ions move toward negative electrode and negative ions to the positive ones. This test method is used to determine chloride migration coefficient in concretes from a non-steady migration experiment. External chloride penetrates into interconnecting pores in concrete as bulk liquid by migration, and chloride ions diffuse further into the saturated pore system. The chloride resistance of concrete is highly dependent on the porosity of concrete in terms of pore size, pore distribution and interconnectivity of the pore system (Cement and Aggregate Concrete Australia, 2009). The chloride migration takes place under three main circumstances. First, the chloride concentration in pore solution must exceed the threshold value, which is also defined as critical value. This threshold value is dependent on inter pore's interconnectivity and composition and availability of the pores solution. Second, concrete has to be moist and contain electrolyte

to permit ion transport. Finally, presence of oxygen is necessary if electrochemical corrosion process is to proceed (Byfors, 1986).

Audenaert et al. (Audenaert et al., 2009) demonstrated that capillary porosity was an adequate parameter to describe the chloride transport in rapid migration test. The authors also noted that connectivity of the pore system had a great influence in resistivity of concrete to chloride ingress. According to a study by Uysal et al., (Uysal et al., 2012) the formation of a less porous, denser microstructure and a discontinuous pore system became critical for reduced chloride ion permeability. King in his study has evaluated the permeability and porosity of concretes containing silica particles. The author concluded that addition of silica fume reduced the size of capillary pores, which increased the possibility of transforming continuous pores into discontinuous ones (King 2012). Yogendran and Langan (Yogendran and Langan, 1987) concluded that micro-silica addition did not necessarily change the pore volume; however, larger pores were subdivided into smaller pores. Nazari and Riahi (Nazari and Riahi, 2011) also stated that the pore structure of concrete was the general embodiment of porosity, pore size distribution, pore scale and pore geometry.

#### **4.1.3.1 Rapid Migration of Studied SCCs at 28- and 90-Day Curing Ages**

For the purpose of this study, twenty-six 28- and 90-days moist-cured samples containing different dosages of nano-silica were tested against chloride ion migration. The chloride ion rapid migration coefficient for 28- and 90-day cured SCCs, the percent difference between chloride ion rapid migration coefficients of nano-silica contained SCCs and the control SCC for both 28- and 90-day curing ages, and the percent difference between 28- and 90-day curing ages chloride ion rapid migration coefficient

results are presented in Table 4.4, while the average migration coefficients as a function of nano-silica content are shown in Figure 4.2. The individual sample results are presented in Appendix B.

Table 4.4: Rapid Migration Coefficients ( $m^2/s \times 10^{-12}$ )

Mixture Designation	28-Day	90-Day	% Reduction from 28 to 90	% Reduction from Control at 28-Day	% Reduction from Control at 90-Day
0-NS	15.56	5.70	63.3	N/A	N/A
1.5-NS	15.05	5.59	62.9	3.3	2
3-NS	14.66	5.48	62.7	5.7	4
4.5-NS	13.7	5.36	60.9	11.9	6.1
6-NS	12.74	4.78	62.5	18.1	16.3
7.5-NS	10.01	4.11	59	35.6	28

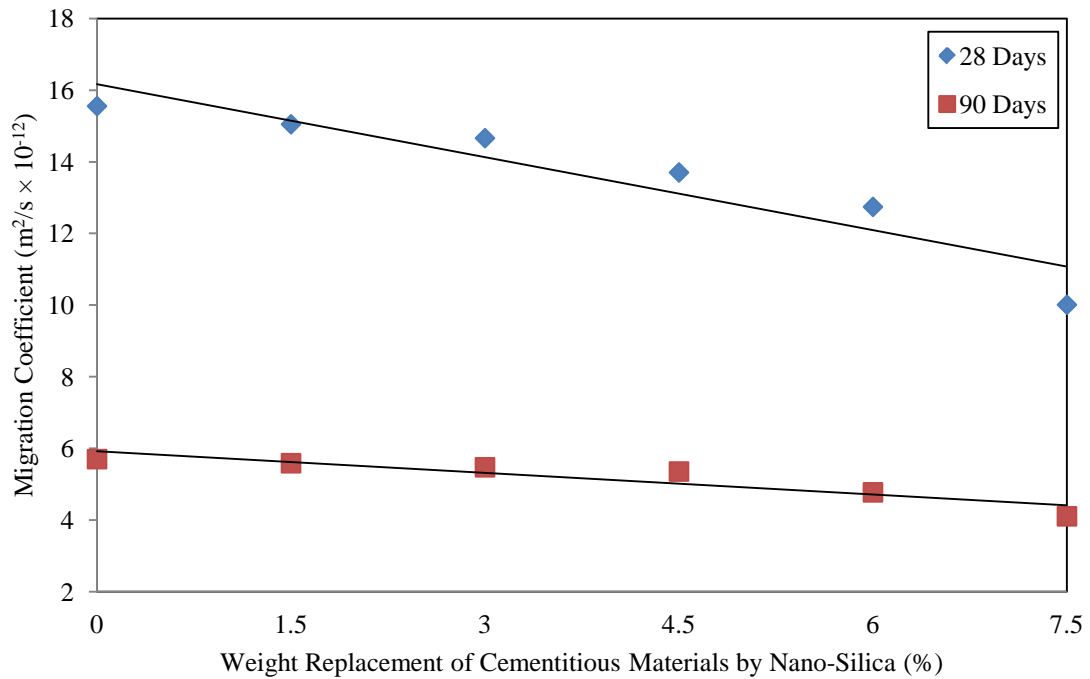


Figure 4.2: Rapid Migration Coefficients of Studied SCCs

The results show that the overall decrease in rapid migration coefficients, with each 1.5% by weight replacement of cementitious materials by nano-silica, was moderate at 28-day curing age. The 28-day rapid migration coefficients decreases ranged from 3 to 36% for nano-silica contained SCCs as compared to that of control SCC. Mixture 1.5-NS had only a 3% decrease in rapid migration coefficient from that of the control SCC. Compared to control SCC, nearly 2% reduction in rapid migration coefficient was observed from 1.5 to 3% replacement level of cementitious materials by nano-silica. From 3 to 6% replacement level, nearly 6% reduction in rapid migration coefficient was observed for every 1.5% replacement of cementitious materials by nano-silica; and lastly, 17.5% reduction was seen from 6-NS to 7.5-NS when compared to that of control SCC. A deduction from the results of silica fume contained SCC reported by Edvardson, can support the hypothesis that reduction in communicating/interconnected pores may have caused complexity and difficulty in movement of chloride ions.

It is believed that rapid migration is greatly affected by pore structure and particularly by the connectivity of pores in concrete matrix. As discovered by Edvardson, one possible cause for the increase in resistance and impermeability of concrete specimens to chloride migration is “pore-blocking effect” due to the pozzolanic reaction of secondary cementitious materials, i.e., fly ash and micro silica (Edvardson, 1998). The pozzolanic reactions in concretes containing nano-silica seemed to be able to develop discontinuous pores system more readily at 28-day curing age. Moreover, as Kong et al. concluded, the improvement in microstructure could be due to adsorption effect of nano-silica in a manner that nano-silica particles adsorpted free water in concrete paste, which improved concrete microstructure (Kong et al., 2012). Furthermore, density of interstitial



spaces inside the skeleton of cement particles may have increased by small agglomerates of C-H-S formed in reaction with nano-silica, which consequently blocked connected pores and improved the pore structure (Kong et al., 2012). In addition, nano-silica particles acted as kernels of hydrated products after hydration began. These new products were able to control crystallization by restricting growth of calcium hydroxide crystals and producing C-S-H compounds, which were capable of filling up voids and densifying the pore structure. Another possible explanation for reduction of rapid chloride migration coefficients of SCCs at 28-day curing age may be due to physical effect of nano-silica fine particles. The nano-silica particles were capable of filling the voids, which could provide a denser structure. As mentioned in Chapter 3, the particle size distribution of cement paste of the studied nano-silica SCCs was enhanced with addition of nano-silica.

At the 90-day curing, there was not a significant reduction in rapid migration coefficient from the control SCC to mixture 1.5-NS with approximately 2% decrease. This improvement in reduction of rapid migration coefficient increased in manner that for every 1.5% replacement level of cementitious materials by nano-silica, 2% reduction in rapid migration coefficients was observed up to mixture 4.5-NS. Mixture 6-NS demonstrated a moderate improvement when compared to that of the control SCC with a reduction of almost 16%. This trend continued in a manner that mixture 7.5-NS showed 28% reduction in rapid migration coefficient when compared to that of the control SCC. On the other hand, the rapid migration coefficients of all SCCs, including control SCC, reduced by nearly 62% from 28- to 90-day curing age. A more plausible explanation for the significant and uniform improvement of rapid chloride migration coefficients of all SCCs may be a denser pore structure resulting in decreased permeability. As fly ash

became more reactive with increasing curing age, it consumed more free calcium hydroxides and produced additional C-S-H compounds into the system. The additional C-S-H compounds reduced the size interconnectivity of the pores, resulting in reduced chloride ion rapid migration coefficients.

#### **4.1.4 Water Penetration**

The penetration is a measure of liquids flow through a porous material caused by pressure force. Water penetration has a direct relationship with permeability of concrete. The permeability of concrete depends on pore structure that is a function of pore size distribution and viscosity of the liquid penetrating to concrete (Zhang and Li, 2011). Water permeability and sorptivity are both affected by size and type of pores (Soneby and Nanukhuttan, 2009). Pore connectivity and pore size distribution play a significant role in permeability. Zhang and Li indicated that there are mainly three types of factors affecting the permeability of concrete: 1) factors affecting the original pore structure of concrete such as water-to-binder ratio, mineral admixtures and additive agents, 2) factors affecting the development of pore structure of concrete such as curing condition, age and activity of binders, and 3) penetration condition such as hydraulic gradient and penetration time (Zhang and Li, 2011).

According to a study conducted by Chung, permeability and water absorptivity of silica fume contained concretes decreased by addition of silica fume. This phenomenon was due to the microscopic pore structure resulting from formation of calcium silicate hydrate (C-S-H) upon the pozzolanic reaction of silica fume with free lime during the hydration of concrete (Chung, 2002). King in his study observed that reduction in the size of capillary pores increased the probability of transformation of continuous pores into

discontinuous ones (King, 2012). Zhang and Li observed that permeability of concrete decreased with increasing strength (Zhang and Li, 2011). Toutanji et al. also reported that concretes containing silica fume showed remarkable reduction in permeability due to denser structure of concretes containing silica fume (Toutanji, 1999).

As studied by Ji, nano-silica particles absorbed calcium hydroxide crystals and reduced size and amount of calcium hydroxide crystals, thus making the interfacial transition zone of aggregates and binding paste matrix denser. These particles can also act as nucleus to tightly bond with calcium silicate hydrate gel particles, making binding paste matrix denser (Ji, 2005)

#### **4.1.4.1 Water Penetration of Studied Nano-Silica Contained SCCs at 28- and 90-Day**

##### **Curing Ages**

For the purpose of this study, a total of thirty-six 28- and 90-days 6×6 inches cured cubes containing different dosages of nano-silica were tested against water penetration. The average water penetration results of the studied SCCs, the percent reduction from 28- to 90-day curing age, and the percent difference between the nano-silica contained SCCs and the control SCC at both 28- and 90-day curing ages are presented in 4.5, while individual sample results are presented in Appendix B. Figure 4.3 shows the average maximum depth of water penetrated into the test samples as a function of nano-silica content.

Table 4.5: 28- and 90-Day Average Water Penetration Depths (mm) of Studied SCCs

Mixture Designation	28-Day	90-Day	% Reduction from 28 to 90	% Reduction from Control at 28-Day	% Reduction from Control at 90-Day
0-NS	12.46	9.94	20.2	N/A	N/A
1.5-NS	11.01	7.48	32	11.7	24.7
3-NS	9.03	6.78	24.9	27.5	31.8
4.5-NS	6.04	4.97	17.6	51.6	50
6-NS	3.74	2.74	26.8	70	72.4
7.5-NS	3.28	2.02	38.3	73.7	79.6

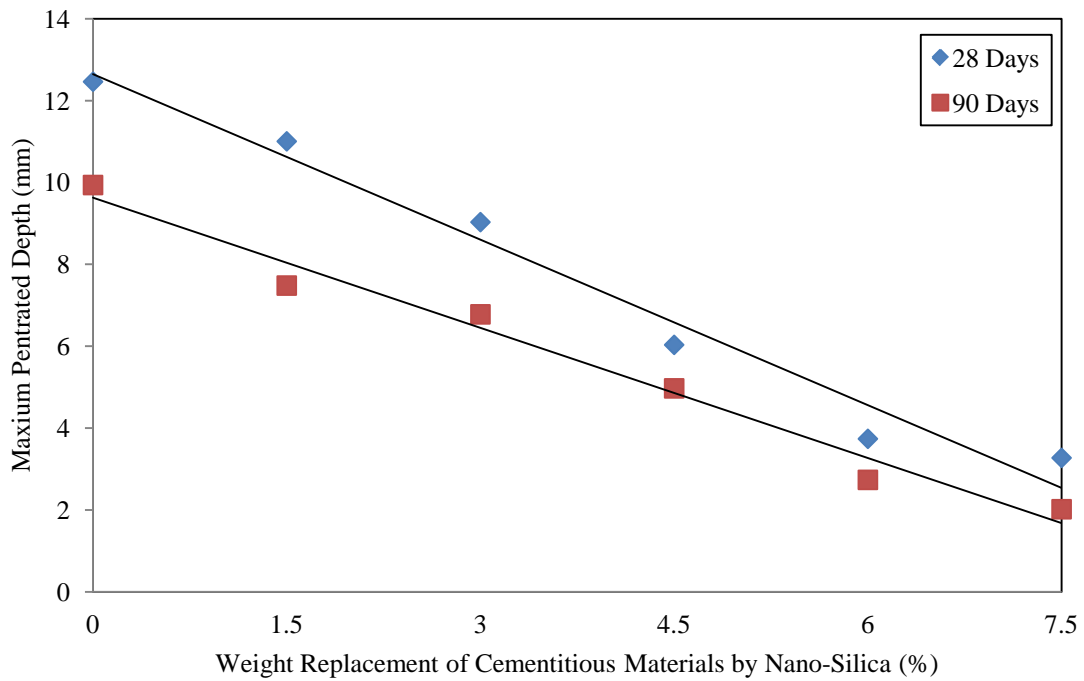


Figure 4.3: Water Penetration Depth of All Concretes

Resistance to water penetration ranged from nearly 12 to 74% when compared to that of control SCC at 28-day curing age. Significant reduction in water penetration depths was observed for all replacement levels of cementitious materials by nano-silica compared to that of control SCC at 28-day curing age up to 6% replacement level. Nearly 12% and 28% increase in resistance to water penetration was observed for Mixture 1.5-

NS and 3-NS from that of control, respectively. Mixtures 4.5-NS showed a significant decrease of 52% from that of control and this difference continued with an increase in partial replacement of cementitious materials up to Mixture 6-NS where the resistance to water penetration was about 70% below than that of control. However, the difference in water penetration depth between Mixture 7.5-NS and the control did not change so much from that of Mixture 6-NS.

The above-mentioned results showed that the permeability of SCCs decreased as nano-silica content increased. According to a study conducted by Chung (Chung, 2002), improvement in permeability was due to improvement of microscopic pore structure resulting from the formation of calcium silicate hydrate (C-S-H), upon pozzolanic reactions of silica with free lime, which strengthened the interface transition zone (between paste and aggregate). As a result, it is reasonable to conclude that addition of nano-silica particles to SCCs modified the pore structure by reducing the size and amount of calcium hydroxide crystals and blocking the connected paths of pores, which resulted in higher resistivity to water penetration under pressure. In addition, it is anticipated, nano-silica particles not only acted as an activator to accelerate cement hydration due to their high reactivity, but also acted as a kernel in cement paste to make the size of calcium hydroxide crystals smaller and the tropism of these crystals more stochastic.

Furthermore, from results of silica fume contained SCC reported by King (King, 2012), it can be deduced that nano-silica was able to reduce the size of capillary pores, which increased the potential of transforming continuous pores into discontinuous blocked pore structures. This physical effect of nano-silica is related to its filling ability

where it acted as a filler to enhance the density of concrete by reducing overall porosity of concrete.

The 90-day water penetration depth of the studied nano-silica SCCs decreased from approximately 25 to 80% when compared to that of control SCC. There was a significant reduction in water penetration depth from the control SCC to mixture 1.5-NS with nearly 25% decrease. Mixtures 3-NS, 4.5-NS, and 6-NS demonstrated more improvement when compared to that of the control SCC with reductions of almost 32, 50, and 72% in water penetration depths, respectively. Similar to the 28-day test results, significant reduction in water penetration depths was observed for all SCC up to mixture 6-NS and only 7% difference between mixtures 6-NS and 7.5-NS was observed when compared to that of control SCC. This improvement is nearly identical to that of observed at 28-day curing age. When the results of 90-day specimens were compared to those of 28-day cured SCCs, an average of 28% reduction in water penetration depth was observed as nano-silica replaced a portion of cementitious materials by weight of 1.5%. This improvement in reduction of water penetration at 90-day curing age can be attributed to continuous pozzolanic reactivity of fly ash with free calcium hydroxides remaining in the system and production of C-H-S crystals reducing the size and amount of available connected pores.

The results of 90-day specimens also revealed that the advantage of nano-silica constrained SCCs over the equivalent control SCC reduced with increasing curing age due to late pozzolanic reactivities of fly ash.

#### ***4.1.5 Capillary Absorption***

This test measures the increase in mass of concrete specimens resulting from absorption of water as a function of time when only one surface of concrete specimens is exposed to water. The rate of ingress of water in this test is largely controlled by absorption due to capillary rise. Capillary is the transport of liquids due to surface tension acting in capillaries. This phenomenon is influenced by viscosity, density and surface tension of the liquid and pore structure (radius, tortuosity and continuity of capillaries) as well as surface energy of the concrete (Cement and Aggregate Concrete Australia, 2009). Generally, concretes with finer pore structures experience greater capillary suction pressures. Mass increase of samples is an indication of absorption of water by concrete specimens. The most significant difference between this test method and Water Absorption test is that in this test only one surface is exposed to water at room temperature while the other surface are sealed simulating water absorption in a member that is in contact with water on one side only. Nano-silica is well-known in reducing size of capillary pores, which increases probability of transforming continuous pores into discontinuous ones (King 2012). This can be explained through presence of small pores in concrete which produces a large capillary force controlling ingress of fluids. Capillary pores are those voids remaining that were originally filled with mixing water. These pores are known to be larger than the C-S-H gel pores and so dominate the transport processes. Yang et al. observed that as the capillary porosity decreases, the capillary pores become smaller and only partially connected (Yang et al., 2006). Water flows within concrete under the action of a capillary force. The strength of the capillary force is determined by the pore structure of the material, yet modified by the local water content.

Therefore, capillary force is strongest when a concrete sample is dry and becomes weaker as the sample saturates (Hall and Yau, 1987).

According to a study conducted by Zhang and Li, with increasing nano-particles ( $\text{TiO}_2$  and  $\text{SiO}_2$ ) content, resulted in decreased total specific pore volume, most likely reduced pore diameter, and weakened refinement on pore structure of concretes (Zhang and Li, 2011). Hall and Yau concluded that water absorption of concrete by the capillary action forces depended on geometry of the porosity (Hall and Yau, 1987). In a study by Sabir et al. pore structure of concrete was examined. These authors revealed that pore system of the cement paste, particularly in the vicinity of the aggregate-paste interface was the most critical feature of the concrete matrix. Aggregates could affect the transport properties of concrete, but they contained discontinuous pores that did not allow water permeability by capillary forces and hence did not contribute to sorptivity (Sabir et al., 1998). These authors also showed that despite the high porosity at the interfacial zone, water movement in concrete was mainly controlled by the bulk of the hardened Portland cement paste, which was the only continuous phase of concrete (Sabir et al., 1998). Yang et al. (Yang et al., 2006) defined capillary pores as those voids remaining that were originally filled with mixing water. The authors believed that early in hydration, the capillary pore space was fully percolated. These pores were much larger than C-S-H gel pores and so dominated the transport processes.

Bentz et al. have discovered that pozzolanic reactions of fly ash and silica contributed to further reduction in capillary porosity of cement pastes containing silica due to their consumption of capillary pore water. Bentz et al. have shown that the relative diffusivity of cement paste was mainly a function of capillary porosity (Bentz et al.,



2000). Thus, as hydration proceeded, the capillary porosity disconnected, while the calcium silicate hydrate became highly percolated.

**4.1.5.1 Capillary Absorption of Studied Nano-Silica Contained SCCs at 28- and 90-**

**Day Curing Ages**

For the purpose of this study, a total of thirty-six 28- and 90-days cured cylinders containing different dosages of nano-silica to replace the same percentage of cementitious materials were tested against capillary absorption of water. The average primary and secondary capillary absorption results obtained for 28- and 90-day curing, the percent reductions from 28- to 90-day curing age, as well as the percent difference between nano-silica contained mixtures and the control SCC are offered in Tables 4.6, and 4.7, respectively. Individual sample results are presented in Appendix B. Figures 4.4 through 4.7 show the primary and secondary absorption of water by SCC specimens.

Table 4.6 summarizes the initial rate of water absorption as the slope of the lines that are the best fit to absorption rate (“I”) plotted against the square root of time. On the other hand, Table 4.7 summarizes the secondary rate of water absorption as the slope of the lines that are the best fit to absorption are “I” plotted against the square root of time.

Table 4.6: Primary Capillary Absorption of Studied SCCs ( $\times 10^{-5}$  mm/s<sup>0.5</sup>)

Mixture Designation	28-Day	90-Day	% Reduction from 28 to 90	% Reduction from Control at 28-Day	% Reduction from Control at 90-Day
0-NS	38.1	35.7	6.1	N/A	N/A
1.5-NS	35	32.8	6.3	8.1	8.2
3-NS	31.6	30.7	2.7	17	14
4.5-NS	26.3	22.1	15.9	30.8	38.1
6-NS	22.7	18.3	19.2	40.4	48.7
7.5-NS	19.5	16.8	13.8	48.8	53

Table 4.7: Secondary Capillary Absorption of Studied SCCs ( $\times 10^{-5}$  mm/s<sup>0.5</sup>)

Mixture Designation	28-Day	90-Day	% Reduction from 28 to 90	% Reduction from Control at 28-Day	% Reduction from Control at 90-Day
0-NS	13.4	9.7	27.4	N/A	N/A
1.5-NS	8	5.8	27.2	40.4	40.2
3-NS	6.9	5.2	24.7	48.6	46.7
4.5-NS	5.8	4.4	25.1	56.4	55
6-NS	5.1	3.5	30.9	62.1	63.9
7.5-NS	4.3	3.1	27.3	68.1	68

Figures 4.4 through 4.7 demonstrate the absorption versus square root of time. The slopes of lines obtained from these graphs determine the initial and secondary rate of water absorption, which are presented in Tables 4.6 and 4.7. The primary capillary absorption refers to the first 6 hours of absorption by samples; whereas the secondary capillary absorption is defined as the slope of the line that is the best fit to absorption rate (“I”) plotted against the square root of time using all measurements from day one to day seven.

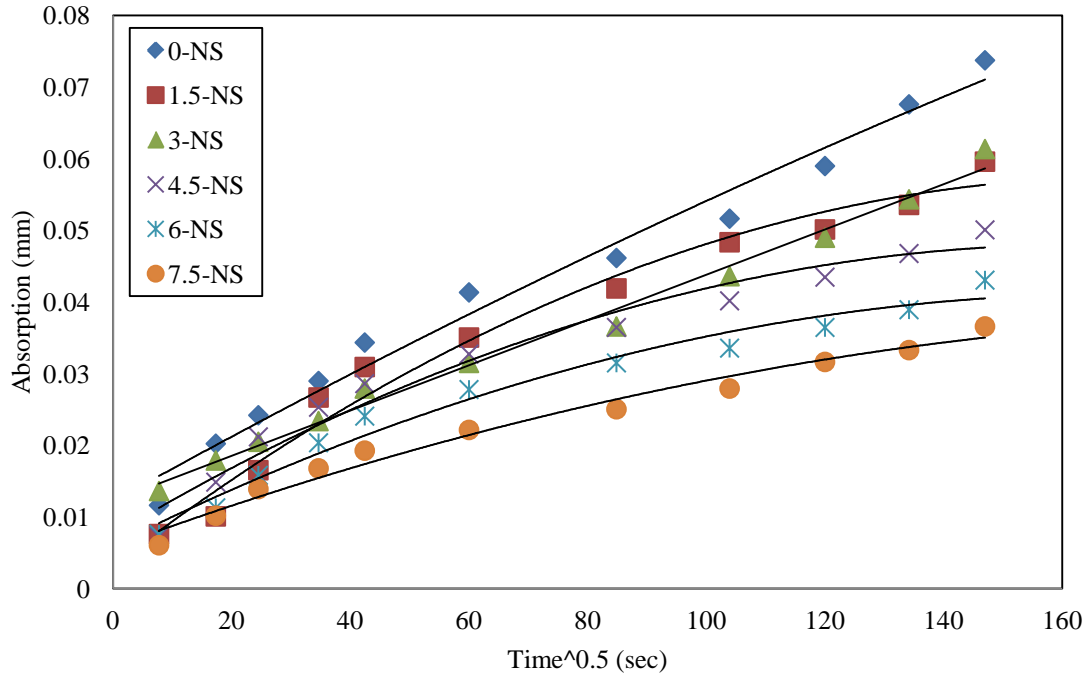


Figure 4.4: Primary Capillary Absorption of Studied SCCs (28-Day Curing Age)

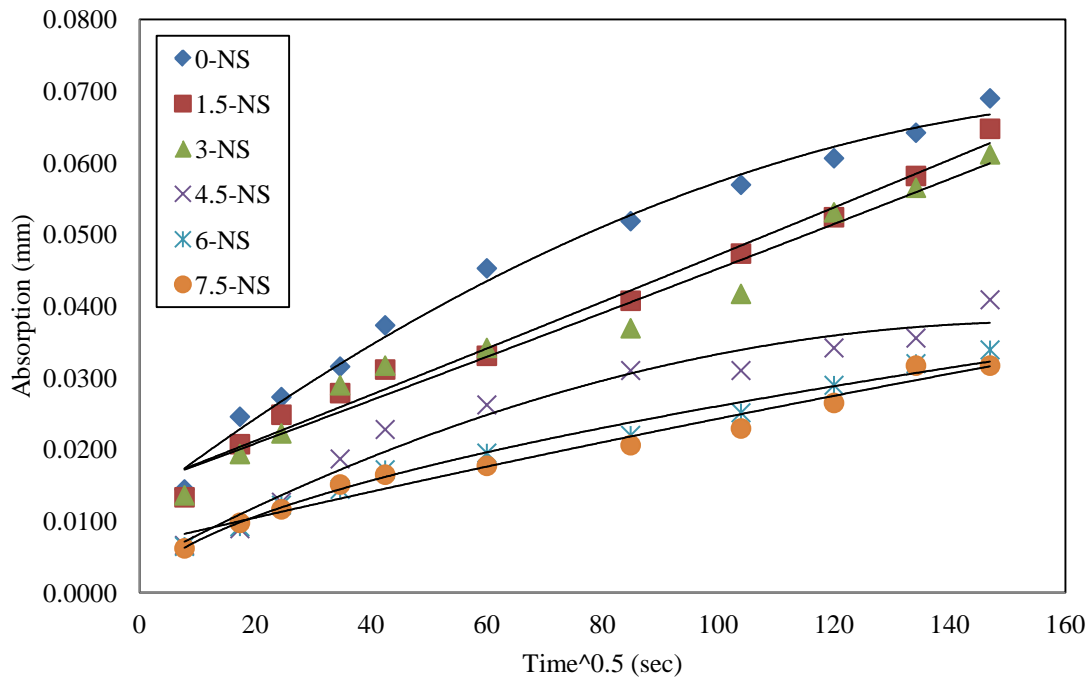


Figure 4.5: Primary Capillary Absorption of Studied SCCs (90-Day Curing Age)

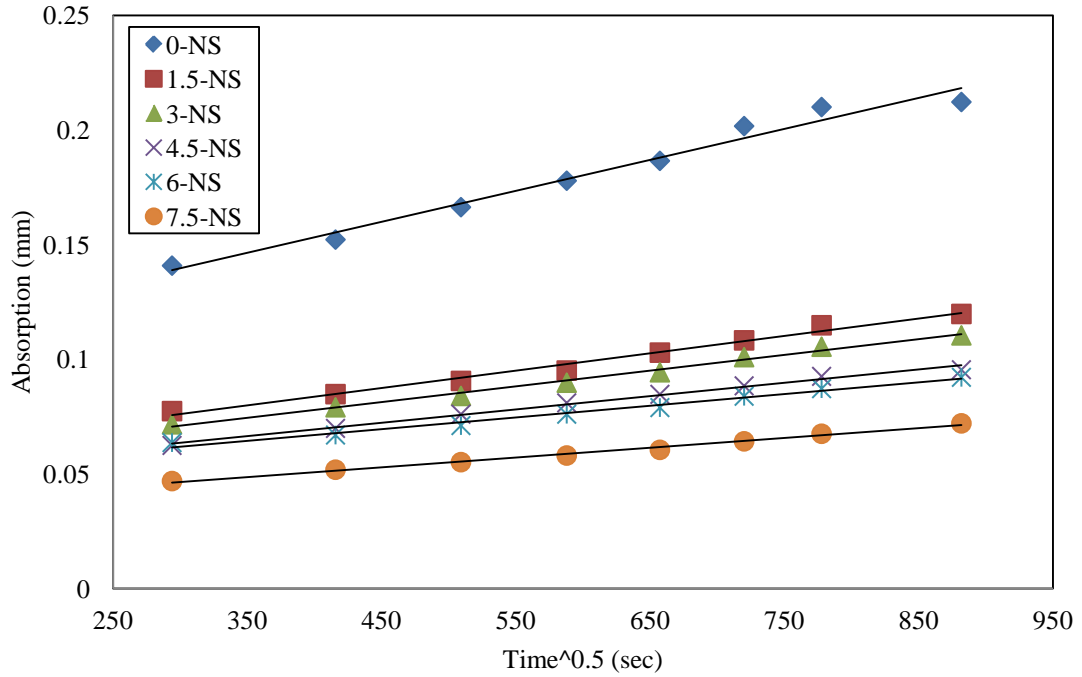


Figure 4.6: Secondary Capillary Absorption of Studied SCCs (28-Day Curing Age)

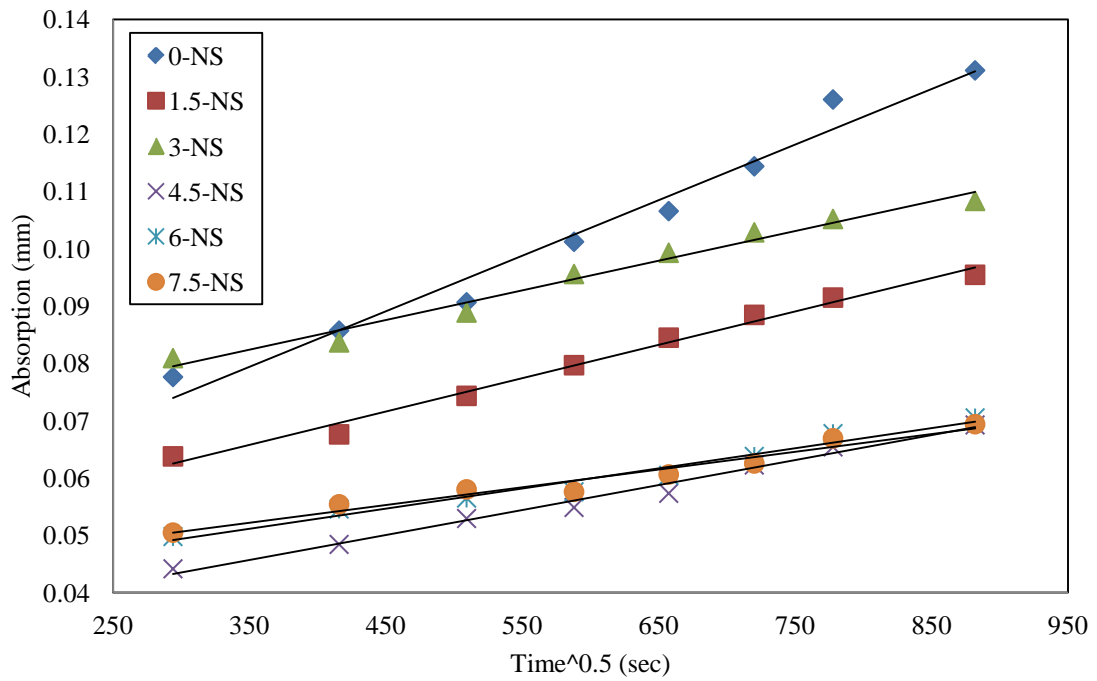


Figure 4.7: Secondary Capillary Absorption of Studied SCCs (90-Day Curing Age)

The overall trend was a decreasing capillary absorption with increasing nano-silica content replacing a portion of the cementitious materials. On average, 10 and 7% reductions in primary and secondary capillary absorption coefficients were observed for every 1.5% replacement of cementitious materials by nano-silica at 28-day curing age when nano-silica contained SCCs were compared to that of Control SCC, respectively.

Similar to water penetration test, the responsible factor for enhancement of concrete to resistance to capillary absorption is the pore structure of concrete. One possible explanation of the overall decreasing primary capillary absorption can be attributed to the highly reactive nano-silica, which was able to reduce size of voids in hydrated cement pastes, thus, making them more impermeable at 28-day curing age by consuming free calcium hydroxides and producing C-H-S crystals.

As reported in Chapter 3, the higher surface area and smaller particle sizes of nano-silica potentially resulted in better packing at interface zones between the cement paste and aggregates. Moreover, nano-silica fine particles may have developed discontinuous and tortuous pores in concrete structure resulting in less absorption of water. Change in the microstructure of the transition zone, reduction of its thickness, associate voids, and microcracks, as well as uniform particle distributions may have been the contributing factors in this test by the addition of nano-silica particles (Kumar, 2008).

The change in primary capillary absorption coefficients of nano-silica contained SCCs from that of control SCC ranged from 8 to 53% at 90-day curing age. On the other hand, 7% decrease in secondary capillary absorption coefficients was observed for every 1.5% replacement of cementitious materials by nano-silica when compared to that of control SCC at 90-day curing age. The results for 90-day curing age displayed a

similar trend to that of 28-day curing with generally decreasing capillary absorption with increasing nano-silica content. In addition, reduction in primary capillary water absorption coefficients for all SCCs from 28- to 90-day curing age ranged from 3 to 19%. Moreover, all SCCs showed nearly 27% reductions in secondary capillary absorption coefficients from 28- to 90-day curing age. Similar reasons (i.e. chemical and physical effects of nano-silica on concrete matrix) may have been responsible for improvement of nano-silica contained SCCs in resistance to capillary water absorption. Fly ash pozzolanic reactivity may have also resulted in production of more C-H-S compounds controlling the connectivity of the pores and pore structure.

#### **4.1.6 Water Absorption**

One of the most important properties of a good quality concrete is low permeability. A concrete with low permeability resist ingress of water (or any liquid) and is not as susceptible to water penetration. It is important to know that permeability of concrete is somewhat different from absorption. Permeability is mostly related to the size of pores, their distribution, and most significantly their continuity. As a result, permeability is not necessarily directly related to absorption; however, water absorptivity, which is more affected by size and type of pores, can have a great effect on permeability of concrete. Volume and size of voids in concrete is the driving factor in this test method regardless of interconnectivity and continuity of pores. The total volume of voids in this test method refers to inter-particle and internal pore volume of particles.

Yogendran and Langan (Yogendran and Langan, 1987) in their studies indicated that micro silica (i.e. silica fume) addition does not necessarily change the pore volume;

however, larger pores are subdivided into smaller pores. As a result, it must be noted that there is a difference between pore structure and pore volume of concrete.

Querica et al. (Querica et al., 2012) have also concluded that nano-silica concretes have very low effective water permeability (less interconnected pores and/or finer pore structure). Yogendran and Langan already reported a similar phenomenon for high performance concrete with silica fume additions, where total porosity was not affected, but permeability was decreased in one order of magnitude (Yogendran and Langan, 2012).

The absorption is divided into three separate tests: absorption after immersion, absorption after immersion and boiling, and volume of air voids. The results of these tests are discussed in the following subsections.

#### **4.1.6.1 Water Absorption after Immersion**

The average absorptions after immersion, percent reduction from 28- to 90-day curing age, percent reduction from control SCC and all other SCCs containing nano-silica at both 28- and 90-day curing ages are given in Table 4.8. The individual results are documented in Appendix B. Figure 4.8 shows the absorption after immersion results of 28 and 90 days curing as a function of replacement percentage of cementitious materials by nano-silica.

Table 4.8: Average Percentage Absorption After Immersion of Studied SCCs

Mixture Designation	28-Day	90-Day	% Reduction from 28 to 90	% Reduction from Control at 28-Day	% Reduction from Control at 90-Day
0-NS	5.98	4.53	24.3	N/A	N/A
1.5-NS	5.72	3.95	31	4.4	12.8
3-NS	5.02	3.68	26.6	16.1	18.7
6-NS	5.24	3.4	35.1	12.4	24.9
7.5-NS	4.72	3.4	28	21.1	25

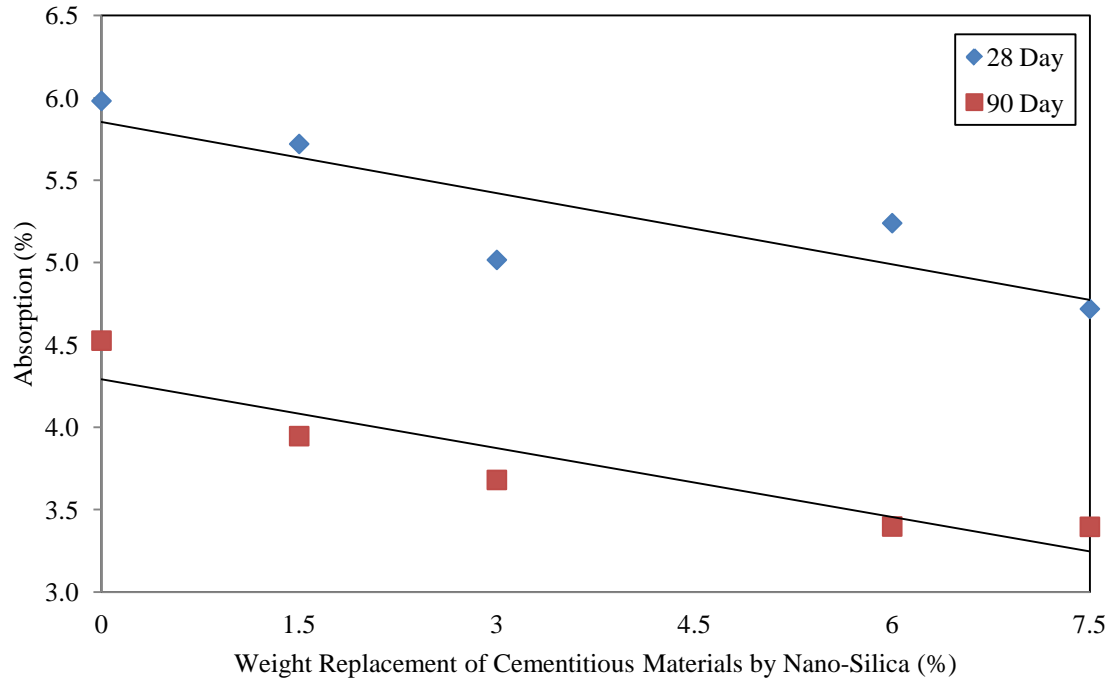


Figure 4.8: Percentage Absorption after Immersion in Water of Studied SCCs

The absorption after immersion results displayed marginal to moderate improvements with nano-silica replacing a portion of the cementitious materials. Mixture 1.5-NS had only 4% decrease in absorption after immersion from that of the control SCC. From this point on, additional replacement of cementitious materials by nano-silica had changes in water absorption after immersion ranging between 12 to 21% when compared to that of the control SCC. Improvement in increasing partial replacement of cementitious materials by nano-silica can be due to its physical and chemical effects. At high replacement levels of cementitious materials by nano-silica, the fine nano-silica particles filled the voids between cement grains much more efficiently than smaller replacement levels. This phenomenon was demonstrated by the particle size distribution curve



presented in Chapter 3. The chemical effect however, can be attributed to ability of nano-silica to produce more C-H-S products, which can better fill up the capillary voids.

At 90-day curing age, the absorption after immersion continued to decrease with increasing nano-silica replacing a portion of the cementitious materials. The percent reduction in water absorption after immersion from the control SCC and all other SCCs containing nano-silica ranged from 13 to 25%. Nearly 20% reduction in water absorption after immersion was observed for every 1.5% replacement of cementitious materials by nano-silica up to Mixture 6-NS. No significant improvement in reduction in water absorption after immersion was observed from mixture 6-NS to 7.5-NS when compared to that of control SCC. On the other hand, nearly 29% reduction in water absorption after immersion was observed from 28- to 90-day curing age for all studied SCC. A fairly uniform reduction in absorption for the 90-day nano-silica contained and control SCCs indicated that the latent pozzolanic reactivity of fly ash was capable to fill the gap between absorption of 90-day nano-silica contained and that of 90-day control SCC.

#### **4.1.6.2 Water Absorption after Immersion and Boiling of Studied Nano-Silica**

##### **Contained SCCs at 28- and 90-day Curing Ages**

Table 4.9 presents the average absorption, percent reduction in absorption from 28- to 90-day curing age, and percent reduction of absorption from control for both 28- and 90-day curing ages of the studied SCCs after immersion and boiling. The individual results for the studied SCCs are documented in the Appendix B. Figure 4.9 demonstrates the absorption after immersion and boiling of 28 and 90 days curing as a function of replacement percentage of cementitious materials by nano-silica.

Table 4:9 Average Percentage Absorption After Immersion and Boiling of Studied SCCs

Mixture Designation	28-Day	90-Day	% Reduction from 28 to 90	% Reduction from Control at 28-Day	% Reduction from Control at 90-Day
0-NS	6.59	5.34	19	N/A	N/A
1.5-NS	6.23	4.95	20.5	5.5	7.3
3-NS	5.75	4.90	14.8	12.7	8.2
6-NS	5.50	4.78	13	16.6	10.5
7.5-NS	5.04	4.64	7.9	23.6	13.1

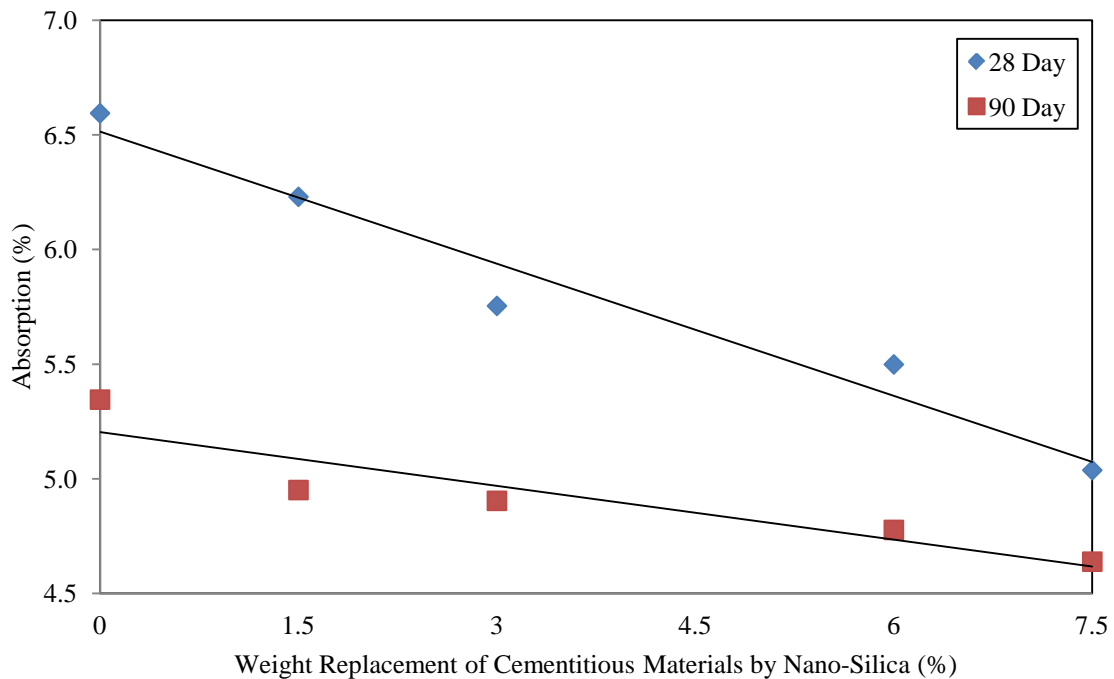


Figure 4.9: Percentage Absorption after Immersion and Boiling in Water of Studied SCCs

The results for 28-day curing of the studied SCCs demonstrated an overall reduction in the water absorbed after immersion and boiling with increasing nano-silica percentage replacing a portion of cementitious materials. However, this reduction was not as significant as compared to other properties earlier reported. When compared to that of

control SCC, reduction in water absorption after immersion and boiling ranged from 5.5 to 24% for all nano-silica contained SCCs. Nearly 6% reduction in water absorption after immersion and boiling was observed for every 1.5% replacement of cementitious materials by nano-silica when compared to that of control SCC. The reduction in absorption after immersion and boiling can be attributed to the similar attributes given to the results obtained for absorption after immersion. The physical effect of nano-silica (i.e. filling ability) allowed for smaller particles to decrease voids between cement grains, thus producing a denser structure. In a similar manner, the increase in production of C-H-S crystals can reduce voids in the system. Lastly, the increase in HRWRA dosage with increasing nano-silica powder content reduced concrete absorption after immersion and boiling due to less mixing water trapped in the system allowing for a better distribution of nano powder particles.

Comparison of 90-day cured nano-silica contained SCCs with that of control SCC revealed that for every 1.5% replacement of cementitious materials by nano-silica, 2% reduction in absorption of water after immersion and boiling was observed. In addition, on average 15% reduction in water absorption was calculated for all studied SCCs from 28- to 90-day curing age. The absorption after immersion and boiling at 90-day curing did not alter significantly between control SCC and nano-silica contained SCCs. The difference in results observed in 28- and 90-day absorption after immersion and boiling is related to fly ash's reactivity. Fly ash reactivity generally does not occur until later curing ages, and when present, produces additional hydrates, which can fill up voids efficiently.

#### **4.1.6.3 Volume of Voids of Studied Nano-Silica Contained SCCs at 28- and 90-day**

##### **Curing Ages**

The volume of voids test follows the absorption after immersion and boiling, and considers the samples suspended weight to determine the total available volume of voids percent by volume of concrete. The average percent volume of voids, percent reduction of these voids from 28- to 90-day curing age, and percent reduction from control SCC to all other SCCs containing nano-silica are presented in Table 4.10. Individual sample results are presented in Appendix B. Figure 4.10 demonstrates the average volume of voids as a function of nano-silica replacing a portion of the cementitious materials for 28- and 90-day cured test samples.

Table 4.10: Percentage Volume of Permeable Pore Space, Voids

Mixture Designation	28-Day	90-Day	% Reduction from 28 to 90	% Reduction from Control at 28-Day	% Reduction from Control at 90-Day
0-NS	15.16	12.63	16.7	N/A	N/A
1.5-NS	14.3	10.91	23.7	5.7	13.6
3-NS	13.1	10.37	20.8	13.6	17.9
6-NS	12.13	9.52	21.5	20	24.6
7.5-NS	11.32	9.26	18.2	25.4	26.7

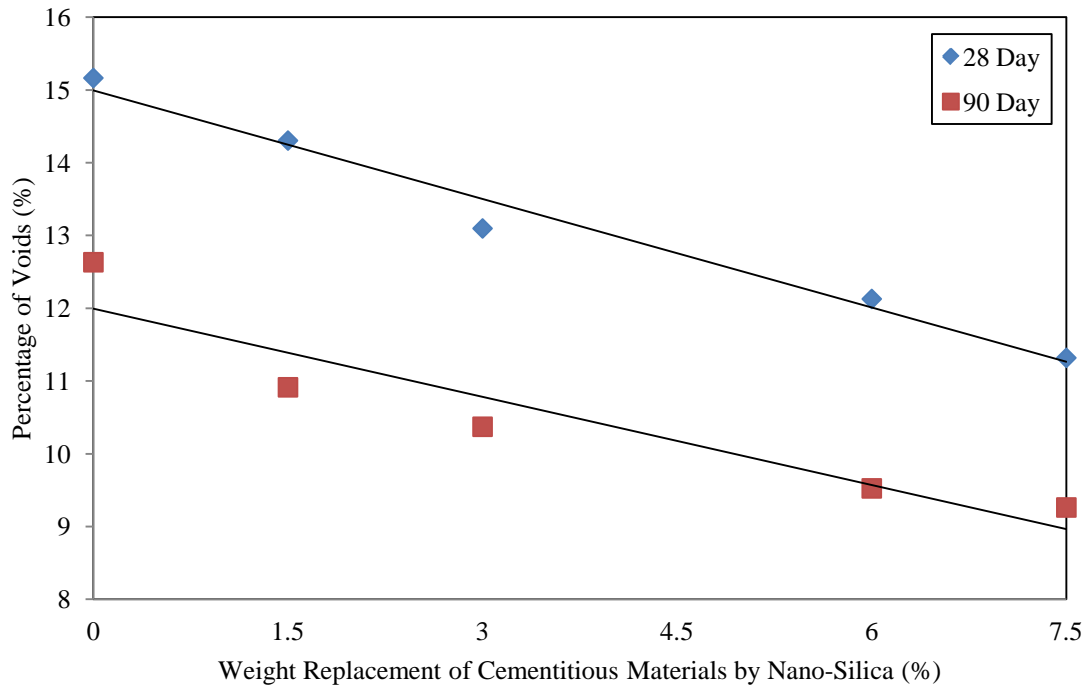


Figure 4.10: Percentage of Voids in Studied SCCs

Comparison of 28-day cured nano-silica contained SCCs with that of control SCC revealed that on average, for every 1.5% replacement of cementitious materials by nano-silica, nearly 6.5% reduction in volume of voids was calculated. As discussed earlier, this improvement can be attributed to formation of C-H-S compounds from reaction of nano-silica particles by calcium hydroxides as well as filling ability of nano-silica particles. The differences between control SCC and nano-silica contained SCCs were similar to the results obtained for absorption after immersion and boiling due to similarity in testing mechanisms.

Addition of nano-silica may have also densified the paste matrix resulting in less voids in cement paste. It is also safe to say that nano-silica acted as a filler occupying pore spaces between grains in the same manner that sand fills the spaces between

particles of coarse aggregates and cement grains fill the spaces between fine aggregate grains.

The 90-day test results of volume of voids revealed that on average for every 1.5% replacement of cementitious materials by nano-silica, 4% reduction in volume of voids was observed when compared to that of control SCC. In addition, nearly 20% reduction in volume of voids was observed from 28- to 90-day curing age for all studied SCCs. A possible explanation for this trend is the available content of fly ash in each studied mixture. Fly ash and calcium hydroxides have the potential to react and form C-H-S crystals that are capable of altering pore structure to some extent. As it was discussed before, combination of nano-silica and fly ash particles elevated transport properties of concretes at 28-day curing age and any improvement thereafter was due to slow pozzolanic activity of fly ash over time.

Although nano-silica particles were able to remarkably reduce the pore volume of concrete mixtures as explained previously for the results attained for Rapid Migration, Water Penetration, and Capillary Absorption tests, most likely the porosity of concrete mixtures was not changed very significantly from 28- to 90-day curing age. It is believed that possibly the continuity of pores in concrete matrices were changed, yet the overall pore volumes did not change drastically. Another explanation for this trend is that by increase in nano-silica content and curing age of concrete specimens, larger pores appeared to have been subdivided into smaller pores.

#### **4.1.7 Rapid Chloride Permeability Test (RCPT)**

In this test, total charge passed through hardened cement matrix over a known time interval is measured, and is then related to chloride permeability by using the

established relationships between the chloride permeability and the total charge passed (Wee et al., 1999). The higher the total charge passes through the hardened cement matrix, the lower its resistance to chloride penetration. Chloride ions migrate inside concrete by way of liquid present in the pores. The pore liquid is a solution containing the dissolved components of hydrated cement (Zofia and Adam, 2013). It is believed that the pore liquid has an electrolyte nature due to presence of several ions such as sodium, potassium, calcium, and hydroxide ions. In RCPT test, all types of ionic movement are measured, which is a drawback and concern associated with this test.

The Rapid Chloride Penetration test is an assessment of concrete's electroconductivity that is affected by chemistry of pore solution, to a large extent, and concrete pore structure, to a lesser extent. Pore structure as discussed earlier is a function of pore size, distribution, and connectivity of pores; which are all affected by hydration of cement, freeze and thaw, and deterioration processes. On the other hand, pore solution is greatly affected by cement composition, supplementary cementitious materials, and inclusion of aggregates (Shi, 2003).

Bentz et al. (Bentz et al., 2000) in a study stated that micro silica (i.e., silica fume) affects both the pore structure and the hydroxide concentration of the pore solution. Ramezani-pour et al. in a study concluded that the conductivity property of the concrete is predominantly governed by the chemical compositions of the pore solutions, although also affected by the pore structure of the concrete (Ramezani-pour et al., 2011). In the same way as aggregates, the hydration products can be considered insulators. Hence, the overall conductivity of concrete is associated with the flow of ions on pore solution. The pore solution provides the paths of least resistance for electrolytic conduction. It is

believed that use of mineral and chemical admixtures can change the composition of the pore solution of concrete (Lizarazo and Lopez, 2011). According to a study conducted by Bentz et al., silica fume not only increased the pore structure discontinuity (high tortuosity and refinement of pore structure), but it also decreased the hydroxide (OH<sup>-</sup>) concentration of the pore solution (Bentz et al., 2000).

**4.1.7.1 Rapid Chloride Permeability of Studied Nano-Silica Contained SCCs at 28- and 90-Day Curing Ages**

The RCPT results of the 28- and 90-day cured control and nano-silica contained SCCs are presented in Table 4.11. Results are presented as the charge passed through the studied SCCs and are measured in coulombs. Lower charges passed indicate higher resistance to chloride ingress. The percent difference between RCPT results obtained for control SCC and nano-silica contained SCCs at both curing ages (i.e. 28- and 90-day) as well as the percent difference from 28- to 90-day curing age of all studied SCCs are presented in Table 4.11. Individual sample results are presented in Appendix B; and Figure 4.11 demonstrates the average charges passed through the SCCs as a function of nano-silica replacing a portion of cementitious materials.

Table 4.11: Total Charge Passed through Studied SCC Specimens (Coulombs)

Mixture Designation	28-Day	90-Day	% Reduction from 28 to 90	% Reduction from Control at 28-Day	% Reduction from Control at 90-Day
0-NS	5651	1507	73.3	N/A	N/A
1.5-NS	4557	1457	68	19.4	3.4
3-NS	4476	1417	68.3	20.8	6
4.5-NS	4049	1434	64.6	28.3	4.9
6-NS	3106	1382	55.5	45	8.3
7.5-NS	2301	1190	48.3	59.3	21.1



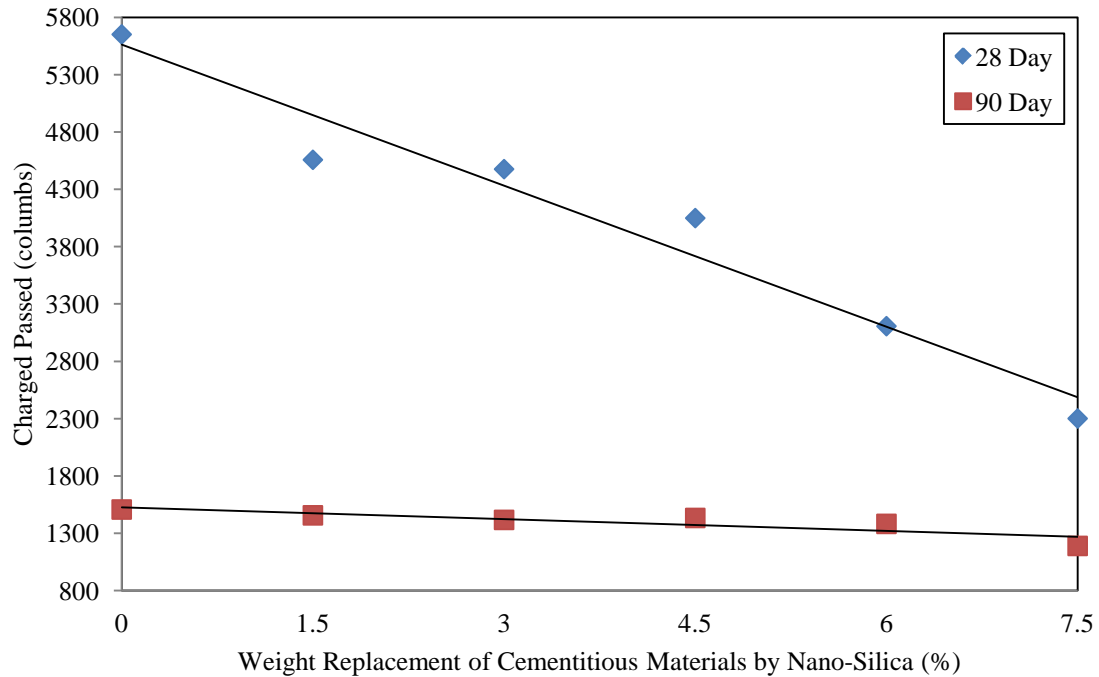


Figure 4.11: Charges Passed through Studied SCCs

Permeation of chloride ions into SCCs reduced with increases in nano-silica content and curing age. On average for every 1.5% replacement of cementitious materials by nano-silica at 28-day curing age, 23% reduction in chloride permeation to the nano-silica contained SCCs, as compared to that of control SCC, was observed up to 4.5% replacement level. Charges passed through Mixtures 6-NS and 7.5-NS were 45 and 59% lower than that of control SCC for 28-day curing age. This improvement of SCCs in resistance to rapid chloride penetration is partially due to pore structure modification of concrete mixtures by addition of nano-silica, which enhanced the interfacial zone of the mixtures due to its pozzolanic reactivity as well as improving the concrete paste through its filler effect. In addition, nano-silica may have affected dilution of pore solution

concentration ( $\text{OH}^-$  used up by chemical reaction) at early age, which caused reduction in electroconductivity of pore solution.

A finer porosity and more precipitated C-S-H gel may have decreased the mobility of the chloride ions into concrete pore solution. Yildirim et al. concluded that lower chloride permeability of the concrete with mineral admixtures such as silica fume is a result of a denser microstructure (Yildirim et al., 2011). As a result, the pozzolanic reaction may have caused lower amount of capillary pores and clogging of the pores, which reduced chloride ion transport in SCCs. Since nano-silica is a finer material than silica fume, the denser microstructure is expected to be attained by nano-silica addition to SCCs.

Results of 90-day rapid chloride penetration test revealed that on average 5% reduction in charges passed through nano-silica contained SCCs when compared to that of control SCC was observed for every 1.5% replacement of cementitious materials by nano-silica up to Mixture 6-NS. Mixture 7.5-NS produced 21% reduction in charges passed through when compared to that of control SCC. The improvement in resistivity of concretes to chloride penetration was more pronounced at 90-day curing. On average, 69% reduction in charges passed through studied SCCs was observed from 28- to 90-day curing age up to mixture 6-NS. Mixtures 6-NS and 7.5-NS showed 56 and 48% reductions in charges passed through them from 28- to 90-day curing age, respectively.

While the results showed a clear trend of improved rapid chloride resistance with an increase in nano-silica content, the individual sample of the same mixture produced higher variations in resistance to chloride penetration than those seen in bulk properties of concretes. It is believed that this variation is due to the electrical potential applied

across the specimen may have heated up the specimen, and because of this, the chloride transportation was significantly accelerated (Wee et al., 1999). It must also be noted that hydroxide ions have a greater ionic conductance than chloride ions. Hence, in a pore solution with a high concentration of  $\text{OH}^-$  ions the test may show misleading results referring to unacceptably high level of chloride permeability. However, the results indicate that the resistance to chloride permeation was increased with increases of nano-silica content of the studied SCCs for both 28 and 90-day curing ages.

The significant reduction in quantity of charge passed through the specimens from 28- to 90-day curing age is mostly due to presence of more pores in solution and more free calcium hydroxide ions and high alkalinity of concrete pore solution at early age. However, at 90-day curing age, most of calcium hydroxide was consumed by reacting with fly ash and the concentration of concrete and associated hydroxide ions in the pore solution decreased significantly, hence, there were less free calcium hydroxide in the pore solution and the pores solution became less electroconductive. Additionally, it is believed that fly ash reduced alkalinity of pore solution over time, which resulted in reduction of electroconductivity. Fly ash reacted with free calcium hydroxide available in pore solution causing fewer ions to migrate through concrete.

#### **4.1.8 Chloride Diffusion Test**

Diffusion is a process by which ions can transport through saturated concrete without flow of water. The driving factor in diffusion is concentration gradients. Diffusion is observed in cases where a concentrated solution is in contact with a more diluted solution; in these cases, ions will migrate between the solutions until they both reach the same concentration. Diffusion in concrete generally refers to transfer of mass of

free molecules or ions in the pore solution resulting in a net flow from regions of higher concentration to regions of lower concentration of the diffusing substance. This transportation mode takes place in fully saturated condition such as fully submerged concrete specimens in salt bath. The most significant factor in diffusion is the concentration gradient of the free chloride ions in the pore solution.

Li et al. (Li et al, 2011) have shown that diffusion of chloride ions is dependent mainly on pore structure of cement paste and ITZ between aggregate and paste matrix. Uysal et al. (Uysal et al., 2012) have shown that chloride ion penetration depends on chloride binding capacity and (ion exchange) of the constituent materials. Chloride ions penetrate into concrete through water filled pores or open pores and some of these ions can react with cement components, mainly tricalciumaluminates ( $C_3A$ ) to form stable chlorocomplexes (Uysal et al., 2012).

#### **4.1.8.1 Chloride Diffusion of Studied SCCs at 28- and 90-Day Curing Ages**

The average chloride content of 28- and 180-day cured SCCs at selected depths are summarized in Table 4.12. Individual sample results are also presented in Appendix B. The percent difference between chloride content of nano-silica contained SCCs and the control SCC for both 28- and 180-day curing ages and the percent difference between 28- and 180-day curing ages chloride content results are presented in Table 4.13.

Table 4.12: Average Chloride Content Measured at Selected Depths of Studied SCCs (gram)

Depth (mm)	0-NS	1.5-NS	3-NS	4.5-NS	6-NS	7.5-NS
28-Day (35 Days in Salt Bath)						
1	0.4336	0.312444	0.316	0.1513	0.15	0.1517
3	0.3588	0.262015	0.2549	0.1477	0.136	0.1352
5	0.2431	0.202651	0.2054	0.1288	0.1262	0.1292
7	0.1939	0.170327	0.1657	0.1159	0.0988	0.1028
9.5	0.1411	0.151453	0.1491	0.1007	0.0938	0.0952
12.5	0.131	0.125878	0.1182	0.1139	0.0651	0.0623
15.5	0.1235	0.117411	0.1006	0.08	0.0867	0.0607
180-Day (60 Days in Salt Bath)						
1	0.3540	0.2143	0.2030	0.1645	0.1579	0.1566
3	0.2914	0.2087	0.1659	0.1463	0.1381	0.1349
5	0.1859	0.1739	0.1369	0.1241	0.1170	0.1143
7	0.1097	0.1066	0.1028	0.0997	0.0976	0.0947
9.5	0.1215	0.1065	0.1027	0.1001	0.0980	0.0938
12.5	0.1070	0.0954	0.0936	0.0951	0.0933	0.0921
15.5	0.1101	0.0978	0.0901	0.0868	0.0817	0.0753

Table 4.13: Percent Reduction from Curing Ages and Control SCC

% Reduction from 28- to 180-Day Curing Age						
Depth (mm)	0-NS	1.5-NS	3-NS	4.5-NS	6-NS	7.5-NS
1	18.36	31.41	35.76	-8.72	-5.27	-3.23
3	18.78	20.35	34.92	0.95	-1.54	0.22
5	23.53	14.19	33.35	3.65	7.29	11.53
7	43.42	37.41	37.96	13.98	1.21	7.88
9.5	13.89	29.68	31.12	0.60	-4.48	1.47
12.5	18.32	24.21	20.81	16.51	-43.32	-47.83
15.5	10.85	16.70	10.44	-8.50	5.77	-24.05
% Reduction from Control at 28-Day						
Depth (mm)	0-NS	1.5-NS	3-NS	4.5-NS	6-NS	7.5-NS
1	N/A	27.94	-1.14	52.12	0.86	-1.13
3	N/A	26.97	2.72	42.06	7.92	0.59
5	N/A	16.64	-1.36	37.29	2.02	-2.38
7	N/A	12.16	2.72	30.05	14.75	-4.05
9.5	N/A	-7.34	1.55	32.46	6.85	-1.49
12.5	N/A	3.91	6.10	3.64	42.84	4.30
15.5	N/A	4.93	14.32	20.48	-8.38	29.99
% Reduction from Control at 180-Day						
Depth (mm)	0-NS	1.5-NS	3-NS	4.5-NS	6-NS	7.5-NS
1	N/A	39.46	5.27	18.97	4.01	0.82
3	N/A	28.38	20.51	11.81	5.60	2.32
5	N/A	6.46	21.28	9.35	5.72	2.31
7	N/A	2.83	3.56	3.02	2.11	2.97
9.5	N/A	12.35	3.57	2.53	2.10	4.29
12.5	N/A	10.84	1.89	-1.60	1.89	1.29
15.5	N/A	11.17	7.87	3.66	5.88	7.83

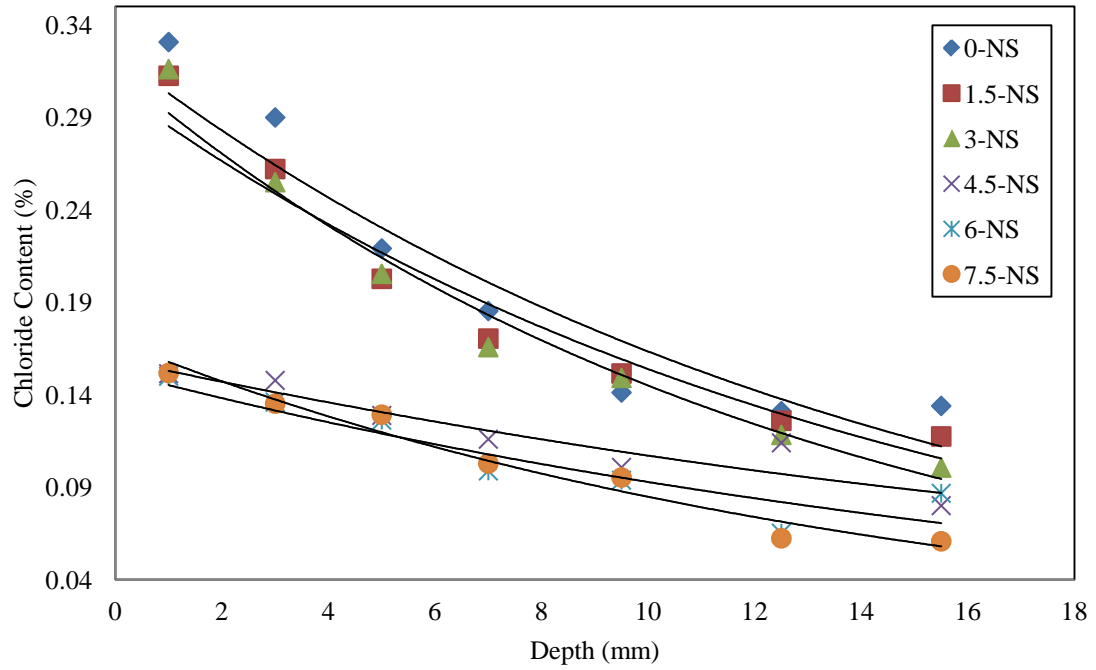


Figure 4.12: Chloride Content of 28-Day Studied SCCs after 35 Days in Salt bath

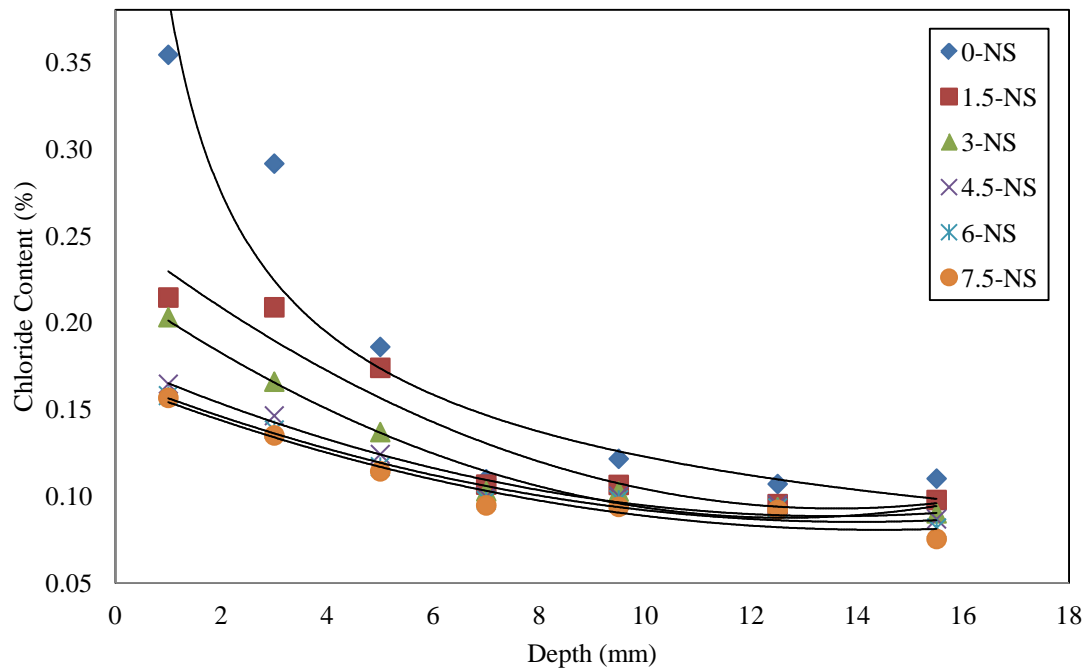


Figure 4.13: Chloride Content of 180-Day Studied SCCs after 60 Days in Salt bath

The 28-day curing results of the studied SCCs indicate a significant reduction of the chloride content. The reduction observed in chloride content of SCCs containing nano-silica is due to physical effect of fine nano-silica particles, which were responsible for formation of less porous, denser microstructure and a discontinuous pore system. An identical trend was observed in Rapid Migration, Capillary Absorption, and Water Penetration test results. Additionally, the nano-particles acted as filler to enhance the density of concrete, which reduced the porosity of concrete. As mentioned in Chapter 3 of this study, increasing nano-silica partial replacement created a finer particle size distribution. The finer particle size distribution of nano-silica enhanced the pore structure of concrete and filled the voids at various size levels.

Nano-silica particles were also able to enhance the concrete pastes chemically by their rapid reaction with free calcium hydroxide, which seemed to be able to create a discontinuous pore system more readily by consuming free calcium hydroxide. In addition, nano-particles acted as kernel in cement paste to make calcium hydroxide crystals smaller and accelerated the cement hydration due to their high activity.

The improvement in resistivity of concrete mixtures to chloride penetration was more pronounced at 180-curing days. Partial replacement of cementitious materials by nano-silica resulted in concrete mixtures with an appreciably lower chloride permeability than control mixture. When compared to the 28-day curing results, the nano-silica exhibited positive influence on reduced chloride diffusion at 180-day curing age. The increased pozzolanic reactivity of fly ash with increased curing age resulted in the formation of additional C-H-S compounds that were responsible for improvement of the pore structure. Connectivity of communicating voids played a huge role in chloride



diffusion at 180-day curing age. Nano-silica particles were able to fill the intergranular space between the cement particles and thus reduce the connectivity and size of the pores system. In addition to refinement of pores, their distribution, and enhancement of pore structure, presence of nano-silica particles may have changed the chemical composition of the pore water and consequently the capacity of binding chloride (Zhang and Gjør, 1996).

#### 4.2 Comparison of Nano-Silica and Micro Silica Based Concretes

Four distinguished tests, in addition to flow properties, were selected to compare the performance and effects of nano-silica with silica fume particles in SCCs. These tests were compressive strength, rapid migration, water penetration, and chloride diffusion. The comparison was made on 28 and 90-day cured samples for both nano-silica and silica fume contained concretes. In addition to transport properties comparison, the degree of reactivity of nano-silica and silica fume was evaluated by performing Thermogravimetric Analysis (TGA) and Differential Scanning Calorimetry (DSC). The comparisons results are presented in the following sections.

##### 4.2.1 Flow Properties Comparison

Table 4.14: Flow Properties Comparison of Nano-Silica and Silica Fume Contained SCCs

Percent NS or SF Replaced	Slump Flow Diameter (mm)		VSI		T <sub>50</sub> (sec)		J-Ring Diameter (mm)		HRWR Admix. Dosage (kg/m <sup>3</sup> )	
	NS*	SF**	NS	SF	NS	SF	NS	SF	NS	SF
0	635	635	1	1	1.04	1.04	25.4	25.4	1.02	1.02
3	635	635	1	1	0.79	0.67	25.4	50.8	3.24	1.54
4.5	635	647.7	1	1	1.01	0.59	25.4	50.8	4.33	1.75
6	647.7	635	1	1	1.81	0.47	38.1	50.8	5.75	1.97
7.5	635	635	1	1	1.66	0.31	38.1	38.1	7.37	2.26

NS\*: nano-silica; SF\*\*: silica fume

The admixtures dosages used for nano-silica contained SCCs were higher than that used for silica fume contained SCCs. This is due to smaller particle size and higher surface area of dry nano-silica particles, which demanded higher dosage of admixture to attain the target flow properties. The amount of time that it took for nano-silica contained SCCs to reach a diameter of 50 centimeter was higher than that of silica fume contained SSCs. Although all concretes had low viscosity ( $2 \text{ sec} < T_{50} < 5 \text{ sec}$ ), silica fume contained concretes had lower viscosity due to the overall larger and broader particle size distribution as mentioned in Chapter 3 of this research study.

#### **4.2.2 Compressive Strengths Comparison**

Average compressive strength of selected SCCs for both nano and micro silica contained SCCs are compared and presented in Table 4.15. Percent increases in compressive strength of SCCs from nano to micro silica are also presented in Table 4.15. Individual sample results are presented in Appendix B. Compressive strength of nano and micro silica are also graphically illustrated in Figure 4.13.

Table 4.15: Compressive Strength Comparison of Nano and Micro Silica Contained SCCs (MPa)

Percent NS or SF Replaced	28-Day		% Increase from NS to SF at 28-Day	90-Day		% Increase from NS to SF at 90-Day
	NS	SF		NS	SF	
0	55.5	55.5	0	70.9	70.9	0
3	59.9	64.9	7.70	73.4	77.5	5.29
4.5	64.3	66.4	3.16	74.9	78.5	4.59
6	67.9	72.1	5.83	77.2	83.1	7.10
7.5	72.5	76.7	5.48	83.9	81.1	-3.45

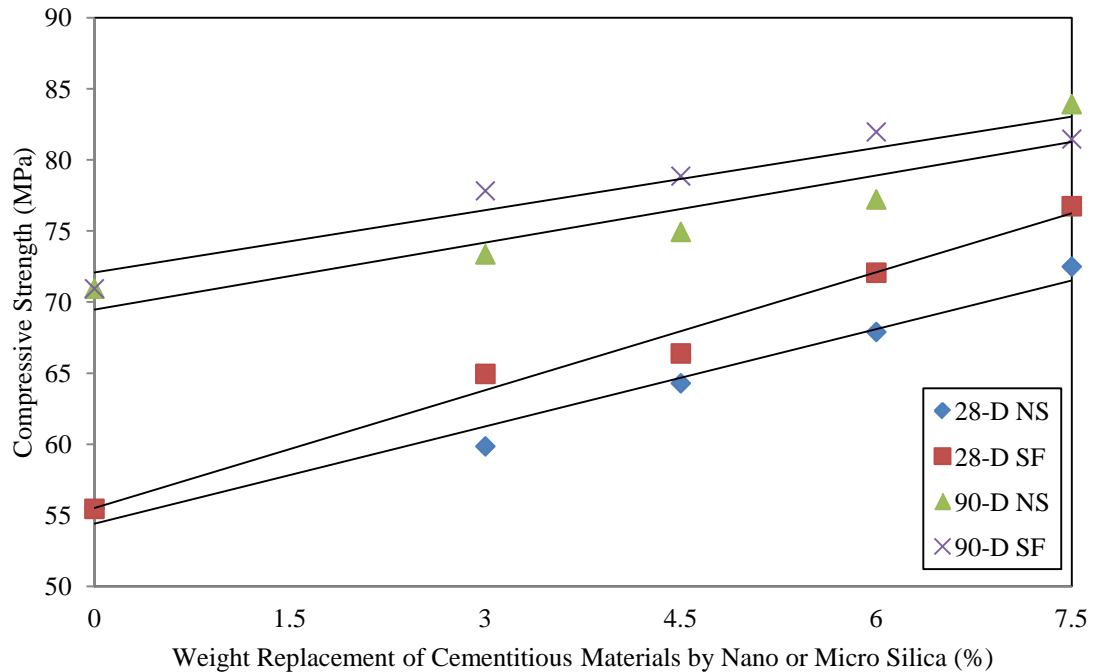


Figure 4.14: Compressive Strength Comparison of NS and SF Contained SCCs

The comparison of compressive strength tests results for both 28- and 90-days curing ages revealed negligible differences in strength gains between nano-silica and silica fume contained concretes. As the replacement for cementitious materials increased from 3 to 7.5%, on average 5% increase in compressive strength was observed for micro silica when compared to that of nano-silica for both 28- and 90-day curing ages. As mentioned in Chapter 3 of this study, the wider particle size distribution of silica fume than that of nano-silica is one possible contributor to higher strength of silica fume contained SCCs than that of nano-silica contained SCCs. As a result, silica fume particles were able to fill various sizes of voids in concrete matrix and produce a denser matrix, which resulted in higher strength. Another possible contributor is the agglomeration caused by difficulties to fully disperse nano-silica particles during mixing. As

summarized in Chapter 3, nano-silica particles were mixed with water and HRWRA in a blender prior to being added to the rest of the concrete ingredients (i.e. fine aggregate, coarse aggregate and fly ash). It is possible that the blender was not capable of de-agglomerating mixed nano-silica with water and as a result, nano particles lose their high surface area due to coagulation. Although dry nano-silica particle sizes provided by the supplier ranged from 15 to 20 nanometer and 97.12% of silica fume particles were finer than 45 micrometer, the nano-silica particles was became highly agglomerated after mixing with water. It is believed that this phenomenon affected both hardened and transport properties of nano-silica contained SCCs by producing relatively poorly organized C-S-H structures.

#### **4.2.3 Rapid Migration Coefficients Comparison**

Average rapid migration coefficients of selected nano and micro silica based SCCs are compared and summarized in Table 4.16 and shown in Figure 4.14, respectively. The percent reduction in rapid migration coefficient from nano to micro silica is also summarized in Table 4.16. In addition, individual sample results are presented in Appendix B.

4.16: Rapid Migration Coefficient Comparison of Nano and Micro Silica Contained SCCs ( $m^2/s \times 10^{-12}$ )

Percent NS or SF Replaced	28-Day		% Reduction from NS to SF at 28-Day	90-Day		% Reduction from NS to SF at 90-Day
	NS	SF		NS	SF	
0	15.56	15.56	0	5.70	5.70	0
3	14.66	13.50	7.92	5.48	5.18	5.40
4.5	13.70	12.90	5.87	5.36	4.99	6.86
6	12.74	11.90	6.62	4.78	4.38	8.30
7.5	10.01	9.20	8.11	4.11	3.74	8.96

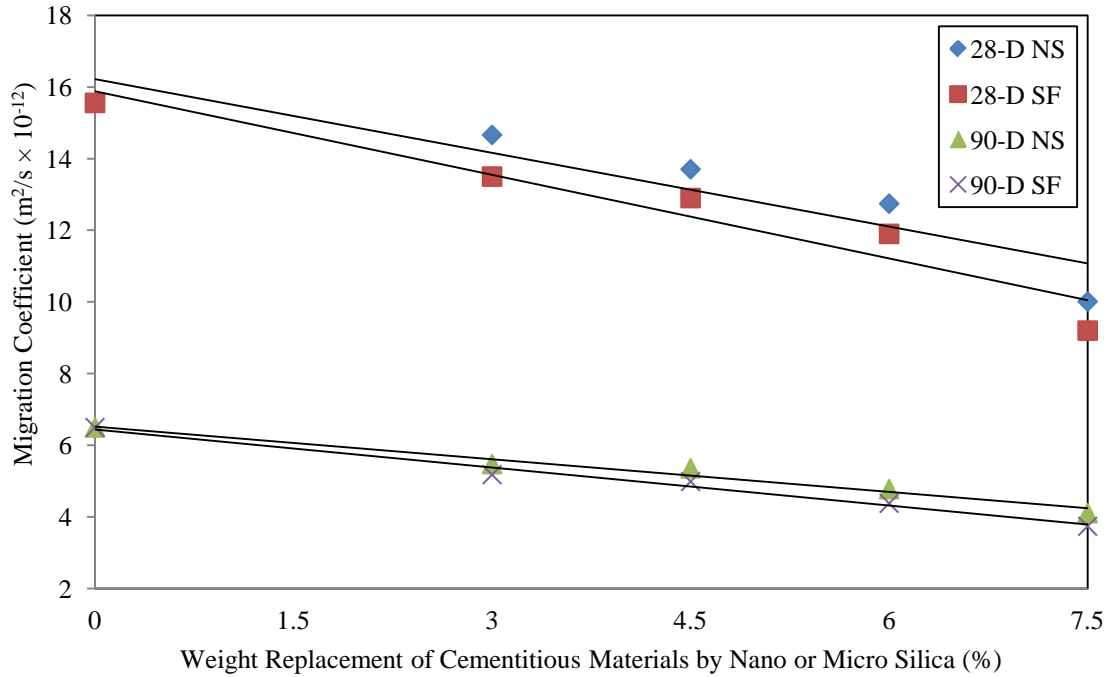


Figure 4.15: Rapid Migration Coefficient Comparison of NS and SF Contained Concretes

In observing 28-day results, silica fume SCCs produced rapid migration coefficients that were lower than those of nano-silica contained SCCs. While no significant variations between low and high replacement of cementitious materials (i.e. 3 vs. 7.5%) were observed, on average, silica fume contained SCCs produced rapid migration coefficients that were nearly 7% lower than that of nano-silica SCCs. A similar trend was observed for 90-day cured specimens. The 90-day cured silica fume contained SCCs produced an average of 7% lower rapid migration coefficient than their equivalent nano-silica concrete. As mentioned earlier, the well-graded size distribution of silica fume, as compared to uniformly graded agglomerated nano-silica SCCs, were able to fill voids more effectively. As discussed earlier in this chapter, reduction in

communicating/interconnected pores has a great influence on chloride ion movements. The agglomerated nano-silica particles also were not able to densify the concrete microstructure to the same extent as silica fume for both 28- and 90-day curing ages, which ultimately resulted in a slightly weaker strength, and lower resistance against rapid chloride emigration for nano-silica contained SCCs.

#### **4.2.4 Water Penetration Comparison**

Average depth of water penetrated into the selected SCCs was measured and compared for both nano and micro silica contained SCCs. The results are tabulated in Table 4.17 and shown in Figure 4.15. The percent reduction in depth of water penetrated into nano-silica SCCs is compared to that of micro silica contained SCCs and presented in Table 4.17. Individual sample results are also presented in Appendix B.

Table 4.17: Water Penetration Depth Comparison of Nano and Micro Silica Contained SCCs (mm)

Percent NS or SF Replaced	28-Day		% Reduction from NS to SF at 28-Day	90-Day		% Reduction from NS to SF at 90-Day
	NS	SF		NS	SF	
0	12.46	12.46	0	9.94	9.94	0
3	9.03	8.48	6.13	6.78	6.48	4.40
4.5	6.04	5.82	3.65	4.97	4.73	4.91
6	3.74	3.31	11.64	2.74	2.52	8.03
7.5	3.28	3.16	3.46	2.02	2.01	-5.61

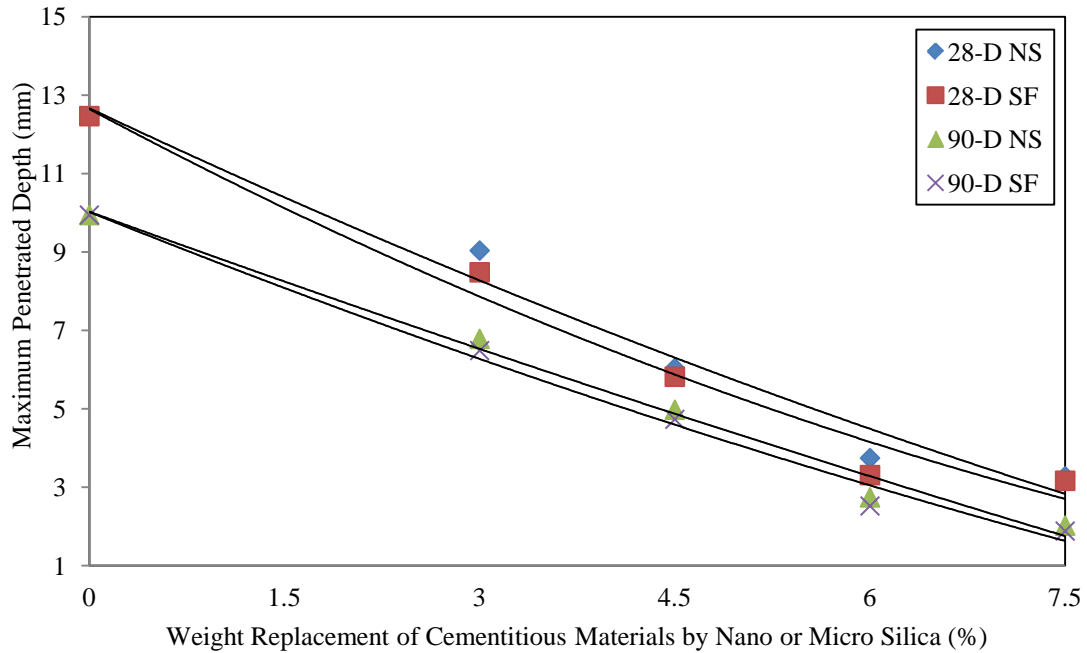


Figure 4.16: Water Penetration Depth Comparison of NS and SF Studied SCCs

The percentage water penetration depth reduction from nano to micro silica contained SCCs varied from 3.5 to 11.5% as their replacement for cementitious materials increased from 3 to 7.5% for 28-day curing age. However, the results revealed that both types of concretes had high resistance to water penetration. The results also showed that the highest reduction in water penetration depth was attributed to 6% replacement level when comparing nano-silica to silica fume contained SCCs. The 90-day curing results indicated 4 to 8% reduction in water penetration depths from nano-silica contained SCCs to the corresponding silica fume-based SCCs. As discussed earlier, although nano-silica particles were finer than of silica fume, the mixing method utilized may have agglomerated nano particles, which ultimately resulted in nano-silica particles not being able to fill pore spaces as effectively as silica fume.

#### 4.2.5 Chloride Diffusion Comparison

Selected mixtures for both nano and micro silica contained SCCs were tested against chloride ion diffusion. Chloride content at selected depths was measured and compared for both nano and micro silica contained SCCs. The results for 28-day curing age is tabulated in Table 4.18 while Table 4.19 presents the chloride content of 180-day cured nano-silica specimens as well as 90-day cured silica fume contained SCCs. Additionally, Table 4.20 presents the percent difference in chloride content between various ages of cured nano and micro silica contained SCCs at the selected depths. Figures 4.16 demonstrate percent difference between 28-day cured nano and micro silica contained SCCs, while Figure 4.17 shows the percent difference between 180-day cured nano-silica and 90-day cured SCCs.

Table 4.18: 28-Day Chloride Content (%) Comparison of Nano and Micro Silica Contained SCCs at Selected Depths

Depth (mm)	Control		3%		4.5%		6%		7.5%	
	NS	SF	NS	SF	NS	SF	NS	SF	NS	SF
1	0.434	0.434	0.316	0.402	0.151	0.378	0.150	0.374	0.152	0.372
3	0.359	0.359	0.255	0.347	0.148	0.297	0.136	0.271	0.135	0.270
5	0.243	0.243	0.205	0.238	0.129	0.208	0.126	0.195	0.129	0.194
7	0.194	0.194	0.166	0.192	0.116	0.140	0.099	0.128	0.103	0.132
9.5	0.141	0.141	0.149	0.121	0.101	0.122	0.094	0.117	0.095	0.117
12.5	0.131	0.131	0.118	0.122	0.114	0.117	0.065	0.112	0.062	0.117
15.5	0.124	0.124	0.101	0.099	0.080	0.110	0.087	0.107	0.061	0.100



Table 4.19: 180-Day Nano-Silica and 90-Day Silica Fume Chloride Content (%)  
Comparison at Selected Depths

Depth (mm)	Control		3%		4.5%		6%		7.5%	
	NS	SF	NS	SF	NS	SF	NS	SF	NS	SF
1	0.354	0.354	0.203	0.224	0.165	0.205	0.158	0.103	0.157	0.102
3	0.291	0.291	0.166	0.215	0.146	0.123	0.138	0.095	0.135	0.100
5	0.186	0.186	0.137	0.158	0.124	0.117	0.117	0.104	0.114	0.098
7	0.110	0.110	0.103	0.131	0.100	0.097	0.098	0.110	0.095	0.087
9.5	0.122	0.122	0.103	0.118	0.100	0.084	0.098	0.091	0.094	0.083
12.5	0.107	0.107	0.094	0.095	0.095	0.081	0.093	0.083	0.092	0.076
15.5	0.110	0.110	0.090	0.089	0.087	0.077	0.082	0.072	0.075	0.070

4.20: Percent Difference in Chloride Content at Selected Depths from Micro to Nano-Silica Contained SCCs

Depth (mm)	28-Day				180-Day NS Compared to 90-Day SF			
	3%	4.5%	6%	7.5%	3%	4.5%	6%	7.5%
1	21.43	59.97	59.87	59.20	9.54	19.76	-53.45	-53.98
3	26.46	49.35	49.83	49.87	22.80	-18.56	-45.06	-34.50
5	13.66	38.02	35.22	33.47	13.46	-5.89	-13.04	-17.23
7	13.47	17.16	22.63	22.36	21.53	-2.89	1.91	-8.60
9.5	-22.92	17.73	19.97	18.84	13.26	-19.88	-7.69	-13.01
12.5	2.88	2.23	41.88	46.62	1.89	-17.26	-12.68	-21.66
15.5	-1.41	27.40	19.05	39.36	-1.81	-13.46	-13.16	-8.03

Negative values in table 4.18 refer to percent reduction in chloride content from nano to micro silica contained SCCs, whereas positive values are indication of percent increase in chloride content from nano to micro silica concrete.

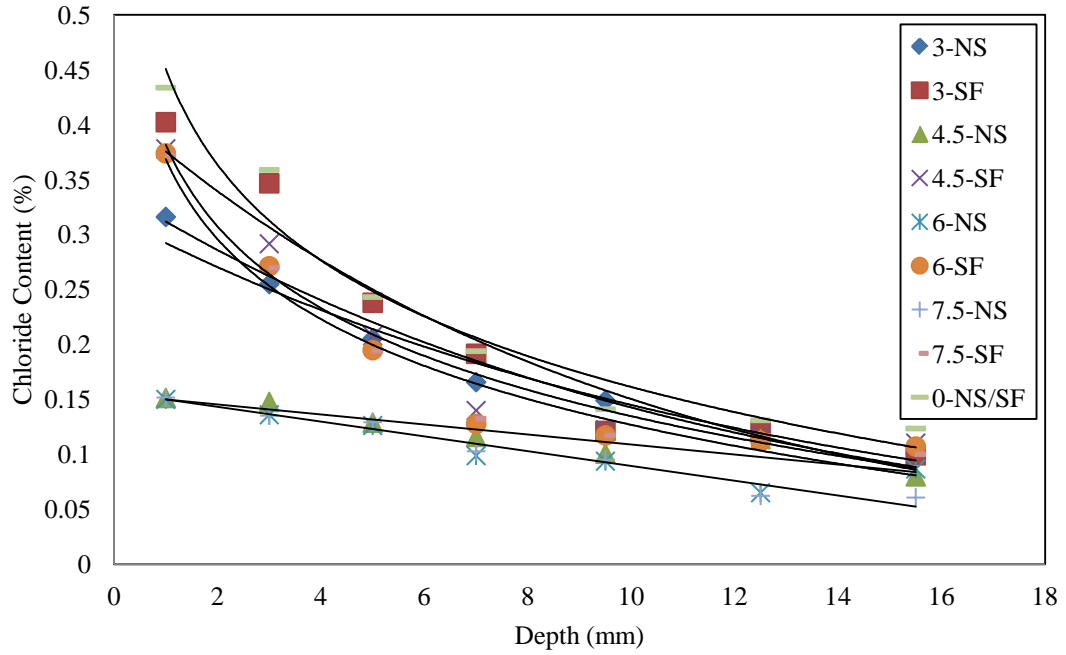


Figure 4.17: Chloride Content of 28-Day Studied Nano and Micro Silica Contained SCCs

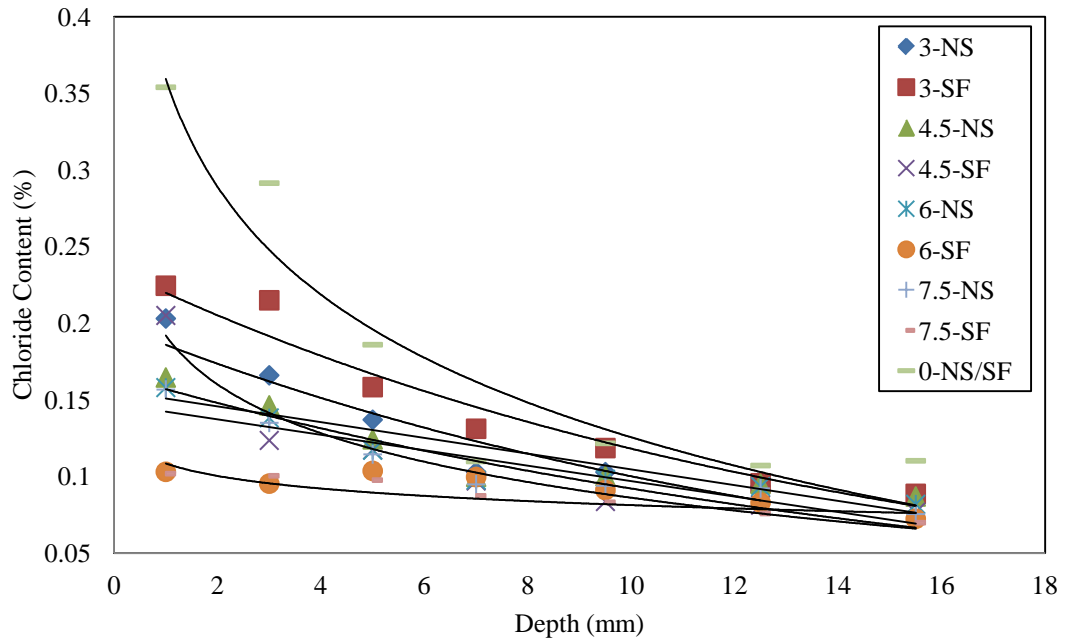


Figure 4.18: Chloride Content of 180-Day Studied Nano-Silica and 90-Day Micro Silica Contained SCCs

Despite the results obtained for previously mentioned tests, the 28-day chloride diffusion test results revealed no reduction from nano to micro silica contained SCCs. This is mainly due to high sensitivity of this test method and high variation in test results. On the other hand, the test results for 180-day cured nano-silica contained SCCs compared to that of 90-day cured silica fume SCCs indicated lower chloride content for silica fume contained SCCs at all selected depths. Although nano-silica contained SCCs were cured for a longer time, silica fume SCCs showed lower chloride content for all replacement levels, mostly after 3% replacement level, and selected depths.

As discussed earlier in this chapter, reduction in interconnected pores has a great influence on difficulty of chloride ion movements. Both mineral admixtures were able to influence the microstructure of concrete matrix, however, one possible reason for better performance of 90-day cured silica fume contained SCCs over 180-day cured nano-silica contained SCCs could be due to agglomerated nano-silica particles which may have not been able to densify the concrete microstructure and to reduce pore spaces of matrix to the great extent silica fume did.

#### **4.2.6 Differential Scanning Calorimetry and Thermogravimetric Analysis**

Further analysis was needed to better understand the behavior of nano-silica and silica fume and their degree of reactivity. The Differential Scanning Calorimetry (DSC) and Thermogravimeter Analysis (TGA) are the most employed test methods to better understand the internal reactions of concrete paste and mortars. Thermogravimetric analysis is used in research and testing to determine the characteristics of cement pastes, the rate of degradation, and absorbed moisture content of materials based on weight

changes. Mass change in materials associated with thermal degradation is quantitatively measured through TGA. Differential Scanning Calorimetry is a thermoanalytical test in which the difference in heat flow rate between a sample and inert reference is measured as a function of time and temperature. In DSC analysis, the crucible temperature increases linearly as a function of time. Once the sample undergoes phase transitions, more or less heat will need to flow to it than to the reference sample to maintain both at the same temperature.

The TGA instrument consists of a highly precised balance with a crucible loaded with the sample. The crucible is placed in a small electrically heated oven with thermocouples to measure the temperature. Analysis is carried out by increasing the temperature gradually and plotting weight against temperature.

Samples containing equal amount of nano-silica and silica fume were prepared. Both samples contained the same amount of lime ( $\text{Ca(OH)}_2$ ) and cured for 28 days. The idea was to detect which one of the two materials consumes higher dosage of calcium hydroxide available in the paste from which the degree of reactivity of the materials could be identified. Table 4.21 summarizes the constituents of nano and micro silica contained samples used for TGA test.

Table 4.21: Constituents of Nano and Micro Silica Contained Samples Used for TGA Test

Nano-Silica Contained Sample			Silica Fume Contained Sample		
Nano-Silica (g)	Lime (g)	Water (g)	Silica Fume (g)	Lime (g)	Water (g)
12.2	150	186.76	12.2	150	146.24

The analysis was done at the FAME-Tech Labs in the University of Nevada, Las Vegas. The TGA/DSC test results are shown in Figures 4.18 through 4.21.

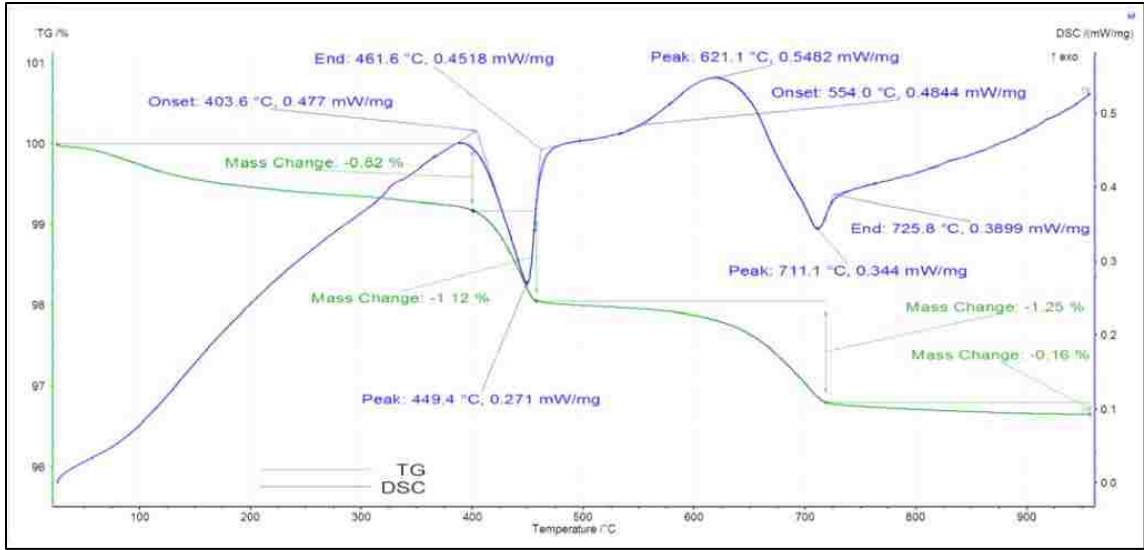


Figure 4.19: Nano-Silica TGA/DSC Test Result (TG Scale in %)

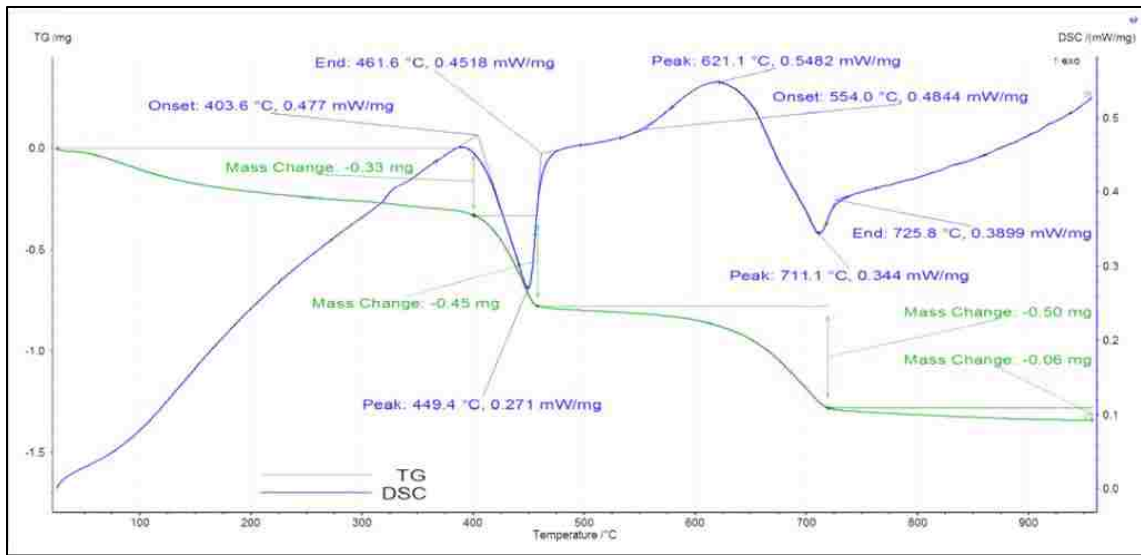


Figure 4.20: Nano-Silica TGA/DSC Test Result (TG Scale in mg)

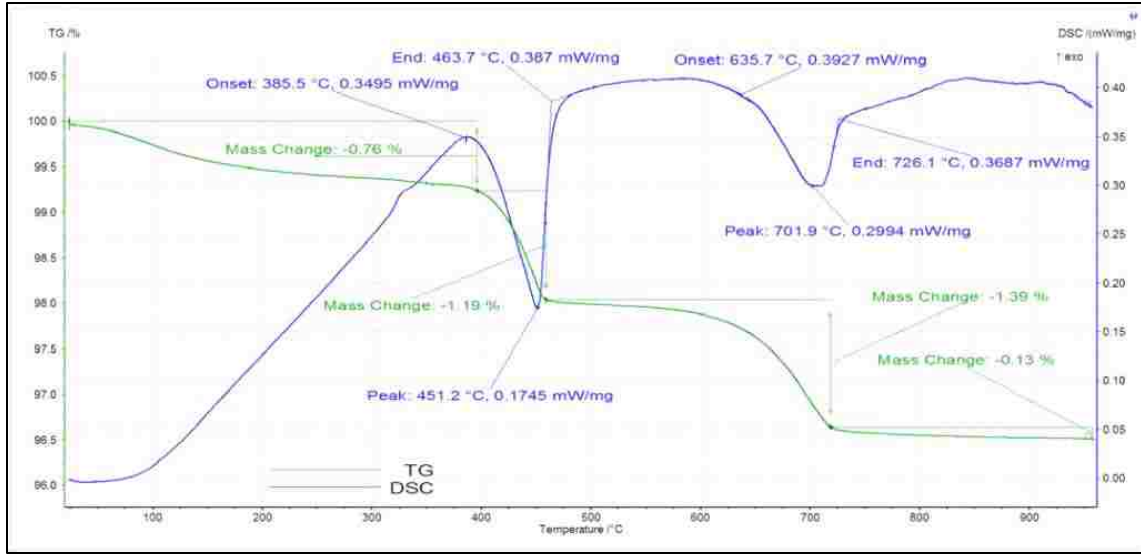


Figure 4.21: Silica Fume TGA/DSC Test Result (TG Scale in %)

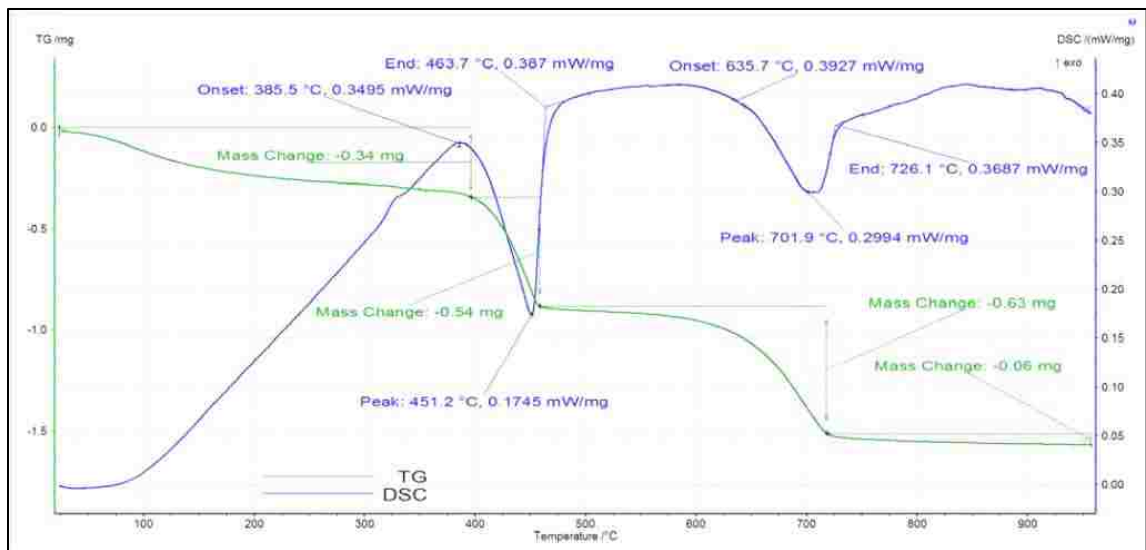


Figure 4.22: Silica Fume TGA/DSC Test Result (TG Scale in mg)

The specimens showed weight loss up to 400°C due to surface water desorption as well as loss of water from C-S-H gel. Further, weight loss at 450°-500°C was due to the thermal decomposition of CH.

The amount of calcium hydroxide ( $\text{Ca}(\text{OH})_2$ ) in the specimen can be calculated directly from the TG curves using the following equation:

$$\text{CH} (\%) = \text{WLCH} (\%) \times \frac{\text{MW}_{\text{CH}}}{\text{MW}_{\text{H}}} \quad (6)$$

where  $\text{WL}_{\text{CH}}$  corresponds to the weight loss attributable to CH dehydration (that is weight loss  $\sim 450\text{-}500^\circ\text{C}$  that is due to the thermal decomposition of  $\text{CH}=\text{Ca}(\text{OH})_2$ ) and  $\text{MW}_{\text{CH}}$  and  $\text{MW}_{\text{H}}$  are the molecular weights of CH (74.01 g/mol) and water (18 g/mol), respectively (Singh et al., 2011). The analysis showed that the nano-silica contained sample contained 4.52% free calcium hydroxide, whereas the silica fume contained sample contained 4.92% free calcium hydroxide. This simply confirmed that the degree of reactivity of the two materials (nano-silica and silica fume) was almost identical.

As alluded to earlier, earlier particle size distribution of nano and micro silica contained SCCs was examined in section 3.2 of this research paper. As it was shown previously in Figure 3.1, silica fume particles sizes ranged from 0.2 to 502 micrometers, and among all of the constituents, higher size concentration was observed for nano-silica particle, which were all within 3.17 to 20 micrometers. The main objective of this analysis was to correlate performance of silica fume compared to nano-silica particles for transport properties of SCCs. It is reasonable to conclude that C-S-H crystals were better improved when micro silica particles were used as compared to nano-silica particles. This was evident by slightly better strength and transport properties displayed by silica fume contained SCCs mainly due to micro silica's wider range of particle sizes and agglomerated of nano-silica when it became in contact with water. As a result, cement paste pores, C-H-S pores and nano-level pores were all better improved by micro silica particles.

As discussed earlier in this chapter, although nano-silica particles were finer particles than micro silica particles prior to mixing, the blending method adopted for this study to disperse nano-silica particles as they became in contact with water was not fully capable of de-agglomerating nano-silica particles. As a result, nano-silica particles were not at their nano level sizes once mixed with other ingredients of the studied SCCs.

### **4.3 Conclusions**

From the results presented in this chapter, the following conclusions can be made.

- The 28-day compressive strength of studied nano-silica SCCs increased from 4 to 31% when compared to that of the control SCC. On the other hand, the 90-day compressive strength of nano-silica contained SCCs improved from 2 to 18% as compared to that of control SCC. The improvement in strength of SCCs at 28-day curing age can be attributed to increased production of C-H-S crystals as well as filling ability of nano-silica particles. The higher strength in 90-day curing age control SCC compared to those of nano-silica SCCs can be attributed to the reduced reactivity of nano-silica and increased reactivity of fly ash over time.

90- to 180-day cured nano-silica concrete produced increases in compressive strengths nearly a half of that from 28- to 90-day curing age. The difference in strength development in control concrete and concrete containing silica over time can be attributed to the rapid formation of an inhibiting layer of reaction product preventing further reaction of silica with calcium hydroxide beyond 90 days. In addition, the highest strength gain over time for the control SCC can be attributed to higher content of reactive fly ash in control SCCs than of all other nano-silica contained SCCs.



- Rapid migration coefficients decreased from 3 to 36% with increasing nano-silica powder replacing a portions of cementitious materials at 28-day curing age. The pozzolanic reactions in concretes containing nano-silica seemed to be able to develop discontinuous pores system more readily at 28-day curing age. In addition, nano-silica particles were capable of filling the voids, which could provide a denser structure. At 90-day curing age, the rapid migration coefficients of nano-silica contained SCCs decreased from 2 to 28% when compared to that of control SCC. The rapid migration coefficients of all SCCs, including control SCC, reduced by nearly 62% from 28- to 90-day curing age. This significant reduction may be a result of denser pore structure due to increase in fly ash reactivity with increasing curing age.
- Water penetration depth levels of nano-silica contained SCCs displayed significant reduction from that of control SCC ranging from 12 to 74% at 28-day curing age and 25 to 80% at 90-day curing age. Nearly 52% difference in water penetration depth was observed between control SCC and Mixture 4.5-NS. Mixtures 6-NS and 7.5-NS showed nearly 70% reductions in water penetration depth when compared to that of control SCC. Decrease in permeability was due to reduction of microscopic pore structure resulting from the formation of calcium silicate hydrate (C-S-H), upon pozzolanic reactions of silica with free lime, which strengthened the interface transition zone (between paste and aggregate). An average of 28% reduction in water penetration depth was observed as nano-silica replaced a portion of cementitious materials by weight of 1.5% when the results of 90-day specimens were compared to those of 28-day cured SCCs. This can be

attributed to continuous pozzolanic reactivity of fly ash with free calcium hydroxides remaining in the system and production of C-H-S crystals reducing the size and amount of available connected pores.

- The overall trend was a decreasing capillary absorption with increasing nano-silica content replacing a portion of the cementitious materials. On average, 10 and 7% reductions in primary and secondary capillary absorption coefficients were observed for every 1.5% by weight replacement of cementitious materials by nano-silica at 28-day curing age when nano-silica contained SCCs were compared to that of Control SCC, respectively. Reduction in primary capillary water absorption coefficients for all SCCs from 28- to 90-day curing age ranged from 3 to 19%. Nearly 27% reduction in secondary capillary absorption coefficients from 28- to 90-day curing age was observed. The smaller particles of nano-silica resulted in improving interfacial zone between the cement paste and aggregates. Moreover, nano-silica fine particles may have developed discontinuous and tortuous pores in concrete structure resulting in less absorption of water.
- The water absorption after immersion, water absorption after immersion and boiling, and volume of voids decreased with increasing nano-silica content at both curing ages. Nearly 20% reduction in volume of voids was observed from 28- to 90-day curing age for all studied SCCs. Fly ash and calcium hydroxides have the potential to react and form C-H-S crystals that are capable of modifying pore structure to some extent. Combination of nano-silica and fly ash particles improved transport properties of concretes at 28-day curing age and any improvement thereafter was due to slow pozzolanic activity of fly ash over time.

It is believed that possibly the continuity of pores and pore shapes in concrete matrices were changed, yet the overall pore volumes did not change drastically. Another explanation for this trend is that through increases in nano-silica content and curing age of concrete specimens, larger pores appeared to have been subdivided into smaller pores.

- On average for every 1.5% replacement of cementitious materials by nano-silica at 28-day curing age, 23% reduction in chloride permeation to the nano-silica contained SCCs was observed when compared to that of control SCC up to 6% replacement level. Charge passed through Mixtures 6-NS and 7.5-NS were 45 and 59% lower than that of control SCC for 28-day curing age. Results of 90-day rapid chloride penetration test revealed that on average 5% reduction in charges passed through nano-silica contained SCCs, as compared to that of control SCC, was observed for every 1.5% replacement of cementitious materials by nano-silica up to mixture 7.5-NS. Mixture 7.5-NS revealed 21% reduction in charges passed through when compared to that of control SCC. On average 69% reduction in charges passed through studied SCCs was observed from 28- to 90-day curing age up to mixture 6-NS. Mixtures 6-NS and 7.5-NS showed 56 and 48%, respectively, reductions in charges passed through them once curing age extended from 28 to 90 days. The significant reduction in quantity of charges passed through the specimens from 28- to 90-day curing age is probably due to presence of more pore in solution and more available calcium hydroxide and high alkalinity of concrete pore solution at early age. However, at 90-day curing age, most of calcium hydroxides were consumed by reacting with fly ash and the concentration

of alkali ions and associated hydroxide in the pore solution decreased significantly, hence, there were less free calcium hydroxide in the pore solution and the pore solution became less electroconductive. Another explanation for decrease in charges passed through specimens at 90-day curing age was due to minor improvement to the pore structure provided by continued reactivity of fly ash producing additional C-H-S crystals.

- Reduction in chloride content of SCCs at selected depths was observed for both 28- and 180-day curing ages when nano-silica contained SCCs were compared to that of control SCC. Additionally, 180-day cured specimens showed significant reduction in chloride content at selected depths compared to their equivalent mixtures cured for 28 days. Filling ability of nano-silica particles as well as transformation of free calcium hydroxide to C-H-S crystals by reacting with nano-silica particles were able to resist chloride ion diffusion at both curing ages. The profound improvement in resistance to chloride diffusion for 180-day cured specimens is mostly due to the increased pozzolanic reactivity of fly ash resulting in the formation of additional C-H-S compounds, which were responsible for improvement of the pore structure.
- Comparison of the results of four distinguished testings (i.e. compressive strength, rapid migration, water penetration, and chloride diffusion) between nano and micro silica equivalently contained SCCs revealed a negligible difference between nano and micro silica performances. From compressive strength results to chloride content of specimens, silica fume contained SCCs showed a minimal superiority over nano-silica contained SCCs. Comparison of 180-day cured nano-

silica contained SCCs with 90-day cured silica fume SCCs in resistance to chloride ion diffusion revealed a significant advantage to silica fume contained SCCs. Although the TGA test showed a minimal difference in reactivity level of nano and micro silica contained samples, it is believed that nano-silica particles were agglomerated during mixing process, which influenced their performance in a nano level as evident through size gradation conducted by Laser Diffraction Size Analyzer. The highly agglomerated nano-silica particles lost their high surface area due to grain growth or loss of the high surface areas where it matters.

## Chapter 5

### Correlations of Variables and Statistical Relationships

This chapter is intended to present statistical analysis obtained from evaluation of the role of mixture constituents and proportions on the studied nano-silica contained self-consolidating concretes. Moreover, statistical relationships between compressive strength and transport properties are summarized in this chapter. Lastly, classifications and a rating system for transport properties of the studied nano-silica contained SCCs are presented.

#### 5.1 Linear Relationship between Compressive Strength and Transport Properties

Linear regression with multiple variable statistical analysis was used to correlate compressive strength and transport properties of the studied nano-silica contained SCCs. Multiple linear regressions was performed to establish relationships between two or more explanatory variable and response variable.

The linear regression equation is generally composed of fit and residual terms. The fit term describes the explanatory variables and can be denoted as  $\beta_0 + \beta_1x_1 + \beta_2x_2 + \dots + \beta_px_p$ , where  $x_1$  and  $x_2$  etc. are the multiple explanatory variables and  $p$  is the number of explanatory variables in the equation. The residual term, however, defines the deviation from observed dependent variable values,  $y$ , from their means. The  $p$ -value is associated with a two-sided test and if an explanatory variable has a  $p$ -value closer to zero, it is more than likely significant.

A adjusted R-Squared ( $R^2$ ) value is used as an indicator of how well the observed data is fitted to the regression line. Higher R-Squared values generally signify better fits of linear models with data. With multiple variables, the R-Squared value can be

misleading, as additional variables will increase the R-Squared value regardless of better or worse fit to the model. The adjusted R-Squared value accounts for the number of predictors in the model and only increases if the new variable improves the model.

Microsoft Excel Regression Analysis tool was used to determine the best linear equation between dependent and independent variables. This unique tool provides R-Squared values, adjusted R-Squared values, explanatory variables coefficients, explanatory variable p-values, and residual plots. These statistical tools were implemented to analyze the effects of nano-silica contained SCC mixture variables on the studied SCC's compressive strength and transport properties. The selected explanatory variables were W/CM (water-to-cementitious materials ratio), NS (nano-silica content replacing cementitious materials), size (average mean particle size of the powder matrix), HRWRA (admixtures dosage in  $\text{kg/m}^3$ ), and age (SCC curing age). By performing multiple linear regressions with the chosen mixture variables, it was possible to examine statistically the extent to which the factors affected individual tests. An example of a multiple linear regression model of compressive strength results is presented in the Appendix C.

All explanatory variables were initially selected for the first trial and the R-squared and adjusted R-squared values were recorded. Explanatory variables with relatively high p-values were then eliminated and regression analysis was repeated. This process was repeated until the optimum adjusted R-squared value was obtained for the model. Some explanatory variables had p-values higher than zero but were found to be significant for optimizing the adjusted R-squared value. Table 5.2 demonstrates the equations for the studied tests obtained by regression analysis. In addition, Table 5.3

demonstrates the final regression analysis with the highest adjusted R-squared value obtained for each individual test.

Subsequent to performing linear regression analysis, correlations between the explanatory variables were investigated. For equations with high correlated variables, one of the variables was omitted and regression analysis was repeated. Table 5.1 summarizes the correlations between the response variables and explanatory variables.

Table 5.1: Correlation for Explanatory Variables

	Age	W/CM	HRWRA	Size	NS
CS	0.87	0.43	0.43	-0.42	0.42
RMT	-0.95	-0.26	-0.26	0.26	-0.25
WP	-0.29	-0.94	-0.93	0.91	-0.94
Cap Abs	-0.35	-0.83	-0.81	0.81	-0.84
% Voids	-0.72	-0.67	-0.66	0.67	-0.67
RCPT	-0.86	-0.38	-0.38	0.38	-0.37
Age	1.00	0.00	0.00	0.00	0.00
W/CM	0.00	1.00	1.00	-0.98	1.00
HRWRA	0.00	1.00	1.00	-0.98	1.00
Size	0.00	-0.98	-0.98	1.00	-0.98
NS	0.00	1.00	1.00	-0.98	1.00

Table 5.2: Equations Resulting from Multiple Regression Analysis of Nano-Silica Contained SCCs

Equation No.	Correlated Equation
1	Compressive Strength (MPa) = 0.138Age+1.988 HRWRA+52.396
2	RMT (10-12) = -0.136Age-0.537HRWRA+19.565
3	Water Penetration (mm) = -0.0313Age-206.039W/CM+124.144
4	Secondary Capillary Absorption = -0.0317Age-1.054HRWRA+12.3137
5	Volume of Voids (%) = -0.0429Age-3.056Size-29.718
6	Rapid Chloride Permeability (Coulombs) = -42.347Age+1529.466NS-16894.3



Table 5.3: Summary of Regression Analyses of Selected Tests

Test	R <sup>2</sup> Value	Adjusted R <sup>2</sup> Value	Influential Variables	Coefficient of Variables	P-Value
Compressive Strength	0.9418	0.934	Intercept	52.3965	2.87E-15
			Age	0.1381	5.38E-10
			HRWRA	1.9883	4.85E-06
Rapid Migration	0.9725	0.9664	Intercept	19.5648	4.38E-10
			Age	-0.1363	3.41E-08
			HRWRA	-0.5375	0.0011
Water Penetration	0.9636	0.9555	Intercept	124.1444	7.31E-08
			Age	-0.03126	0.0012
			W/CM	-206.039	1.33E-07
Capillary Absorption	0.7802	0.7313	Intercept	12.3137	3.70E-06
			Age	-0.0317	0.05121
			HRWRA	-1.0544	0.00057
Volume of Voids	0.9663	0.9566	Intercept	-29.719	0.00032
			Age	-0.043	1.80E-05
			Size	-3.0559	2.60E-05
Rapid Chloride Permeability	0.8905	0.8662	Intercept	-16894.3	0.0277
			Age	-42.3468	2.61E-05
			Size	1529.466	0.0074

Amongst all of the factors, age was the common factor and had the major impact on improvement of studied SCCs. Compressive strength and rapid migration statistical analyses revealed that only age and HRWRA dosage had impact on enhancement of strength of SCCs and their resistance to chloride migration. Among the two, age had the most effective influence. From water penetration test analysis, it was observed that age and W/CM ratio were the two factors affecting the enhancement of SCCs. However, for this test, W/CM ratio played a more significant role than the age. Age, W/CM, and HRWRA all had influential role in improving of resistance of SCCs to secondary capillary absorption of water and reduction of pores. Among these factors, age had the greatest influence. On the contrary, W/CM and nano-silica content were the only two

factors influencing the improvement of SCCs in reduction of percent volume of voids. Age and nano-silica content were the only two factors affecting the improvement of SCCs in impermeation to rapid chloride permeability.

## **5.2 Correlations between the Studied Tests**

The purpose of this section is to investigate correlations between compressive strength and studied transport properties tests. It should be noted that the proposed relationships are valid for the testing results obtained for this study. Correlations are associations between two variables where the association indicates that as one variable's value changes, the other variable's value should also change. A weak correlation refers to occasional change in variables, whereas a strong correlation indicates the frequent change of variables. Correlation between two variables may indicate association; however, it is not causation.

Microsoft Excel was used to determine the correlations between the test results of the studied nano-silica contained SCCs. The correlations between the studied compressive strength (CS) and transport properties which included volume of voids (VOV), secondary capillary absorption (CA), water penetration depth (WP), rapid chloride penetration test (RCPT), and rapid migration test (RMT) are shown in Tables 5.4 and 5.5. Blank spaces shown in the table were left intentionally to avoid repetition of the same correlation value. If the absolute correlation value was closer to magnitude of one, it indicated a strong correlation while a value close to zero indicated a weak correlation. Positive values indicated a positive correlation where changes in value should be observed in the two variables in the same direction. When the correlation value was negative, the two variables change in opposite directions. Table 5.4 presents the

correlation between the studied tests on 28-curing age nano-silica contained SCCs and Table 5.5 summarizes the correlation between the studied tests for 90-curing age nano-silica contained SCCs.

Table 5.4: Correlation between the Studied Tests for 28-Day Cured Nano-Silica Contained SCCs

	CS	RCPT	RMT	WP	VOV	CA
CS	1					
RCPT	-0.97	1				
RMT	-0.98	0.95	1			
WP	-0.96	0.94	0.89	1		
VOV	-0.95	0.97	0.91	0.97	1	
CA	-0.98	0.94	0.91	0.99	0.98	1

Table 5.5: Correlation between the Studied Tests for 90-Day Cured Nano-Silica Contained SCCs

	CS	RCPT	RMT	WP	VOV	CA
CS	1					
RCPT	-0.97	1				
RMT	-0.98	0.96	1			
WP	-0.87	0.83	0.90	1		
VOV	-0.78	0.81	0.82	0.95	1	
CA	-0.73	0.73	0.74	0.93	1	1

As it is seen from Tables 5.4 and 5.5, secondary capillary absorption had the highest positive correlations. Secondary capillary absorption had the highest correlation with water penetration at 28-day curing age and with volume of voids at 90 days of curing. This indicated that as absorption rate decreased, a somewhat similar decrease maybe observed in water penetration results. Rapid chloride permeability test (RCPT) results had a high positive correlation with RMT results with correlation values of 0.95 and 0.96 for 28- and 90-day curing ages, respectively. The high correlation may be a result of rapid chloride penetration and rapid migration being similarly affected by

modification to the pore structure. Correlation of secondary capillary absorption with all other studied tests, except for water penetration and volume of voids, decreased with increase in curing time (see Tables 5.4 and 5.5). Table 5.4 shows that all of the studied tests had high correlations with one another. On the other hand, Table 5.5 shows that those correlations either weakened or strengthened by increase in curing time.

Lastly, compressive strength had high negative correlations with all of the studied tests, which indicates any decrease or increase observed in the studied tests may reflect the opposite trend for compressive strength results. The correlations between the secondary capillary absorption and rapid migration, percent volume of voids, and water penetration tests are shown in Figures 5.1 through 5.3.

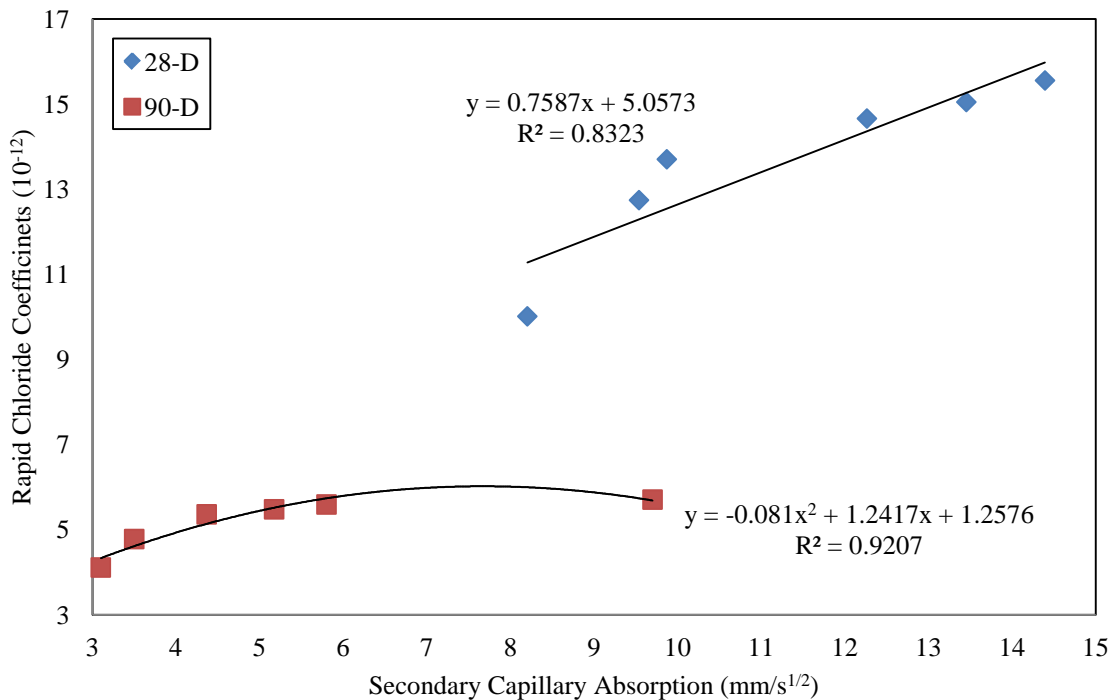


Figure 5.1: Correlation between Secondary Capillary Absorption and Rapid Chloride Coefficients of 28- and 90-Day Cured Nano-Silica Contained SCCs

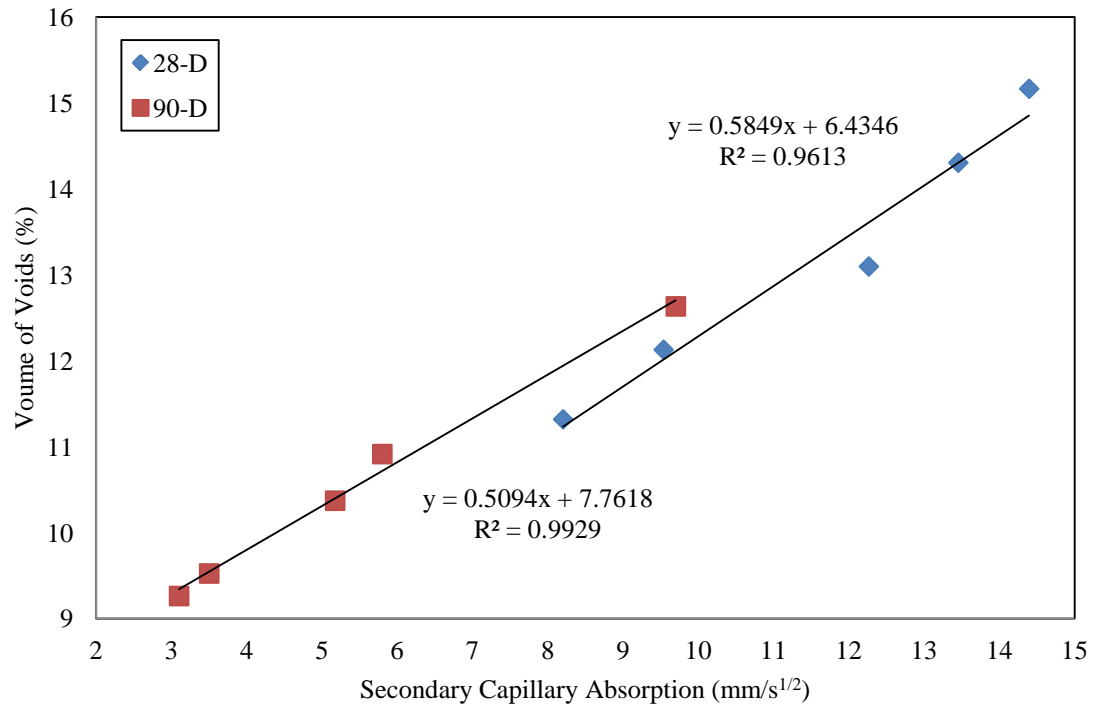


Figure 5.2: Correlation between Secondary Capillary Absorption and Percent Volume of Voids of 28- and 90-Day Cured Nano-Silica Contained SCCs

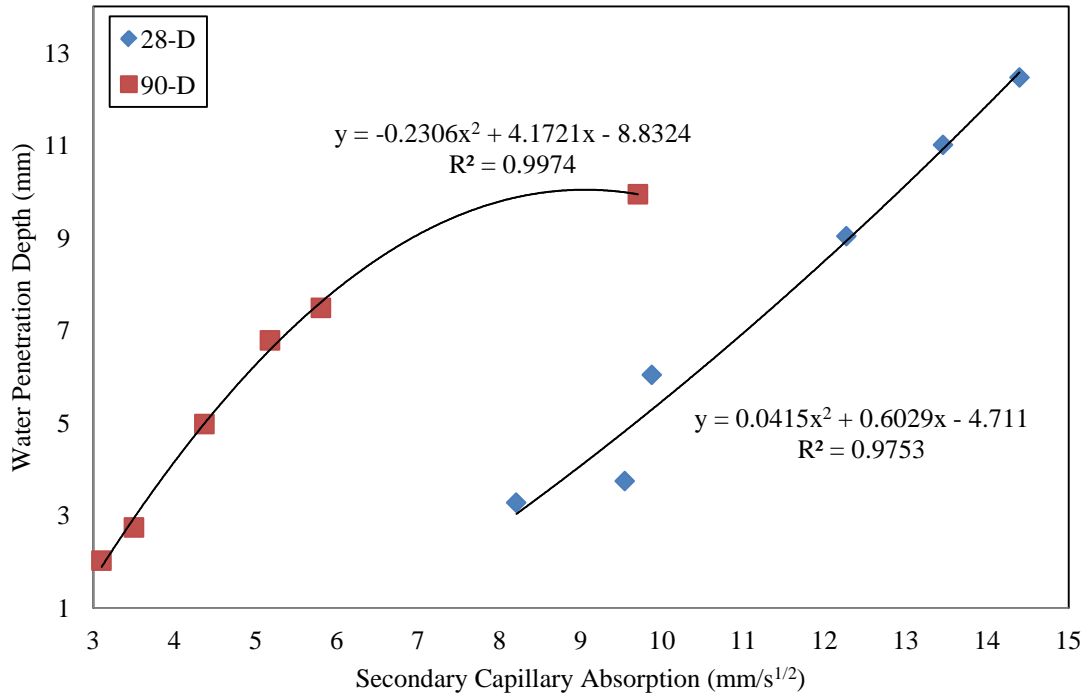


Figure 5.3: Correlation between Secondary Capillary Absorption and Water Penetration Depths of 28- and 90-Day Cured Nano-Silica Contained SCCs

Rapid migration results exhibited strong correlation with water penetration, volume of voids, and rapid chloride permeability test (RCPT) test results for both 28- and 90-day cured SCCs. For instance, rapid migration correlations with water penetration test results were 0.89 and 0.90 for 28- and 90-day curing ages, respectively (see Figure 5.4). As discussed earlier, improvement of pore structure by nano-silica fine particles are expected to produce similar trends between the tests that are highly dependent on pore structure, shape and size of pores, and volume of voids.

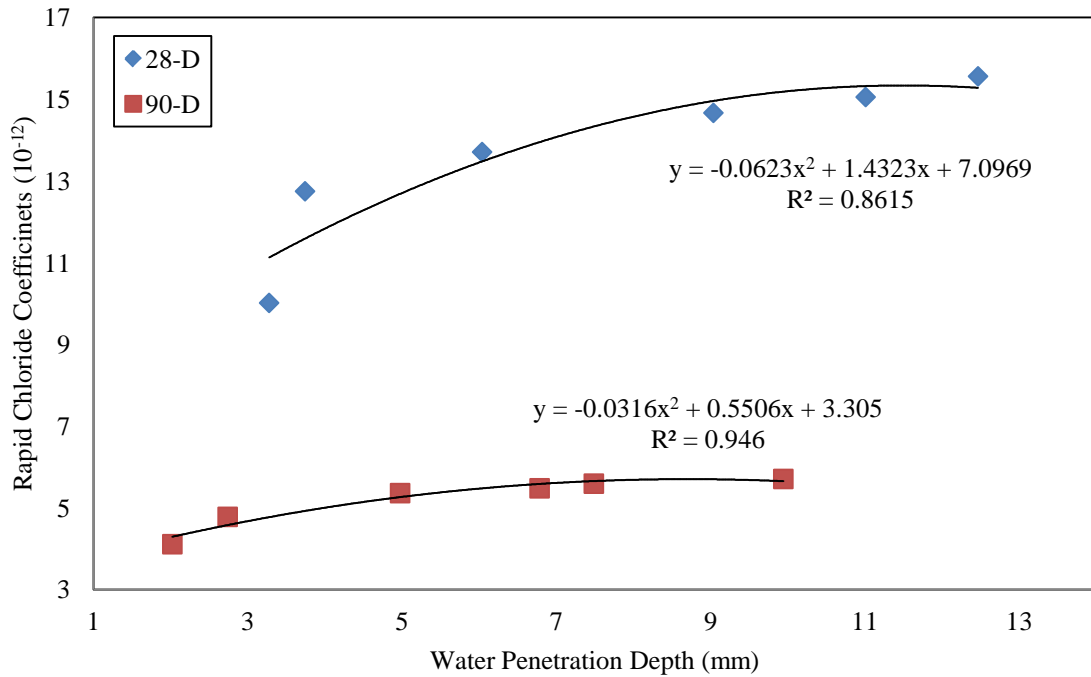


Figure 5.4: Correlation between Water Penetration Depths and Rapid Migration Coefficients of 28- and 90-Day Cured Nano-Silica Contained SCCs

Correlations between compressive strength and all other transport property tests appeared to be strong for 28 days of curing. These correlations slightly decreased for water penetration, volume of voids, and secondary capillary absorption with increase in curing time to 90 days, yet the correlations were still moderately strong (i.e. -0.87, -0.78, and -0.73, respectively). Correlations between compressive strength and all other studied tests are shown in Figures 5.5 through 5.9.

Strong correlations are expected as many of the transport and mechanical tests are dependent on concrete pore structure. Less porous concretes with little penetration to water and other substances should result in higher strengths and resistance to ion penetration.

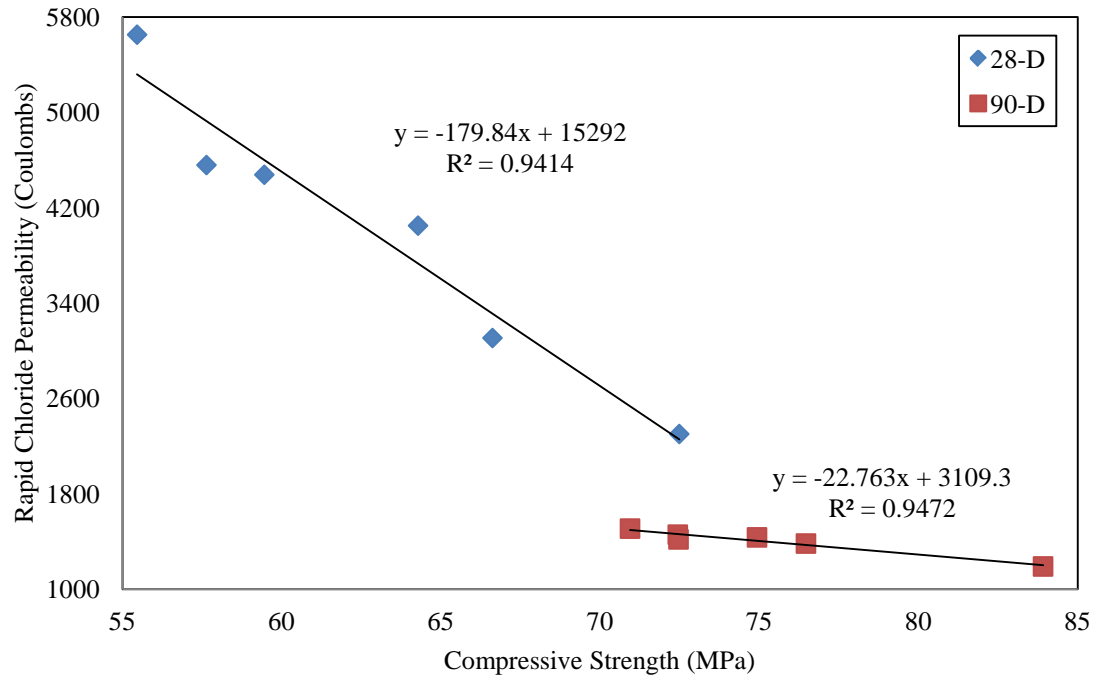


Figure 5.5: Correlation between Compressive Strength and Rapid Chloride Permeability of 28- and 90-Day Cured Nano-Silica Contained SCCs



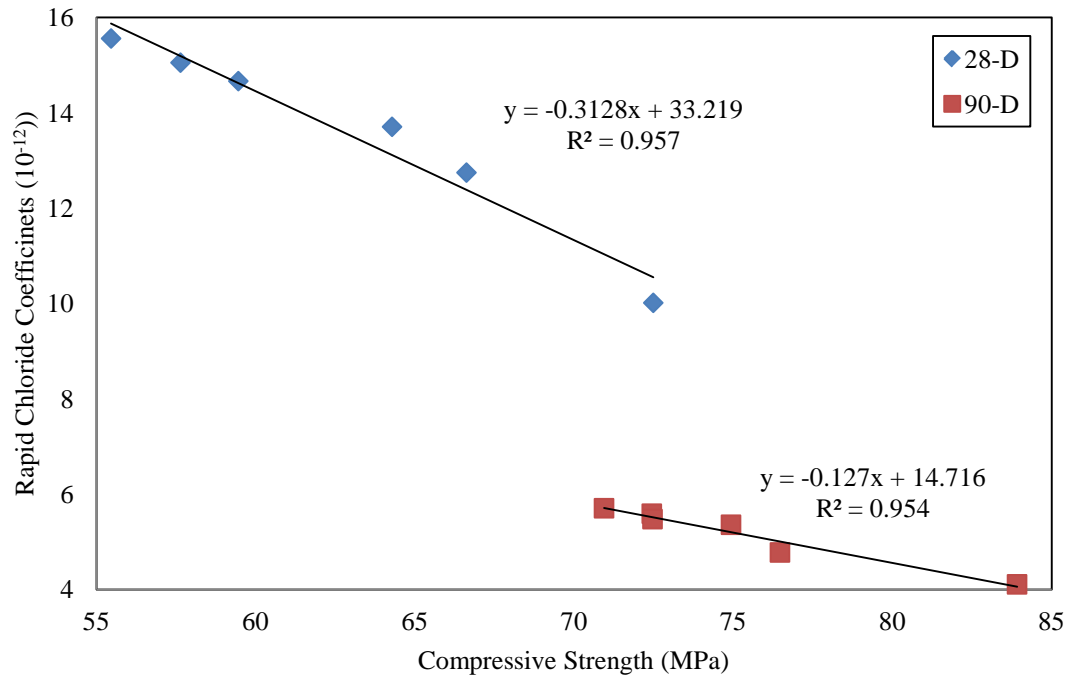


Figure 5.6: Correlation between Compressive Strength and Rapid Migration of 28- and 90-Day Cured Nano-Silica Contained SCCs

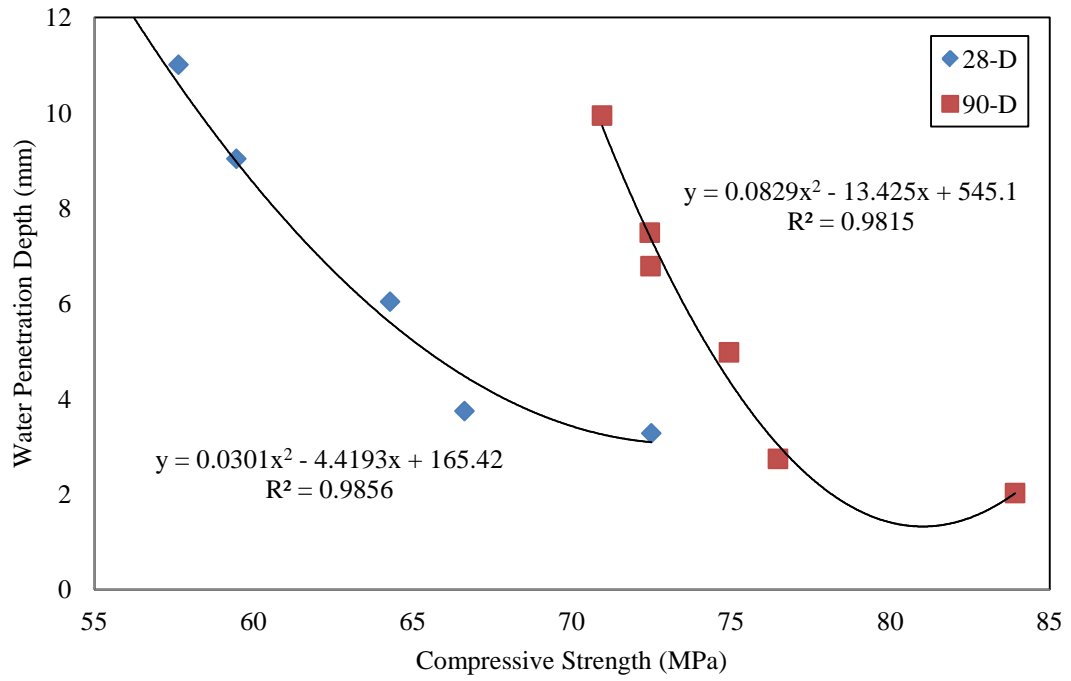


Figure 5.7: Correlation between Compressive Strength and Water Penetration Depth of 28- and 90-Day Cured Nano-Silica Contained SCCs

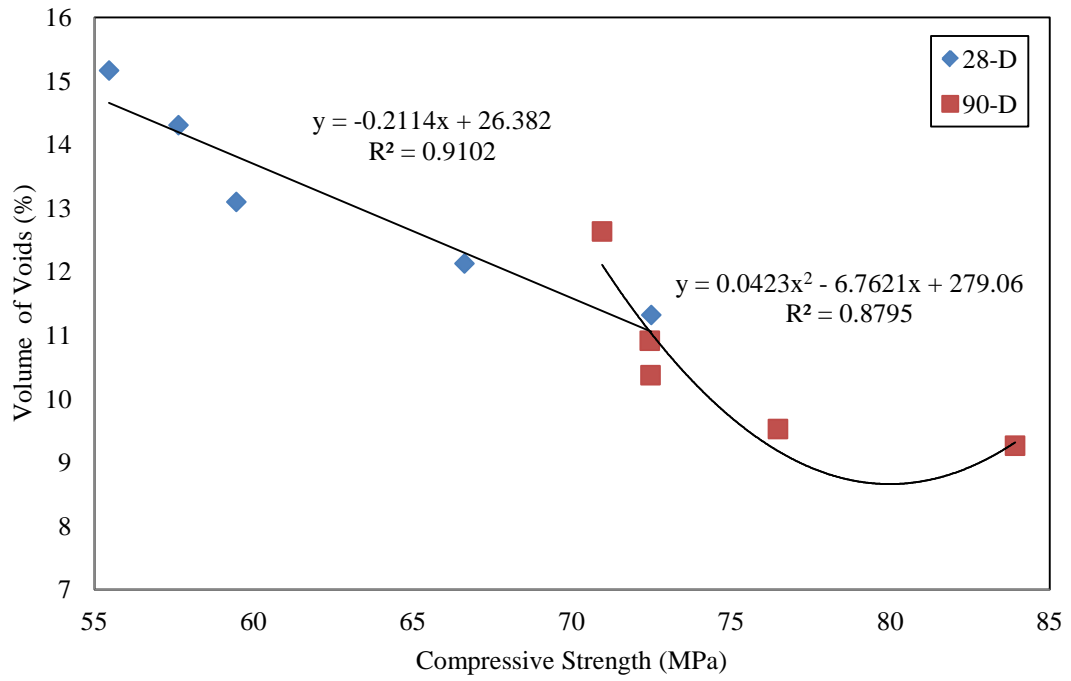


Figure 5.8: Correlation between Compressive Strength and Percent Volume of Voids of 28- and 90-Day Cured Nano-Silica Contained SCCs

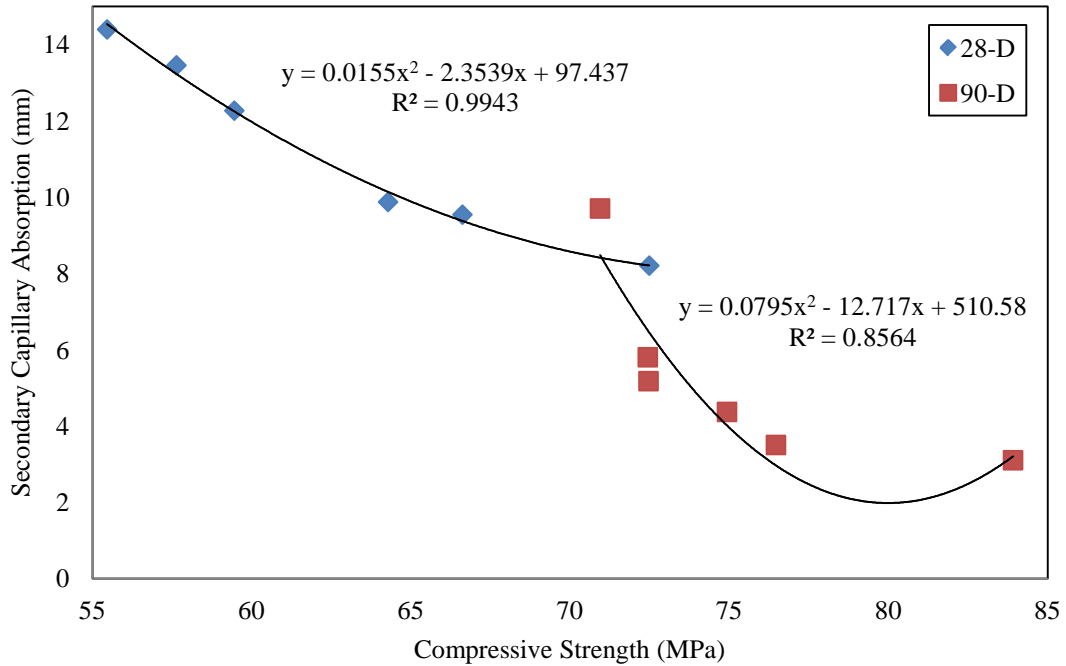


Figure 5.9: Correlation between Compressive Strength and Secondary Capillary Absorption of 28- and 90-Day Cured Nano-Silica Contained SCCs

### 5.3 Classifications of Transport Properties of the Studied SCCs

After defining the transport processes and evaluating the performance of SCCs containing nano and micro silica, the key question is "how will these transport properties affect the durability of a structure?" In Table 5.6, the first column shows the actual concrete properties that are likely to affect. The second column shows the transport properties and the final column shows the deterioration processes that result from the corresponding transport properties.

Table 5.6: Properties of Concrete Matrix, Transport Properties, and Deterioration Processes Caused by the Transport Processes

Properties of concrete matrix	Transport processes	Deterioration processes
Pore interconnection	Capillary suction	Freezing and thawing
Fluid Chemistry & pore interconnection	Electromigration (RCPT & RMT)	Reinforcement corrosion
Pore interconnection	Pressure driven flow (Water Penetration)	Freezing and thawing
Total pore volume (porosity)	Diffusion	Reinforcement corrosion
Total pore volume (porosity)	Water absorption	Freezing and thawing & strength

Depending on the type of environmental and climatic conditions to which a concrete structure or element is exposed to, a specific transport process may be chosen to evaluate and examine long-term durability. For instance, concrete elements in tidal zones are subject to capillary suction process. As a result, additional care must be taken regarding pore interconnection when designing these types of elements. Moreover, concrete elements that are exposed to seawater are highly recommended to be tested against chloride diffusion and rapid chloride migration.

Selective transport properties, which were evaluated in previous chapters, have suggested classification ranges to quantify the extent of chloride ion resistivity and durability of SCCs. These transport properties were rapid chloride permeability test (RCPT), rapid migration test (RMT), and volume of voids. The classification criteria for the above-mentioned tests are presented in Tables 5.7 through 5.9. Following the Table 5.9, the studied SCCs are classified in Table 5.10 according to the suggested criteria.

Table 5.7 summarizes the rapid chloride permeability test's range of charges passed and their corresponding permeability rates.

Table 5.7 : Rapid Chloride Permeability Range of Chloride Ion Penetrability Based on Charge Passed

Charge passed (Coulombs)	Chloride Ion Penetrability
> 4000	High
2000 - 4000	Moderate
1000 - 2000	Low
100 - 1000	Very low
< 100	Negligible

Table 5.8 presents the chloride ingress resistance criteria of rapid migration coefficients.

Table 5.8: Chloride Ingress Resistance Criteria Based on Rapid Migration Coefficients

$D < 2 \times 10^{-12} \text{ m}^2/\text{s}$	very good resistance against chloride ingress
$D < 8 \times 10^{-12} \text{ m}^2/\text{s}$	good resistance against chloride ingress
$D < 16 \times 10^{-12} \text{ m}^2/\text{s}$	moderate resistance against chloride ingress
$D > 16 \times 10^{-12} \text{ m}^2/\text{s}$	not suitable for aggressive environment

The durability classification provided by VicRoads based on apparent volume of permeable voids is shown in Table 5.9.

Table 5.9: Durability Classification Based on Apparent Volume of Permeable Voids

Durability Classification Indicator	Vibrated Cylinders (AVPV %)	Rodded Cylinders (AVPV %)	Cores (AVPV %)
Excellent	<11	<12	<14
Good	11-13	12-14	14-16
Normal	13-14	14-15	16-17
Marginal	14-16	15-17	17-19
Bad	>16	>17	>19

Table 5.10 classifies the studied nano-silica contained SCCs for both 28- and 90-day curing ages based on the above-mentioned rating criteria.

Table 5.10: Nano-Silica Contained SCC Classification

Mixture Designation		0-NS	1.5-NS	3-NS	4.5-NS	6-NS	7.5-NS
RCPT (Coulombs)	28-D	5651	4557	4476	4046	3106	2301
		High	High	High	High	Moderate	Moderate
	90-D	1507	1457	1417	1434	1382	1190
		Low	Low	Low	Low	Low	Low
RMT ( $\text{m}^2/\text{s} \times 10^{-12}$ )	28-D	15.56	15.05	14.66	13.7	12.74	10.01
		Moderate	Moderate	Moderate	Moderate	Moderate	Moderate
	90-D	5.7	5.59	5.48	5.36	4.78	4.11
		Good	Good	Good	Good	Good	Good
Volume of Voids (%)	28-D	15.16	14.3	13.1	N/A	12.13	11.32
		Marginal	Normal	Good	N/A	Good	Excellent
	90-D	12.63	10.91	10.37	N/A	9.52	9.26
		Good	Excellent	Excellent	N/A	Excellent	Excellent

Results of RCPT test showed that at 28-day curing age only 6% and 7.5% NS SCCs had “moderate” chloride permeability and the rest of the SCCs showed “high” chloride permeability. On the contrary, all 90-day cured SCCs had “low” chloride permeability. It appeared that 6% and higher replacement of cementitious materials by nano-silica produced SCCs that effectively resisted chloride penetration at 28-day curing age. This could be the result of better pore structure or dilution of the pore solution constituents as discussed previously in Chapter 4 of this study. Moreover, increases in curing age resulted in high resistible SCCs for all replacement levels. As discussed in Chapter 4 of this study, improvement in rapid chloride impermeability was due to transformation of pores into a smaller discontinuous network as well as reduction in fly ash effect in electroconductivity of pore solution.

Results of RMT test showed that all SCCs at 28 days of curing ranked “moderate” against chloride ingress. However, after 90 days of curing, all SCCs ranked “good” against chloride ingress. The difference in rapid migration criteria between 28- and 90-

day curing ages however confirmed that fly ash's latent reactivity greatly improved chloride ingress resistance.

The improvement in durability through volume of voids of studied SCCs ranged from marginal to excellent at 28 days of curing. The control SCC had marginal durability. With 1.5 percent of nano-silica replacing a portion of the cementitious materials, the durability became normal. This trend was continued and 3-NS and 4.5-NS mixtures showed good durability. Lastly, 7.5 percent replacement of cementitious materials by nano-silica resulted in excellent durability. Durability of control SCC improved from marginal to good and all other SCCs obtained excellent durability once curing age was extended from 28 to 90 days. As discussed in Chapter 4, the improvements observed are mostly due to physical effect (i.e. filling ability) of nano-silica powder, which acted as filler.

#### **5.4 Conclusions**

According to the statistical analyses performed, the following conclusions can be made:

- Correlations between the studied tests were investigated. It was found that secondary capillary absorption, rapid chloride migration, percent volume of voids and water penetration had the strongest correlations. Rapid chloride permeability had also strong correlations with rapid chloride migration for both curing ages (i.e. 28 and 90 days). Lastly, compressive strength had negative strong correlations with all other studied tests at 28-day curing age. These correlations slightly decreased for water penetration, volume of voids, and secondary capillary



absorption with increase in curing time to 90 days, yet the correlations were still moderately strong.

- The studied SCCs were classified based on the results of rapid chloride permeability, rapid migration, and volume of voids. It was found that only Mixtures 6-NS and 7.5-NS mixtures had moderate chloride impermeability at 28 days of curing and all other mixtures had high permeation. However, at 90-day curing age, all mixtures showed low chloride permeability. All mixtures had moderate resistivity to chloride migration at 28-day curing age, and became in good rating factor after 90 days of curing. Based on the volume of voids classifications, the control SCC had marginal durability; Mixture 1.5-NS showed normal durability, and Mixtures 3-NS and 6-NS produced good durability. Lastly, 7.5 percent by weight replacement of cementitious materials by nano-silica resulted in excellent durability. Durability of control SCC improved from marginal to good, whereas all nano-silica contained SCCs showed excellent durability at 90-day curing age.

## Chapter 6

### Conclusions and Recommendations

This investigation was intended to evaluate the influence of nano-silica as a partial replacement of ordinary Portland cement (OPC) on transport properties of self-consolidating concretes (SCCs). Nano-silica was used to replace a portion of the cementitious materials at varying percentages by weight ranging from 1.5 to 7.5%. Flow properties (slump flow, VSI,  $T_{50}$  flow time, and J-Ring) and bulk characteristics such as compressive strength of the investigated SCCs were evaluated. The studied transport properties were absorption, water penetration, rapid chloride permeability, capillary absorption, rapid migration, and chloride diffusion. Additionally, four distinguished and selected bulk and transport properties of nano-silica contained SCCs (i.e. compressive strength, water penetration, rapid migration, and chloride diffusion) were compared to equivalent SCCs containing silica fume. Silica fume replaced a portion of cementitious materials at levels of 3, 4.5, 6, and 7.5% by weight. Lastly, statistical analyses were performed to establish the most suitable relationships between the studied transport properties and compressive strength with several independent variables.

#### 6.1 Conclusions

The main findings and conclusions of this study are presented below.

- Nano-silica particle sizes ranged from 15 to 20 nanometer and 97.22% of silica fume particles were finer than 45 micrometer. However, once these particles were mixed and blended with water and were analyzed by Laser Diffraction Size Analyzer, silica fume particle sizes ranged from 0.2 to 502 micrometers and nano-silica particle size distribution changed to a relatively narrow based of 3.17 to 20

micrometers. Addition of water to nano-silica particles caused these particles lose their high surface area due to grain growth and agglomeration. The adopted blending procedure was unable to de-agglomerate the agglomerated nano-silica during batching of concrete.

- Particle size distribution of cementitious powder as functions of nano-silica powder replacing a portion of cementitious materials revealed finer gradation for nano-silica contained SCCs as opposed to that of control SCC.
- The results of flow properties showed slump flows within the target value of  $635 \pm 25$  mm and  $T_{50s}$  of less than 2.66 seconds for all SCCs. Additionally, J-ring results were within 19 to 38 mm, well within the 51 mm limit. All SCCs had acceptable visual stabilities. No segregation, coning, or bleeding was observed for any of the studied SCCs.
- Comparison of nano-silica contained SCCs to that of control SCC revealed increases from 4 to 31%, 2 to 18%, and 1.6 to 10.5% for 28-, 90-, and 180-day curing ages, respectively. The improvement in compressive strengths increased by 22 and 11% from 28- to 90- and 90- to 180-day curing ages, respectively. Highest improvement was gained by control SCC due to its higher fly ash content than that of nano-silica contained SCCs.
- Reduction in interconnected pores of nano-silica contained SCCs resulted in rapid chloride migration coefficients ranging from 3 to 36% and 2 to 28% for 28- and 90-day curing ages when compared to control SCCs. Moreover, rapid chloride migration coefficient of all studied concretes reduced by an approximately 60% once curing age was extended from 28 to 70 days.

- All SCC samples were exposed to water pressure for 72 hours and their penetrated water levels were compared. A large reduction in water penetration depth from control SCC to nano-silica contained SCCs, ranging from 12 to 74% and 25 to 80% at 28- and 90-day curing age, respectively, was observed. While the results of nano-silica contained SCCs compared to that of control SCC varied, Mixtures 6-NS and 7.5-NS showed nearly similar results when compared to control SCC for both curing ages. Comparison of 28- and 90-day curing age results revealed an average of 28% reduction in water penetration depth with increase in curing age for all investigated SCCs.
- The ability of SCCs in absorbing water through capillary suction mechanism was tested and the results were compared amongst all SCCs. Comparing nano-silica contained SCCs to control SCC revealed that, on average, 10 and 7% reductions in primary and secondary capillary absorption coefficients, respectively, were observed for every 1.5% replacement of cementitious materials by nano-silica at 28-day curing age. Reduction in primary capillary water absorption coefficients for all SCCs from 28- to 90-day curing age ranged from 3 to 19% and nearly 27% reduction in secondary capillary absorption coefficients from 28- to 90-day curing age was observed. Chemical and physical effects of nano-silica as well as continuous pozzolanic reactivity of fly ash were the main contributors to reductions in capillary absorption of nano-silica contained SCCs.
- Three distinctive features of water absorption test, absorption after immersion, absorption after immersion and boiling, and volume of voids were studied. A similar trend was observed for the aforementioned absorption features. Nearly

20% reduction in volume of voids was observed from 28- to 90-day curing age for all studied SCCs mainly due to late pozzolanic reactivity of fly ash. Results showed that the volume of voids did not vary significantly with inclusion of nano-silica. It is believed that nano-silica was able to divide larger pores into smaller pores; however the overall pore volume did not change significantly.

- Improvement in both pore solution, to a larger extent, and pore structure, to a less extent, of nano-silica contained SCCs resulted in higher resistance to chloride ions permeation. Charges passed through nano-silica contained SCCs were lower than of control SCC at both curing ages. High variation in resistance to chloride ion penetration was observed for individual sample of the same mixture, yet all samples showed improvement in chloride ion resistance. On average 69% reduction in charges passed through studied SCCs was observed with an increase in curing age from 28 to 90 days for concretes containing less than 6% nano-silica by weight of cementitious materials. For Mixtures 6-NS (6% nano-silica) and 7.5-NS (7.5% nano-silica) showed 56 and 48% reductions in charges passed, respectively, with an increase of curing age from 28 to 90 days.
- The diffusion of chloride ions into concretes reduced by inclusion of nano-silica into concrete mixtures, as well as, increases in curing age. Partial replacement of cementitious materials by nano-silica resulted in SCCs with an appreciably lower chloride permeability than control SCC. Reduction in chloride content of SCCs at selected depths was observed for both 28- and 180-day curing ages when nano-silica contained SCCs were compared to that of control SCC. Additionally, 180-

day cured specimens showed significant reduction in chloride content at selected depths as compared to their equivalent mixtures cured for 28 days.

- A comparison of flow properties between nano-silica contained and silica fume SCCs showed a higher amount of High-Range-Water-Reducing Admixture (HRWRA) needed for nano-silica contained SCCs to achieve a similar flowability. This finding is attributed to the smaller particle sizes and higher surface area of nano-silica particles.
- The comparison of compressive strength tests results for both 28- and 90-days curing ages produced a negligible difference in load-bearing capacity between nano-silica and silica fume contained concretes. Nearly 5% increase in compressive strength was observed for silica fume contents when compared to that of nano-silica mixtures for both 28- and 90-day curing ages.
- All rapid chloride migration coefficients of silica fume contained SCCs were lower than of those for nano-silica contained SCCs by an average of nearly 7%.
- Maximum depth of water penetrated through nano and micro silica contained SCCs were also compared. The results indicated that silica fume contained SCCs had better resistance to water penetration by an average of less than 12% at both curing ages.
- No significant difference was observed between nano and micro silica contained SCCs in resistance to chloride diffusion at 28-day curing age. On the other hand, the test results for 180-day cured nano-silica contained SCCs, compared to that of 90-day cured silica fume SCCs, indicated a lower chloride content for silica fume contained SCCs at all selected depths.

- The better performance of silica fume contained SCCs over nano-silica contained SCCs can be attributed to the agglomerated wet and uniformly graded nano-silica particles which were unable to fill pore spaces and densify paste microstructure as good as well-graded silica fume did.
- The reactivity of nano and micro silica contained samples in consumption of calcium hydroxide was evaluated by Differential Scanning Calorimetry and Thermogravimetric Analyses (TGA). Although the TGA test showed a minimal difference in reactivity level of nano and micro silica contained samples.
- As discussed earlier in this chapter, although dry nano-silica particles had larger surface area than dry micro silica particles prior to mixing, the adopted blending method was found insufficient to de-agglomerate wet nano-silica particles, this inhibiting their expected performance at nano level and limiting availability of reactive silica surface area.

## **6.2 The Key Outcomes**

The key outcomes and conclusions of this study are summarized below.

- Overall evaluation of both nano and micro silica performances for both 28 and 90-day curing ages showed that nano and micro silica particles improved transport properties of SCCs significantly. This was because nano and micro silica particles were finer than cement particles; hence, they acted as fillers to fill spaces between the cement grains. This greater fineness increased the rate at which nano and micro silica hydrated and thus accelerated strength development.
- Hydration reaction between cement and water produced calcium silicate hydrate. These crystals were hexagonal and were arrayed in the interfacial transition zone

(ITZ), between aggregates and binding paste matrix, which was detrimental to the water permeability resistant capacity. Nano and micro silica particles were very active due to their enormous specific surface area. Hence, nano and micro silica reacted with calcium hydroxide crystals very quickly, and produced calcium silicate hydrate gel. As a result, the size and amount of the calcium hydroxide silicate crystals were reduced and the calcium silicate hydrate gel filled the voids to improve the density of the interfacial transition zone (ITZ) and the binding paste matrix.

- Nano and micro silica particles filled the voids of calcium silicate hydrate gel structure and made the binding paste matrix denser. They also acted as nucleus to tightly bond with C-S-H gel particles. As a result, the stability of the hydration product structure was improved, which resulted in enhancement in mechanical and transport properties of SCCs.
- Addition of nano-silica and silica fume improved the consistency of the SCCs and reduced potential for bleeding, segregation, and conning.
- Silica particles served on two levels in SCCs. The first contribution was chemical effect: the pozzolanic reactions of free (soluble) calcium hydroxide formed more C-S-H gel at final stages. The second contribution was due to physical effect: silica particles (both nano and micro) were smaller than cement particles, and were able to fill the micro voids in the young and partially hydrated cement paste, thus, increasing the final density of concrete.



### **6.3 Recommendations**

Future studies on the inclusion nano-silica powder as a partial replacement of cementitious materials may include:

1) De-agglomeration of wet nano-silica:

Different methods of de-agglomeration of nano-silica particles can be studied to investigate the most effective de-agglomeration method in order to allow nano-silica to contribute at nano level. Sonication, homogenization, and stirring, as well as different mixing time periods assigned for each method are amongst a few procedures that can be used to ascertain the effectiveness of de-agglomeration for wet nano-silica.

2) Evaluation of durability of nano-silica powder contained SCCs and its relation to transport properties:

Durability of nano-silica contained SCCs can be evaluated by studying sulfate attack, alkali silica reactivity, acid resistance, and abrasion testing. From the findings of these testing, a theoretical transport property index can be established to reflect the relationship between transport properties and durability of SCCs.

## Appendix A

### Conversion Factors

$$1 \text{ mm} = 0.0394 \text{ inch}$$

$$1 \text{ nm} = 10^{-9} \text{ m} = 3.94 \times 10^{-8} \text{ inch}$$

$$1 \text{ kg} = 2.20 \text{ lb}$$

$$^{\circ}\text{C} = (5/9) (^{\circ}\text{F} - 32)$$

$$1 \text{ MPa} = 145 \text{ psi}$$

$$1 \text{ kg/m}^3 = 1.684 \text{ lb/yd}^3 = 0.0624 \text{ lb/ft}^3$$

$$1 \text{ kg/m}^3 = 0.0624 \text{ lb/ft}^3$$

$$1 \text{ ml/100 kg} = 0.0153 \text{ oz/cwt}$$

## Appendix B

### Results of Individual Testing

Compressive Strength of Studied Nano-Silica Contained SCCs (MPa)

Mixture Designation		0-NS	1.5-NS	3-NS	4.5-NS	6-NS	7.5-NS
28-Day	Samples	56.8	58	58.7	62.4	64.1	75.1
		57.2		60.9	64.7	69.4	71.9
		53.7		57.3	58.8	65.7	66.4
		55.8	58.8		65.7	66.4	70.5
		53.8	57.3	58.8	65.7	66.4	70.5
Average	55.5	57.7	59.5	64.3	66.6	72.5	
90-Day	Samples	68.3	74.3	70.7	78.1	75	87
		75.2	74.3	74.3	76.9	76.4	80.8
		69.3	68.8	72.4	69.8	78	
	Average	70.9	72.5	72.5	74.9	76.5	83.9
180-Day	Samples	81.6	82.5	82.4	83.6	84.8	91.7
			78.1	82.6	84.9	86.7	93.4
	Average	81.6	80.3	82.5	84.3	85.8	90.2

Rapid Migration Coefficient Comparison of Nano and Micro Silica Contained SCCs ( $m^2/s \times 10^{-12}$ )

Percent NS or SF Replaced	28-Day		% Reduction from NS to SF at 28-Day	90-Day		% Reduction from NS to SF at 90-Day
	NS	SF		NS	SF	
0	15.56	15.56	0	5.70	5.70	0
3	14.66	13.50	7.92	5.48	5.18	5.40
4.5	13.70	12.90	5.87	5.36	4.99	6.86
6	12.74	11.90	6.62	4.78	4.38	8.30
7.5	10.01	9.20	8.11	4.11	3.74	8.96

Water Penetration Depth of Studied Nano-Silica Contained SCCs (mm)

Mixture Designation	28-Day				90-Day			
	Samples			Average	Samples			Average
0-NS	12.45	12.19	12.75	12.46	9.80	9.55	10.46	9.94
1.5-NS	10.16	10.16	12.70	11.01	6.60	7.90	7.95	7.48
3-NS	9.17	9.58	8.36	9.03	6.12	6.99	7.24	6.78
4.5-NS	6.50	5.97	5.64	6.04	5.06	5.02	4.85	4.97
6-NS	3.91	3.81	3.51	3.74	3.06	2.72	2.44	2.74
7.5-NS	3.07	3.51	3.25	3.28	2.10	2.02	1.94	2.02

Primary Capillary Absorption of Studied Nano-Silica Contained SCCs  
( $\times 10^{-5}$  mm/s<sup>0.5</sup>)

Mixture Designation		0-NS	1.5-NS	3-NS	4.5-NS	6-NS	7.5-NS
28-Day	Samples	0.00038	0.00035	0.00032	0.00023	0.00023	0.00019
		0.00038	0.00035	0.00032	0.00026	0.00023	0.0002
		0.00038	0.00035	0.00031	0.0003	0.00022	0.0002
	Average	0.00038	0.00035	0.00032	0.00026	0.00023	0.0002
90-Day	Samples	0.00031	0.00033	0.00031	0.00022	0.00019	0.00018
		0.00035	0.00032	0.00032	0.00023	0.00018	0.00016
		0.00041	0.00033	0.0003	0.00022	0.00018	0.00017
	Average	0.00036	0.00033	0.00031	0.00022	0.00018	0.00017

Secondary Capillary Absorption of Studied Nano-Silica Contained SCCs  
( $\times 10^{-5}$  mm/s<sup>0.5</sup>)

Mixture Designation		0-NS	1.5-NS	3-NS	4.5-NS	6-NS	7.5-NS
28-Day	Samples	0.000133	0.000079	0.00007	0.000056	0.000049	0.000045
		0.000135	0.000081	0.000071	0.000066	0.000053	0.000046
		0.000133	0.000079	0.000065	0.000053	0.00005	0.000037
	Average	0.000134	0.00008	0.000069	0.000058	0.000051	0.000043
90-Day	Samples	0.000081	0.000064	0.000052	0.000044	0.000031	0.000032
		0.000105	0.000056	0.000052	0.000045	0.000038	0.00003
		0.000105	0.000054	0.000052	0.000042	0.000036	0.000031
	Average	0.000097	0.000058	0.000052	0.000044	0.000035	0.000031

Percentage Absorption After Immersion of Studied Nano-Silica Contained SCCs (%)

Mixture Designation	28-Day				90-Day				
	Samples			Average	Samples				Average
0-NS	6.21	5.35	6.38	5.98	4.82	3.26	5.50		4.53
1.5-NS	5.56	5.88		5.72	4.058	3.829	3.952		3.95
3-NS	4.81	4.71	5.53	5.02	3.003	4.326	3.713		3.68
6-NS	4.21	2.22	9.29	5.24	1.723	3.458	3.864	4.545	3.40
7.5-NS	4.40	3.04	5.04	4.72	3.084		3.708		3.40

Percentage Absorption After Immersion & Boiling of Studied Nano-Silica Contained SCCs (%)

Mixture Designation	28-Day				90-Day				
	Samples			Average	Samples			Average	
0-NS	6.49	6.62	6.68	6.59	5.35	5.23	5.45	5.34	
1.5-NS	6.02	6.50	6.17	6.23	4.87	4.99	5.00	4.95	
3-NS	5.43	5.33	6.50	5.75	5.68	3.51	5.52	4.90	
6-NS	4.67	2.18	9.65	5.50	5.55	4.90	3.89	4.78	
7.5-NS	4.78	3.35	5.30	5.04	4.03	4.15	5.73	4.64	

Percent Volume of Permeable Pore Space, Voids of Studied Nano-Silica Contained SCCs (%)

Mixture Designation		0-NS	1.5-NS	3-NS	6-NS	7.5-NS
28-Day	Samples	15.009	13.869	12.364	10.627	10.684
		15.156	14.873	12.174	5.208	
		15.326	14.169	14.75	20.547	
	Average	15.16	14.3	13.1	12.13	11.32
90-Day	Samples	13.41	11.262	8.014	5.559	9.103
		11.297	10.572	12.033	8.944	
		13.189	10.905	11.066	11.464	
				12.13		
Average	12.63	10.91	10.37	9.52	9.26	

Total Charge Passed through Studied Nano-Silica Contained SCCs  
(Coulombs)

Mixture Designation		0-NS	1.5-NS	3-NS	4.5-NS	6-NS	7.5-NS
28-Day	Samples	5679	4795	4089	4777	2785	2376
		4938	4319		3387	3291	2244
		6118	4558	4863	3601	3243	2283
		5869			4431		
	Average	5651	4557	4476	4049	3106	2301
90-Day	Samples	1420	1434	1627	1437	1395	1121
		1677		1603	1356		1171
		1425	1479	1456		1508	1369
				981	1177		
	Average	1507	1457	1417	1434	1382	1190

Chloride Content Measured at Selected Depths of 28-Day Cured Studied Nano-Silica Contained SCCs (gram)

Depth (mm)	1	3	5	7	9.5	12.5	15.5
0-NS	0.4246	0.3862	0.2242	0.1746	0.1246	0.1367	0.1370
	0.4426	0.3313	0.2619	0.2132	0.1576	0.1253	0.1099
Average	0.4336	0.3588	0.2431	0.1939	0.1411	0.1310	0.1235
1.5-NS	0.4614	0.3822	0.2483	0.1952	0.1788	0.1182	0.0838
	0.2691	0.2535	0.2184	0.1799	0.1462	0.1321	0.1374
	0.2068	0.1504	0.1413	0.1359	0.1294	0.1274	0.1311
Average	0.3124	0.2620	0.2027	0.1703	0.1515	0.1259	0.1174
3-NS	0.3289	0.2230	0.1712	0.1366	0.1200	0.0865	0.0729
	0.3032	0.2868	0.2395	0.1949	0.1782	0.1499	0.1282
Average	0.3160	0.2549	0.2054	0.1657	0.1491	0.1182	0.1006
4.5-NS	0.1464	0.1446	0.1208	0.1151	0.0925	0.1139	0.0900
	0.1563	0.1509	0.1368	0.1168	0.1089	0.1139	0.0700
Average	0.1513	0.1477	0.1288	0.1159	0.1007	0.1139	0.0800
6-NS	0.1521	0.1316	0.1006	0.0899	0.0835	0.0692	0.0867
	0.1479	0.1404	0.1518	0.1077	0.1040	0.0610	0.0867
Average	0.1500	0.1360	0.1262	0.0988	0.0938	0.0651	0.0867
7-NS	0.1254	0.1162	0.1060	0.0865	0.0768	0.0590	0.0607
	0.1780	0.1541	0.1523	0.1192	0.1136	0.0657	0.0607
Average	0.15172	0.13517	0.12918	0.10281	0.09523	0.06235	0.0607

Chloride Content Measured at Selected Depths of 180-Day Cured  
Studied Nano-Silica Contained SCCs (gram)

Depth (mm)	1	3	5	7	9.5	12.5	15.5
0-NS	0.3818	0.2773	0.1787	0.1098	0.1117	0.1080	0.1258
	0.3263	0.3055	0.1930	0.1097	0.1312	0.1059	0.0944
Average	0.3540	0.2914	0.1859	0.1097	0.1215	0.1070	0.1101
1.5-NS	0.2239	0.2214	0.1833	0.0932	0.1123	0.0954	0.0977
	0.2048	0.1960	0.1644	0.1200	0.1007	0.0954	0.0979
Average	0.2143	0.2087	0.1739	0.1066	0.1065	0.0954	0.0978
3-NS	0.2405	0.1775	0.1371	0.1086	0.1106	0.1017	0.0966
	0.1655	0.1543	0.1367	0.0970	0.0948	0.0856	0.0836
Average	0.2030	0.1659	0.1369	0.1028	0.1027	0.0936	0.0901
4.5-NS	0.1615	0.1429	0.1164	0.1000	0.0995	0.0895	0.0865
	0.1675	0.1497	0.1317	0.0994	0.1006	0.1007	0.0871
Average	0.1645	0.1463	0.1241	0.0997	0.1001	0.0951	0.0868
6-NS	0.1584	0.1380	0.1159	0.0911	0.0955	0.0897	0.0822
	0.1573	0.1383	0.1181	0.1040	0.1004	0.0969	0.0812
Average	0.1579	0.1381	0.1170	0.0976	0.0980	0.0933	0.0817
7-NS	0.1589	0.1396	0.1182	0.0944	0.0955	0.0925	0.0753
	0.1542	0.1303	0.1104	0.0950	0.0922	0.0917	0.0753
Average	0.1566	0.1349	0.1143	0.0947	0.0938	0.0921	0.0753

Compressive Strength of Studied Micro Silica Contained SCCs (MPa)

Mixture Designation		0-NS	3-SF	4.5-SF	6-SF	7.5-SF
28-Day	Samples	56.8	62.9	65.9	80.6	81.3
		53.7	67.4	67	71.6	68
		57.2		67.3	68.4	80.4
		55.8	64.5	65.3	67.6	77.3
		53.8				
	Average	55.5	64.9	66.4	72.1	76.7
90-Day	Samples	68.3	78.8	73	82.7	80.7
		75.2	74.9	84.2		81.3
		69.3	79.8	79.4	81.2	82.3
			77.7			
	Average	70.9	77.8	78.9	82.0	81.5



Rapid Migration Coefficients of Studied Silica Fume Contained SCCs ( $m^2/s \times 10^{-12}$ )

Mixture Designation	28-Day				90-Day			
	Samples			Average	Samples			Average
0-NS	17.69	14.79	14.18	15.56	5.83	5.46	5.07	5.70
					6.54	4.88	6.45	
3-SF	13.49	13.47	13.60	13.52	5.05	5.20	5.28	5.18
4.5-SF	12.99	13.17	12.56	12.91	4.94	5.03		4.99
6-SF	11.57	11.99	12.10	11.89	4.59	4.31	4.26	4.38
7.5-SF	9.20	9.30	9.03	9.18	3.68	3.66	3.89	3.74

Water Penetration Depth of Studied Silica Fume Contained SCCs (mm)

Mixture Designation	28-Day				90-Day			
	Samples			Average	Samples			Average
0-NS	12.45	12.19	12.75	12.46	9.80	9.55	10.46	9.94
3-SF	8.51	8.47	8.46	8.48	6.51	6.50	6.44	6.48
4.5-SF	5.88	5.76	5.81	5.82	4.71	4.72	4.75	4.73
6-SF	3.31	3.33	3.28	3.31	2.52	2.49	2.54	2.52
7.5-SF	3.12	3.22	3.15	3.16	2.01	1.99	2.03	2.01

Chloride Content Measured at Selected Depths of 28-Day Cured Studied Silica Fume Contained SCCs (gram)

Depth (mm)	1	3	5	7	9.5	12.5	15.5
0-SF	0.4246	0.3862	0.2242	0.1746	0.1246	0.1367	0.1370
	0.4426	0.3313	0.2619	0.2132	0.1576	0.1253	0.1099
Average	0.4336	0.3588	0.2431	0.1939	0.1411	0.1310	0.1235
3-NS	0.3515	0.3328	0.2210	0.1633	0.0994	0.1187	0.0783
	0.4530	0.3603	0.2548	0.2196	0.1432	0.1246	0.1200
Average	0.4022	0.3466	0.2379	0.1915	0.1213	0.1217	0.0992
4.5-SF	0.3733	0.2795	0.1767	0.1157	0.1075	0.0982	0.1016
	0.3827	0.3037	0.2389	0.1640	0.1373	0.1347	0.1187
Average	0.3780	0.2916	0.2078	0.1399	0.1224	0.1165	0.1102
6-SF	0.3635	0.2430	0.1738	0.1179	0.1031	0.1039	0.0993
	0.3841	0.2993	0.2158	0.1374	0.1314	0.1202	0.1148
Average	0.3738	0.2711	0.1948	0.1277	0.1172	0.1120	0.1071
7.5-SF	0.3734	0.2641	0.1573	0.1186	0.1177	0.1158	0.1142
	0.3701	0.2753	0.2311	0.1463	0.1169	0.1177	0.0860
Average	0.3718	0.2697	0.1942	0.1324	0.1173	0.1167	0.1001

Chloride Content Measured at Selected Depths of 90-Day Cured Studied  
Silica Fume Contained SCCs (gram)

Depth (mm)	1	3	5	7	9.5	12.5	15.5
0-SF	0.3818	0.2773	0.1787	0.1098	0.1117	0.108	0.1258
	0.3263	0.3055	0.193	0.1097	0.1312	0.1059	0.0944
Average	0.354	0.2914	0.1859	0.1097	0.1215	0.107	0.1101
3-NS	0.2575	0.2252	0.234	0.1791	0.0705	0.0613	0.0925
	0.1913	0.2046	0.0824	0.0829	0.1664	0.1296	0.0845
Average	0.2244	0.2149	0.1582	0.131	0.1184	0.0954	0.0885
4.5-SF	0.1967	0.1083	0.0981	0.0869	0.0746	0.0715	0.0744
	0.2133	0.1386	0.1362	0.1069	0.0924	0.0907	0.0786
Average	0.205	0.1234	0.1172	0.0969	0.0835	0.0811	0.0765
6-SF	0.0959	0.085	0.1023	0.1116	0.0907	0.078	0.0676
	0.11	0.1053	0.1048	0.0875	0.0912	0.0876	0.0767
Average	0.1029	0.0952	0.1035	0.0995	0.091	0.0828	0.0722
7.5-SF	0.1	0.0948	0.0998	0.0846	0.081	0.0777	0.0704
	0.1035	0.1058	0.0953	0.0899	0.0851	0.0738	0.069
Average	0.1017	0.1003	0.0975	0.0872	0.083	0.0757	0.0697

## **Bibliography**

American Association of State Highway and Transportation Officials. "Standard Specification for Portland Cement." AASHTO M 85, Washington D.C.

American Association of State Highway and Transportation Officials. "Standard Specification for Fine Aggregate for Portland Cement Concrete." AASHTO M 6, Washington D.C.

American Association of State Highway and Transportation Officials. "Standard Specification for Fine Aggregate for Portland Cement Concrete." AASHTO M 43, Washington D.C.

American Association of State Highway and Transportation Officials. "Standard Specification for Coal Fly Ash and Raw or Calcined Natural Pozzolan for Use in Concrete." AASHTO M 295, Washington D.C.

American Association of State Highway and Transportation Officials. "Standard Specification for Chemical Admixtures for Concrete." AASHTO M 194, Washington D.C.

American Association of State Highway and Transportation Officials. "Standard Method of Test for Slump of Hydraulic Cement Concrete." AASHTO T 119, Washington D.C.

American Concrete Educational Bulletin E4-03. (2003). "Chemical Admixtures for Concrete." ACI Committee E-701 Materials for Concrete for Construction, E4-1 to E4-12, Farmington Hills, Mi.

American Concrete Institute (2003). "Guide for the Use of High Range Water Reducing Admixtures (Superplasticizers) in Concrete," ACI Committee 212, 212.3 R1-212.3R13, Farmington Hills, MI.

American Concrete Institute. (1981). "Specifications for Structural Concrete for Buildings." ACI Committee 310, Farmington Hills, MI.

American Concrete Institute. (1997). "State-of-the-Art Report on High-Strength Concrete" ACI Committee 363, Farmington Hills, MI.

American Concrete Pavement Association. (2013). "What are admixtures."

<[http://www.pavement.com/Concrete\\_Pavement/Technical/FATQ/Materials/Admixtures.asp](http://www.pavement.com/Concrete_Pavement/Technical/FATQ/Materials/Admixtures.asp)> (Sept. 7, 2013).

American Society for Testing and Materials (ASTM). (2011). "Standard Performance Specification for Hydraulic Cement." C 1157-11, West Conshohocken, Pa.

American Society for Testing and Materials (ASTM). (2013). "Standard Specification for Blended Hydraulic Cements." C 595-13, West Conshohocken, Pa.

American Society for Testing and Materials (ASTM). (2012). "Standard Specification for Expansive Hydraulic Cement." C 845-12, West Conshohocken, Pa.

American Society for Testing and Materials (ASTM). (2013). "Standard Specification for Concrete Aggregates." C 33-13, West Conshohocken, Pa.

American Society for Testing and Materials (ASTM). (2012). "Standard Specification for Portland Cement." C 150-12, West Conshohocken, Pa.

American Society for Testing and Materials (ASTM). (2012). "Specification for Coal Fly Ash and Raw or Calcined Natural Pozzolan for Use in Concrete." C 618-12a, West Conshohocken, Pa.

American Society for Testing and Materials (ASTM). (2013). "Standard Specification for Chemical Admixtures for Concrete." C 494-13, West Conshohocken, Pa.

American Society for Testing and Materials (ASTM). (2013). "Standard Specification for Chemical Admixtures for Use in Producing Flowing Concrete." C 1017-13, West Conshohocken, Pa.

American Society for Testing and Materials (ASTM). (2013). "Standard Practice for Making and Curing Concrete Test Specimens in the Laboratory." C 192-13a, West Conshohocken, Pa.

American Society for Testing and Materials (ASTM). (2012). "Standard Test Method for Compressive Strength of Cylindrical Concrete Specimens." C 39-12, West Conshohocken, Pa.

American Society for Testing and Materials (ASTM). (2013). "Standard Practice for Use of Unbonded Caps in Determination of Compressive Strength of Hardened Concrete Cylinders." C 1231-13, West Conshohocken, Pa.

American Society for Testing and Materials (ASTM). (2013). "Measurement of Rate of Absorption of Water by Hydraulic-Cement Concretes." C1585-13, West Conshohocken, Pa.

American Society for Testing and Materials (ASTM). (2013). "Standard Test for Density, Absorption, and Voids in Hardened Concrete." C 642-13, West Conshohocken, Pa.

American Society for Testing and Materials (ASTM). (2011). "Standard Test Method for Determining the Apparent Chloride Diffusion Coefficient of Cementitious Mixtures by Bulk Diffusion." C 1556-11a, West Conshohocken, Pa.

American Society for Testing and Materials (ASTM). (2009). "Standard Test Method for Slump Flow of Self-Consolidating Concrete." C 1611-09be1, West Conshohocken, Pa.

American Society for Testing and Materials (ASTM). (2009). "Standard Test Method for Passing Ability of Self-Consolidating Concrete by J-Ring." C 1621-09b, West Conshohocken, Pa.

American Society for Testing and Materials (ASTM). (2012). "Standard Test Method for Electrical Indication of Concrete's Ability to Resist Chloride Ion Penetration." C 1202-12, West Conshohocken, Pa.

American Concrete Institute. (2007). "Self-Consolidating Concrete." ACI Committee 237, 30, Farmington Hills, MI.

Atahan, H.N. and Dikme, D. (2011). "Use of Mineral Admixtures for Enhanced Resistance against Sulfate Attack." *Construction and Building Materials*, 25, 3450-3457.

Audenaert, K., Yuan, Q., and Schutter, G.De. (2010). "On the Time Dependency of the Chloride Migration Coefficient in Concrete." *Construction and Building Materials*, 24, 396-402.

Azamirad, H., and Beheshti zadeh, D. (2005). "A Criticism of Self-Compacting Concrete." 30th Conference on Our World in Concrete & Structures, Singapore, Article Online ID: 100030023.

Bentz, D.P., Jensen, O.M., Coats, A.M., and Glasser, F.P. (2000). "Influence of Silica Fume on Diffusivity in Cement-Based Materials I. Experimental and Computer Modeling Studies on Cement Pastes." *Cement and Concrete Research*, 30, 953-962.

Boston University School of Public Health. (2013). "Multiple Linear Regression Analysis." <[http://sphweb.bumc.bu.edu/otlt/MPH-Modules/BS/BS704\\_Multivariable/BS704\\_Multivariable7.html](http://sphweb.bumc.bu.edu/otlt/MPH-Modules/BS/BS704_Multivariable/BS704_Multivariable7.html)> (Mar. 4, 2014).

Byfors, K., Hansson, C.M., and Tritthart, J. (1986). "Pore Solution Expression as a Method to Determine the Influence of Mineral Additives on Chloride Binding." *Cement and Concrete Research*, 16, 760-770.

Cement Concrete & Aggregates Australia. (2009). "Chloride Resistance of Concrete." Technical Report, 1-37.

Chung, D.D.L (2002). "Improving Cement-Based Materials by Using Silica Fume." *Journal of Materials Science*, 37, 673-682.

Chang, T.P., Shih, J.Y., Yang, K.M., and Hsiao, T.C. (2007). "Material Properties of Portland Cement Paste with Nano-Montmorillonite." *Springer Science Business Media*, 42, 7478-7487.

Claisse, P. (2005). "Transport Properties of Concrete." Coventry University, Coventry CV1 5FB, 1-16.

Diawara, Hamidou. (2008). "Parametric study of self-consolidating concrete" Ph.D. thesis, University of Nevada, Las Vegas, Las Vegas, NV.

Dolado, J.S., Campillo, I., Erkizia, E., Ibanez, J.A., Porro, A., Guerrero, A., and Goni S. (2007) "Effect of Nanosilica Additions on Belite Cement Pastes Held in Sulfate Solutions." *Institute of Construction Science, Madrid, Spain*, 3973-3976.

Domone, P.L. (2006). "Self-Compacting Concrete: An Analysis of 11 Years of Case Studies." *Cement & Concrete Composites*, 28, 197-208.

Douglas, P. (2004). "Properties of Self-Consolidating Concrete Containing Type F Fly Ash." A Master Thesis In Field of Civil Engineering, PCA R&D Serial No. 2619, 1-74.

Edvardsen, C., and Jepsen, M.T. (1998). "Chloride Migration Coefficients from nano-Steady-State Migration Experiments at Environment-Friendly Green Concrete."

Technical Paper, 1-7.

European Committee for Standardization (CEN). (2000). "Testing hardened concrete – Part 8: Depth of penetration of water under pressure." EN 12390-8:2000, Brussels.

European Federation of Concrete Admixture Associations (EFNARC). (2002).

"Specification and Guidelines for Self-Compacting Concrete." Furnham, Surrey, UK.

European Federation of Concrete Admixture Associations (EFNARC). (2006).

"Guidelines for Viscosity Modifying Admixtures for Concrete." Furnham, Surrey, UK.

Felekoglu B., Turkel, S., and Baradan, B. (2007) "Effect of Water/Cement Ratio on the Fresh and hardened Properties of Self-Compacting Concrete." Building and

Environment, 42, 1795-1802.

Goodier, C. (2003). "Development of Self-Compacting Concrete." Proceedings of the Institution of Civil Engineers, Structures & Buildings 156, 405-414.

Grace Construction Products. (2005). "An Introduction to Self-Consolidating Concrete (SCC)." Technical Bulletin TB-1500, 1-6.

Hall, C., and Yau, M.H.R. (1987). "Water Movement in Porous Building Materials-IX.

The Water Absorption and Sorptivity of Concretes." Building and Environment, 22, 77-82.

Iures, L. and Bob C. (2010). "The Future Concrete: Self-Compacting Concrete."

Buletinul Institutului Politehnic Din Iasi, Publicat de, Universitatea Tehnica, 94-100.



- Jalal, M., pouladkhan, A.R., Ramezaniapour, A.K., and Norouzi, H. (2012). "Effects of Silica Nanopowder and Silica Fume on Rheology and Strength of High Strength Self-Compacting Concrete." *Journal of American Science*, 8(4), 270-277.
- Ji, T. (2005). "Preliminary Study on the Water Permeability and Microstructure of Concrete Incorporating Nano-SiO<sub>2</sub>." *Cement and Concrete Research*, 35, 1943-1947.
- Jo, B.W., Kim, C.H., T, G.H., and Park, J.B. (2007). "Characteristics of Cement Mortar with Nano-SiO<sub>2</sub> Particles." *Construction and Building Materials*, 21, 1351-1355.
- Khayat, K. H. (1999). "Workability, testing, and performance of self-consolidating concrete." *ACI Materials Journal*, 96(3), 346-354.
- King, D. (2012). "The Effect of Silica Fume on the Properties of Concrete as Defined in Concrete Society Report 74, Cementitious Materials." 37th Conference on Our World in Concrete 7 Structures, Singapore, Article Online ID: 100037011.
- Kong, D., Du, X., Wei, S., Zhang, H., Yang, Y., and Shah, S. (2012). "Influence of Nano-Silica Agglomeration on Microstructure and Properties of the Hardened Cement-Based Materials." *Construction and Building Materials*, 37, 707-715.
- Li, G. (2004). "Properties of High-Volume Fly Ash Concrete Incorporating Nano-SiO<sub>2</sub>." *Cement and Concrete Research*, 34, 1043-1049.
- Li, H., Xiao, H.G., Yuan, J., and Ou, J. (2004). "Microstructure of Cement Mortar with Nano-Particles." *Composites, Part B*, 35, 185-189.
- Li, H., Zhang, M.H., and Ou, J.P. (2006). "Abrasion Resistance of Concrete Containing Nano-Particles for Pavement." *Wear*, 260, 1262-1266.

- Lizarazo Marriaga, J., and Lopez Tepez, L.G. (2011). "Effect of Silica Fume Addition on the Chloride-Related Transport Properties of High-Performance Concrete." ISSN 0012-7353, 105-110.
- Maghsoudi, A.A., and Dahooei, F.A. (2007). "Effect of Nanosacale Materials in Engineering Properties of Performance Self Compacting Concrete." The International Congress on Civil Engineering, 1-8.
- Maghsoudi, A.A., Maghsoudi, M., and Noori, M. (2009). "Effect of Nano Particles on SCC." Civil Engineering Department, Shahid Bahonar University of Kerman & International Center for Science, High Technology & Environmental Science, 1-13.
- Najigivi, A., and Rashi, S.A. (2012). "Water Absorption Control of Ternary Blended Concrete with Nano-SiO<sub>2</sub> in Presence of Rice Husk Ash." Materials and Structures, 45, 1007-1017.
- National Ready Mixed Concrete Association. (2004). "Concrete in Practice." CIP 37-Self-Consolidating Concrete (SCC), 1-3.
- Nazari, A., and Riahi, S. (2010). "Microstructural, Thermal, Physical and Mechanical Behavior of the Self-Compacting Concrete Containing SiO<sub>2</sub> Nanoparticles." Materials Science and Engineering, A527, 7663-7672.
- Nordtest. (1999). "Chloride Migration Coefficient from Non-Steady-State Migration Experiments." NT Build 492, Espoo, Finland.
- Okamura H. and Ouchi M. (2003) "Self-Compacting Concrete." Journal of Advanced Concrete Technology, Vol. 1, No. 1, 5-15.

Oltulu, M., and Sahin, R. (2013). "Effect of Nano-SiO<sub>2</sub>, nano-Al<sub>2</sub>O<sub>3</sub> and nano-Fe<sub>2</sub>O<sub>3</sub> Powders on Compressive Strengths and Capillary Water Absorption of Cement Mortar Containing Fly Ash: A Comparative Study." *Energy and Building*, 58, 292-301.

Oltulu, M., and Sahin, R. (2011). "Single and Combined Effects of nano-SiO<sub>2</sub>, nano-Al<sub>2</sub>O<sub>3</sub> and nano-Fe<sub>2</sub>O<sub>3</sub> Powders on Compressive Strengths and Capillary Permeability of Cement Mortar Containing Silica Fume, *Materials Science and Engineering*, A 528, 7012-7019.

Qing, Y., Zenan, Z., Deyu, K. and Rongshe, C. (2007). "Influence of Nano- SiO<sub>2</sub> Addition on Properties of Hardened Cement Paste Compared with Silica Fume." *Construction and Building Materials*, 21, 539-545.

Querica, G., Spiesz, P., Husken, G., and Brouwers, J. (2012). "Effects of Amorphous Nano-Silica Additions on Mechanical and Durability Performance of SCC Mixtures." *International Congress on Durability of Concrete*, 1-15.

Ramezani-pour, A.K., Pilvar, A., Mahdikhani, M., and Moodi, F. (2011). "Practical Evaluation of Relationship between Concrete Resistivity, Water Penetration, Rapid Chloride Penetration and Compressive Strength." *Construction and Building Materials*, 25, 2472-2479.

Ransinchung G.D., Kumar, B., and Kumar, V. (2009). "Assessment of Water Absorption and Chloride Ion Penetration of Pavement Quality Concrete Admixed with Wollastonite and Microsilica." *Construction and Building Materials*, 23, 1168-1177.

Sabet, F.A., Libre, N.A, and Shekarchi, M. (2013). "Mechanical and Durability Properties of Self Consolidating High Performance Concrete Incorporating natural Zeolite, Silica Fume and Fly Ash." *Construction and Building Materials*, 44, 175-184.

Sabir, B.B., Wild, S., and O'Farrell, M. (1998). "A Water Sorptivity Test for Mortar and Concrete." *Materials and Structures*, 31, 568-574.

Sahmaran, M., Yaman, I., and Tokyay, M. (2009). "Transport and mechanical properties of self-consolidating concrete with high volume fly ash." *Cement and Concrete Composites*, 31(2), 99-106.

Said, A.M., Zeidan, M.S., Bassunoni, M.T., and Tian, Y. (2012). "Properties of Concrete Incorporating Nano-Silica." *Construction and Building Materials*, 36, 838-844.

Senff, L., Hotza, D., Repette, W.L, Ferreira, V.M., and Labrincha, J.A. (2010). "Mortars with Nano-SiO<sub>2</sub> and Micro-SiO<sub>2</sub> Investigated by Experimental Design." *Construction and Building Materials*, 24, 1432-1437.

Shi, C. (2003). "Another Look at the Rapid Chloride Permeability Test (ASTM C1202 or ASSHTO T277)", CJS Technology Inc., Ontario, Canada.

Siddique, R. (2013). " Compressive Strength, Water Absorption, Sorptivity, Abrasion Resistance and Permeability of Self-Compacting Concrete Containing Coal Bottom Ash." *Construction and Building Materials*, 47, 1444-1450.

Sonebi, M., and Nanukuttan, S. (2009). "Transport Properties of Self-Consolidating Concrete." *ACI Materials Journal*, Technical Paper, Title No. 106-M20, 161-166.

Tande, S.N., and Mohite, P.B. (2007) "Application of Self-Compacting Concrete." 32nd Conference on Our World in Concrete & Structure, Singapore, Article Online ID: 100032055.

Toutanji, H.A. (1999). "Properties of Polypropylene Fiber Reinforced Silica Fume Expansive-Cement Concrete." *Construction and Building Materials*, 13, 171-177.

- Uysal, M., Yilmaz, K., and Ipek, M. (2012). "The Effect of Mineral Admixtures on Mechanical Properties, Chloride Ion Permeability and Impermeability of Self-Compacting Concrete." *Construction and Building Materials*, 27, 263-270.
- Wee, T.H., Suryavanshi, A.K., and Tin, S.S. (1999). "Influence of Aggregate Fraction in the Mix on the Reliability of the Rapid Chloride Permeability Test." *Cement and Concrete Composites*, 21, 59-72.
- Wild, S., Sabir, B.B, and Khatib, J.M. (1995). "Factors Influence Strength Development of Concrete Containing Silica Fume." *Cement and Concrete Research*, 25 (7), 1567-1580.
- Yang, C.C., Cho, S.W., and Wang, L.C. (2006). "The Relationship between Pore Structure and Chloride Diffusivity from Ponding Test in Cement-Based Materials." *Materials Chemistry and Physics*, 100, 203-210.
- Yang, F. (2004). "Self-Consolidating Concrete." *Concrete Technology*, 1-21.
- Yildirim, H., Ilica, T., and Sengul, O. (2011). "Effect of Cement Type on the Resistance of Concrete Against Chloride Penetration." *Construction and Building Materials*, 25, 1282-1288.
- Yogendran, V., and Langan B.W. (1987). "Utilization of Silica Fume in High Strength Concrete." *Proceedings of Utilization of High Strength Concrete*, Stavanger, Tapir Publisher Trondheim, Norway.
- Zhang, M.H., and Islam, J. (2012). "Use of Nano-Silica to Reduce Setting Time and Increase Early Strength of Concretes with High Volumes of Fly Ash or Slag." *Construction and Building Materials*, 29, 573-580.

Zhang, M.H, and Li, H. (2011). "Pore Structure and Chloride Permeability of Concrete Containing Nano-Particles for Pavemetn." *Construction and Building Materials*, 25, 608-616.

Zhang, T., and Gjorv, O.E. (1996). "Diffusion Behavior of Chloride Ions in Concrete." *Cement and Concrete Research*, 26, 6, 907-917.

Zofia, S., and Adam, Z. (2013). "Theoretical Model and Experimental Tests on Chloride Diffusion and Migration Processes in Concrete." *11th International Conference on Modern Building Materials, Structures and Techniques*, 57, 1121-1130.

## **Curriculum Vitae**

Department of Civil and Environmental Engineering and Construction

Howard R. Hughes College of Engineering

The Graduate College

Borhan Moradi

### Address:

2500 Vista Mar Drive, Las Vegas, Nevada, 89128

### Degrees:

Bachelor of Science, Civil and Environmental Engineering, 2011

University of Nevada, Las Vegas

Master of Science, Civil and Environmental Engineering, 2014

University of Nevada, Las Vegas

### Special Honors:

Graduate & Professional Student Association (GPSA) Honorable Mention Award

### Publications:

- Ghafoori, N., Islam, M., Nyknahad, D., Moradi, B., (INVITED) “Comparison of Fly Ash, Lithium Nitrate, and Nano-Silica for Reduction of Alkali-Silica Reactivity,” Proceedings

of the 2<sup>nd</sup> International Conference on Future Concrete, December 12 – 14, 2011, Dubai, United Arab Emirate, pp. 1-11 (CD proceedings).

- Ghafoori, N., M., Nyknahad, D., Moradi, B., and Beasley, S., (INVITED) “Sulfate Resistance of Very High Early Strength Concrete Pavements,” Proceedings of the 2<sup>nd</sup> International Conference on Future Concrete, December 12 – 14, 2011, Dubai, United Arab Emirate, pp. 1-8 (CD proceedings).

Thesis Title: Transport Properties of Nano-Silica Contained Self-Consolidating Concrete

Thesis Examination Committee:

Chairperson: Dr. Nader Ghafoori, Ph.D.

Committee Member: Dr. Samaan Ladkany, Ph.D.

Committee Member: Dr. Mohamed Kaseko, Ph.D.

Committee Member: Dr. Spencer Steinberg, Ph.D.

Graduate College Faculty Representative: Dr. Samir Moujaes, Ph.D.